RF PLASMA THIN FILM DEPOSITION: SILICON OXIDE AND YTTRIUM CONTAINING FILMS

BY

CHRISTOPHER R. NORTON

A THESIS
SUBMITTED TO THE FACULTY OF

ALFRED UNIVERSITY

IN PARTIAL FULFILLMENT OF THE REQUIREMENTS
FOR THE DEGREE OF

MASTER OF SCIENCE

IN

ELECTRICAL ENGINEERING

ALFRED, NEW YORK

AUGUST, 2004

RF PLASMA THIN FILM DEPOSITION: SILICON OXIDE AND YTTRIUM CONTAINING FILMS

BY

CHRISTOPHER R. NORTON

B.S. STATE UNIVERSITY OF N.Y. AT ALFRED (2002)

SIGNATURE OF AUTHOR (Signature on file)

APPROVED BY (Signature on file)
XINGWU WANG, ADVISOR

(Signature on file)
JALAL BAGHDADCHI, ADVISORY COMMITTEE

(Signature on file)
JOSEPH ROSICZKOWSKI, ADVISORY COMMITTEE

(Signature on file)
JIANXIN TANG, CHAIR, ORAL THESIS DEFENSE

ACCEPTED BY (Signature on file)
ALASTAIR CORMACK, DEAN,
SCHOOL OF ENGINEERING

TO MICAH, C. J., AND JENELLE

ACKNOWLEDGMENTS

The author would like to thank Dr. Xingwu Wang for all of his help during the course of this study. I would also like to thank Mrs. Rosalie Di Raimondo, whose knowledge of Alfred University was invaluable. I appreciate also the help of Mr. David Hunt whose knowledge of the RF Plasma system greatly helped my endeavor. Dr. Pipal and Ms. Michele Mitchell of the Chemistry Department also have my thanks. Thanks also go to Mr. Jeffrey Johnson of the Ceramic College Physical Plant and all of his crew for their assistance in assembling the RF Plasma Deposition System. Mr. Alan Ormsby and the personnel of the machine shop were instrumental in the development of the vacuum system. Also, I would like to thank Mr. Ward Votava for his instruction in regards to the electron microscope. I would also like to extend my appreciation to Dr. Richard Marlor, Dr. Tuan Dang, Mr. Mark Grossman, and Mr. Eric Pavlina for their assistance in analyzing samples.

TABLE OF CONTENTS

LIST OF TABLES

LIST OF FIGURES

Abstract

The atmospheric RF plasma thin film deposition system was reassembled and used to deposit SiO_2 coatings. These coatings were deposited on microscope glass slide substrates as well as the exterior of cylindrical glass tubes. An aluminum rod was also used as a substrate.

The atmospheric system was modified to work as a vacuum system so thin film coatings could be deposited on the interior of glass tubes. A water cooled coil was obtained to provide the energy necessary to form plasma. The existing aerosol mist delivery system was modified to work in a vacuum. Silicon dioxide and yttrium containing films were deposited in a vacuum.

Coatings were analyzed with SEM and EDS analysis at Alfred University. Coatings were also analyzed with ESCA, SNMS, FTIR-ATR, SEM, and EDS at the labs of Osram Sylvania.

I INTRODUCTION

Between 1988 and 1997 an atmospheric RF plasma aerosol mist deposition system was developed at Alfred University.[1] Many different types of oxide films were deposited including magnesium oxide, aluminum oxide, yttrium oxide, indium-tin oxide and silicon oxide. One of the objectives of this study was to modify the thin film deposition system so that a comparative study could be made. That is, a study of films deposited under different pressures.

In this study, nano-sized SiO_2 will be used as the precursor for deposition on glass microscope slides. Furthermore, cylindrical substrates will be utilized. In addition, aluminum nitrate and yttrium nitrate will be used as precursors for deposition of thin film on the interior of glass tubes.

A. Background on Thin Film

Thin Film deposition involves the vaporization of a target material and the subsequent condensation (or deposition) of this vapor onto a substrate. Any material onto which the vapor will condense can be used as a substrate.[2] Several techniques are used to supply the energy necessary to vaporize the target material. Among these techniques are Atmospheric Pressure Chemical Vapor Deposition, Atmospheric RF Plasma Deposition, Laser Deposition, Sputtering, and Electron Beam Deposition.[3] Also, depending upon the desired type of thin film and the technique used, deposition can occur under atmospheric pressure or in a vacuum.

1. Applications of Thin Film

There are many industrial applications of thin film. Coatings can be conductive, non conductive, or protective. For instance, protective coatings are applied to engine turbine blades in the aeronautical industry. Critical automotive wear components such as valves

and rings are coated to increase their lifetime. The aerospace industry utilizes coatings to protect optical components against the rigors of space such as the lenses of the Hubble telescope. The requirement here is to engineer the film so that it doesn't change the optical properties of the lenses. The ability to apply a protective coating on glass will find application in the eyeglass industry.

Surgical tools and equipment are coated to add lubrication for easier insertion of instruments. Cutting tools and drill bits can be coated for added toughness and increased lifetime. There has recently been experimentation using thin film coatings on the leads to heart pacemakers to shield them from the heating effects of magnetic resonance imaging. If successful, people with medical implants will be able to undergo this valuable diagnostic procedure.

There are many applications in the electronics industry. Conductive and non conductive coatings can be used together to form capacitors or possibly inductors on silicon chips. This could greatly decrease the size of electronic equipment.

The Atmospheric RF process offers high quality and increased speed because it eliminates the need to apply the coating in a vacuum.

B. Plasma Processing of Thin Film

1. Plasma Spray

Plasma processing is used extensively in the fabrication of thin films, semiconductors, and superconductors. This process can be classified as either microwave, RF or DC.[1] Plasmas generated at atmospheric pressure (760 Torr) do not posses the disadvantages experienced while operating under vacuum conditions.[4] The main difference is that higher voltages are needed to break down the plasma gas at 760 Torr. Figure I-1 demonstrates several plasma generation devices.

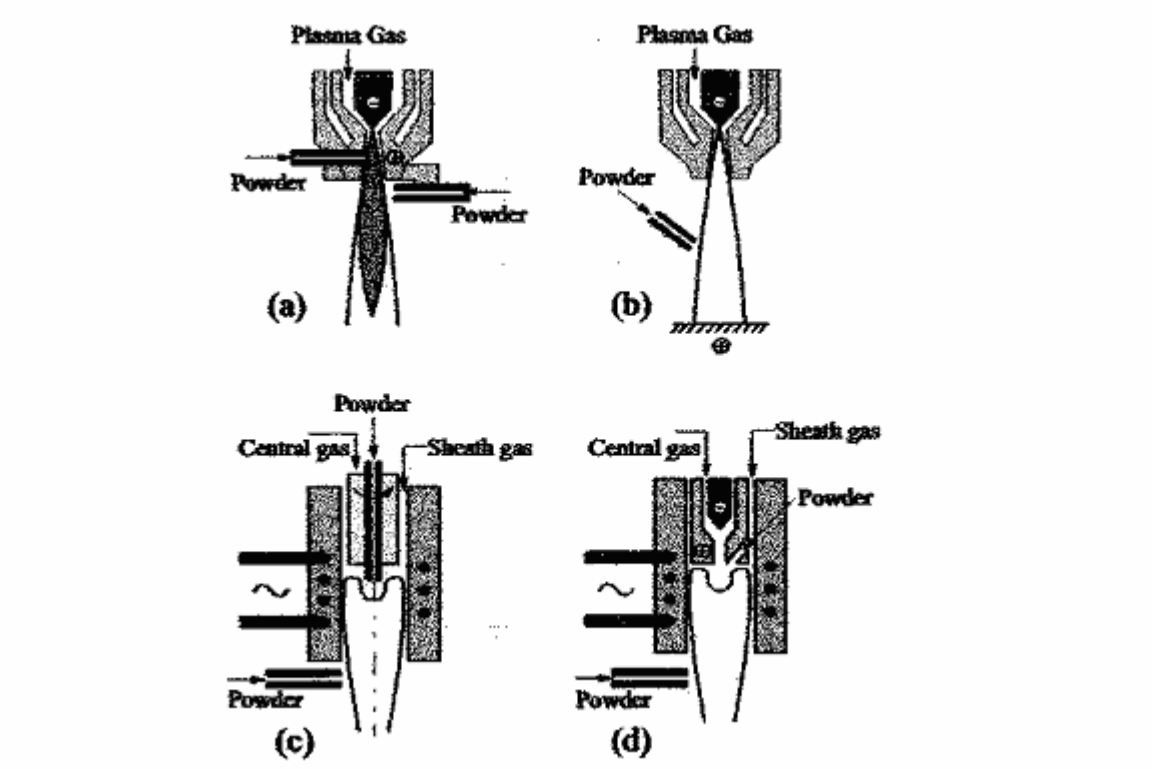

Figure I-1. Thermal plasma generation devices (a) d.c. plasma torch (b) d.c. transferred arc (c) r.f. induction plasma torch (d) d.c./r.f. hybrid plasma torch[5]

2. Plasma Physics

Plasma consists of a partially ionized gas with equal numbers of positive and negative charged particles and a different number of neutral particles.[5] When an external energy source is applied to a plasma gas, gas molecules become ionized and electrons break away from the positively charged nuclei. Because of the small mass of the electrons, they respond more readily than the heavier ions and are therefore the dominant charge carriers.[1] The motion of the ions can be considered negligible in typical plasma processing systems.

Because of their moderately conductive nature, they are affected by both electric and magnetic fields. The force acting on a moving particle in an electro-magnetic field can be described by:

$$\mathbf{F} = q\mathbf{v} \times \mathbf{B}$$

where q is the charge of the particle, v is its velocity, and B is the strength of the electro-magnetic field measured in Tesla. A particle will experience a spiral motion in an electro-magnetic field with a frequency of rotation of:

$$\omega = q\mathbf{B}/m$$

where m is the mass of the particle.

As stated above, the breakdown voltage V_b of a gas must be exceeded in order to generate plasma. V_b is a function of the electrode spacing d and the pressure p according to the equation:

$$V_b = Bpd / (\ln[Apd] - \ln[\ln[1+1/\gamma_{se}]]$$

where A and B are experimentally determined constants and γ_{se} is the secondary electron emission coefficient of the cathode. Figure I-2 demonstrates the dependence of breakdown voltage on electrode spacing and pressure. The breakdown voltage for argon appears to be about 2500v at 760 Torr with a 5mm gap distance. Figure I-2 clearly demonstrates that more energy is required to break down plasma gases at atmospheric pressure as opposed to plasma gases in a vacuum.

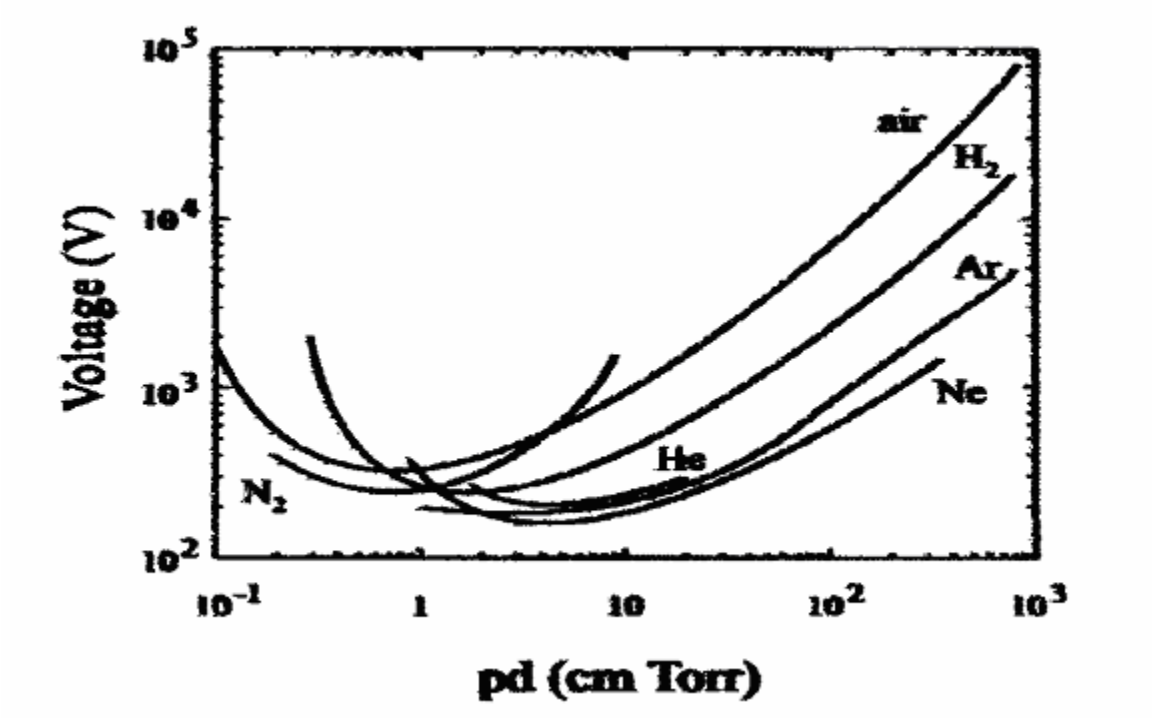

Figure I-2. Breakdown Potential in various gases as a function of p and d[4]

In an inductively coupled plasma torch, a plasma is generated by inductive coupling of energy into the plasma.[5] The power levels of induction plasmas range from a few kW to 500kW with confinement tube diameters from 18 to 100mm. The Tafa plasma torch used in this study utilizes 5 turns of water cooled copper coil surrounding a water cooled quartz confinement tube. The inner diameter of the quartz tube is 40 mm. At 20% power, the torch operates at 7kW at a frequency of 3.2MHz.

Figure I-3 demonstrates the dependency of electron temperature and Ion temperature on pressure. At pressures below 1 Torr the collision rate between ions and electrons is relatively small. When atmospheric pressure is reached, the faster moving electrons carry much more energy than the slower moving ions.[1]

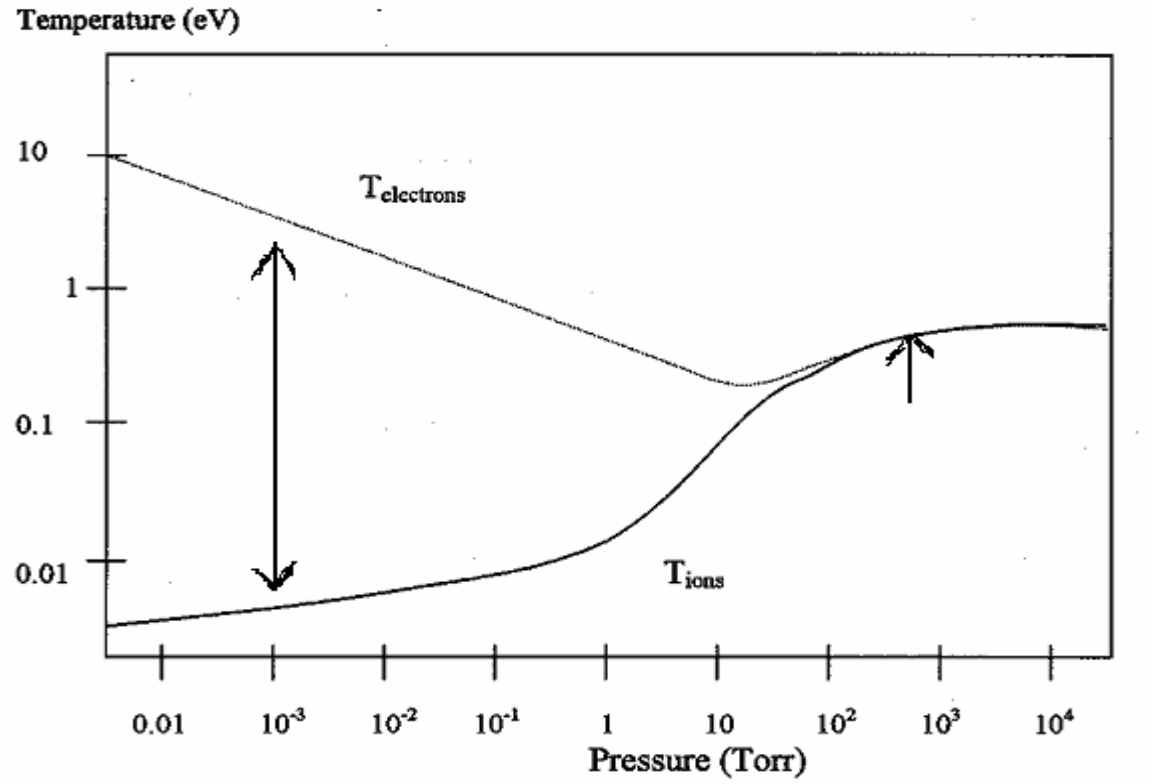

Figure I-3. Dependence of Electron Temperature and Ion Temperature on Pressure[1]

The longer arrow in figure I-3 demonstrates the approximate pressure obtained by the modified RF deposition system, a vacuum of approximately $20x10^{-3}$ Torr. The shorter arrow shows atmospheric pressure of 760 Torr.

II EXPERIMENTAL PROCEDURES – ATMOSPHERIC SYSTEM

A. Radio Frequency Generator

A radio frequency (RF) plasma deposition system will be used in this study. The system makes use of an RF generator to supply the electro-magnetic field required by a plasma generator. Radio frequency wave generation makes use of high voltage alternating current, converts it to high voltage direct current, and then oscillates the DC signal to mimic an alternating current signal. The reason for this is that the plasma torch requires a very stable energy source free of the fluctuations experienced with commercially delivered AC power. The RF generator used for this study is a model TAFA32*30MC manufactured by Lepel in 1975. This high frequency generator makes use of vacuum tube technology and is rated at 230 volts and 160 amps. It is designed to operate at a frequency of 4 MHz and is capable of delivering thirty kilowatts of power.

1. Vacuum Tube Capacitors

When the system was assembled it was decided to increase the capacitance in the tank circuit. This effectively reduced the operating frequency of the generator and possibly made the system more stable. Figure II-1 demonstrates the type of vacuum tube capacitors utilized in this generator.

2. Power Vacuum Tube

The power vacuum tube is a voltage control device and acts much like a field effect transistor whereas a bias current controls the power output. Because of the high heat generated by the tube, the entire system is cooled with fans and a circulating water system. Figure II-2 depicts the ML-315 vacuum tube.

Figure II-1. Vacuum Tube Capacitors

3. Grid Control

Proper tuning of the RF generator is extremely important.[6] Over-driving or under-driving the power tube will eventually result in overheating and failure. A variable

Figure II-2. ML-315 Power Vacuum Tube

inductor in the grid control circuit controls the amount of bias current applied to the tube. If the grid current is too small, an excess amount of current passes through the variable inductor and arcing occurs between the turns of the coil. The gird control is currently set at 17.10 as demonstrated in Figure II-3.

Figure II-3. Grid Control

B. Plasma Generator

A plasma generator supplies the energy necessary to vaporize the target material. The generator used in this study is a TAFA Model 27*08. The assembly consists of a quartz tube surrounded by five turns of 3/32" copper wire to form a coil. When a voltage is placed across this coil, a magnetic field is generated inside the quartz tube. Figure II-4 demonstrates the operation of the torch.

Figure II-5 provides a photograph of the plasma torch in operation. At the time this picture was taken, SiO_2 was being deposited on a soda lime silicate glass slide. The bluish flame (with a hint of purple) is produced by the silicon dioxide target material being introduced to the torch. The color of the flame is different for various target materials. The leads can be seen connected to the RF generator. The leads not only function as positive and negative terminals but also provide cooling water to the torch.

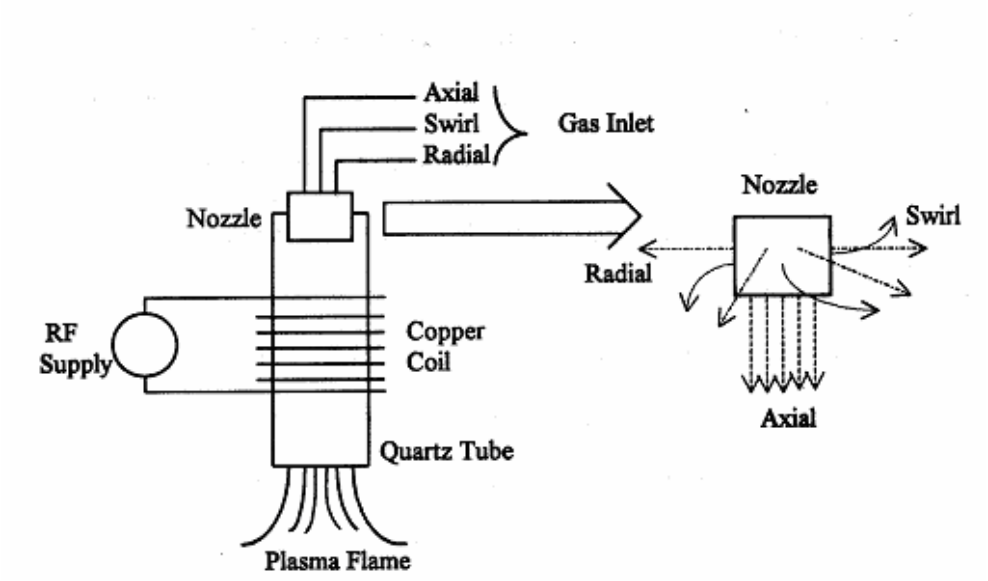

Figure II-4. Plasma Torch[2]

Like the RF generator, the torch is water cooled to help with heat dissipation. The center section of the torch is encased in Teflon. Argon gas enters the reactor through a gas nozzle and is distributed in axial, radial, and swirl directions as shown in Figure II-4.

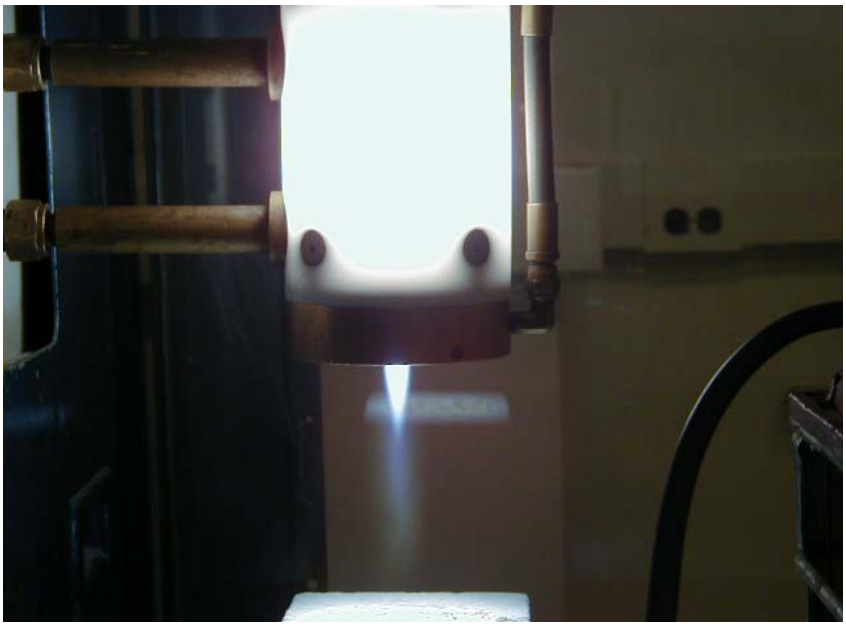

Figure II-5. TAFA Model 27*08 Plasma Torch

When the argon gas is introduced to the torch and enters the magnetic field inside the quartz tube, it is partially ionized to form a plasma region.[2] Figure II-6 demonstrates the temperature profile of this plasma region. As can be seen, the temperature in the center of the plasma region can reach 10,000°K (about 17,500°F). This region is where the target material is vaporized. The newly formed vapor travels through the torch and out the bottom where it condenses onto a substrate.

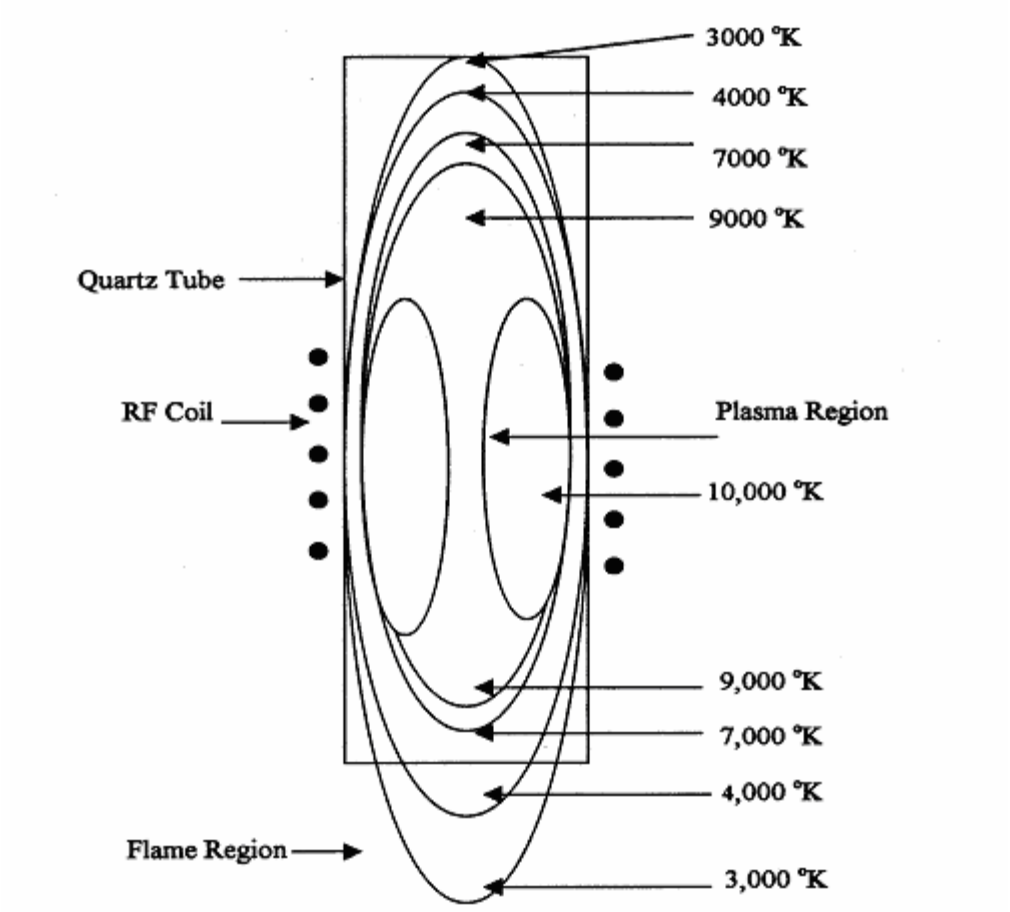

Figure II-6. Plasma Torch Temperature Profile[1]

C. Aerosol Mist Delivery System

An aerosol mist procedure developed and patented by Alfred University is used to deliver the target material to the plasma torch. The mist system produces more homogenous films than the old procedure of introducing a powder to the plasma region.[2]

Figure 11-7 demonstrates how an ultrasonic nebulizer is used to create an aerosol mist from a solution of the target material. An aerosol mist is a suspension of ultramicroscopic solid or liquid particles in air or gas, such as fog or smoke. Argon is used as the carrier gas to transport the mist to the plasma generator.

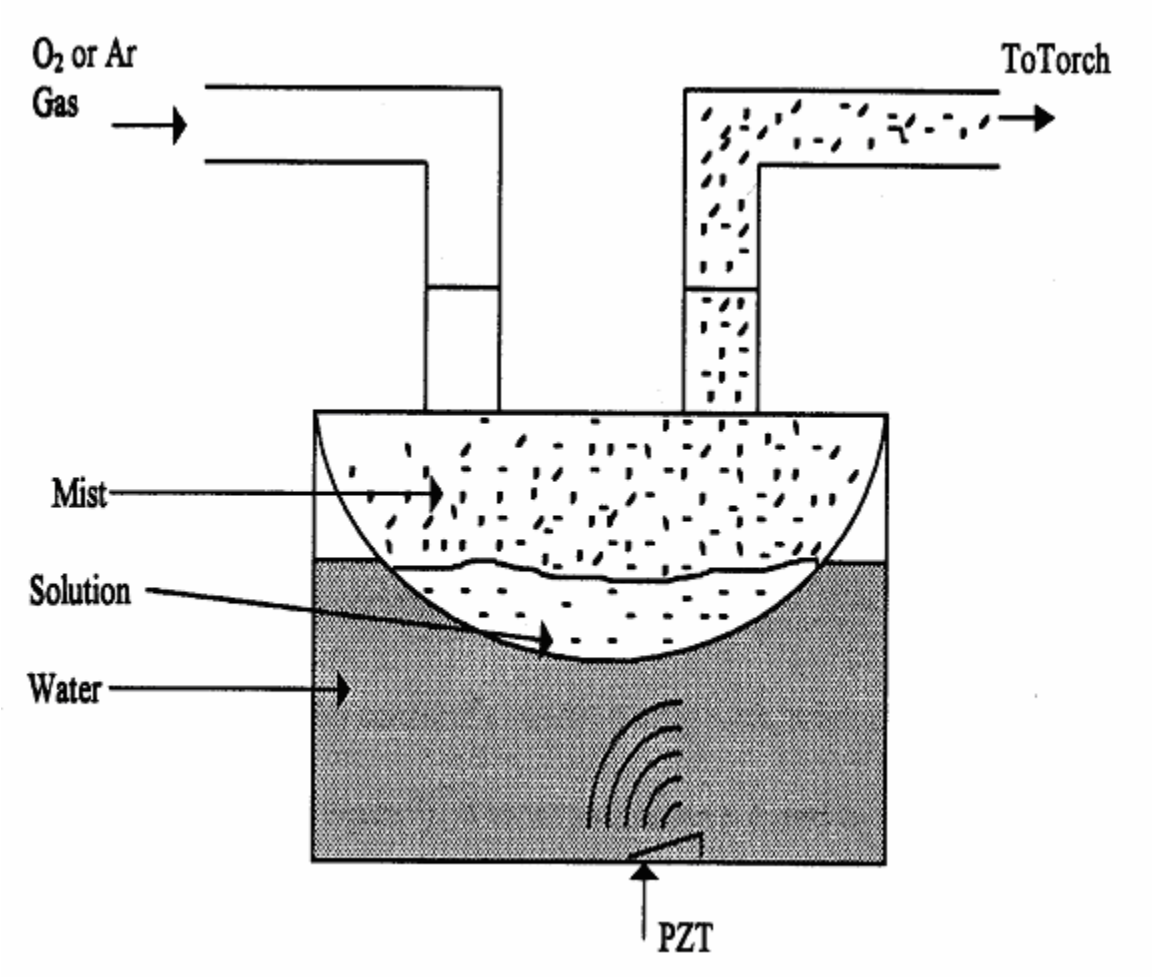

Figure 11-7. Creation of Aerosol Mist[1]

The Devilbiss model Ultra-Neb 99 nebulizer used in this experiment works much better after it has operated for a time. It was noted that the plasma torch began to flicker about half way through the runs when the nebulizer power was set on high. This flickering suggested an unstable plasma region which was caused by excessive loading. This excessive loading was caused by the increased flow of target material. This idea was confirmed several times when the plasma became so unstable that the torch went out. Turning the nebulizer power down reduced this loading effect and allowed the runs to

continue to the desired length of time. The problem was solved by letting the nebulizer run on full power (without the target material present) for at least ten minutes prior to starting a run. Figure II-8 is a schematic representation of how the nebulizer, plasma generator, and substrate assemblies work together.

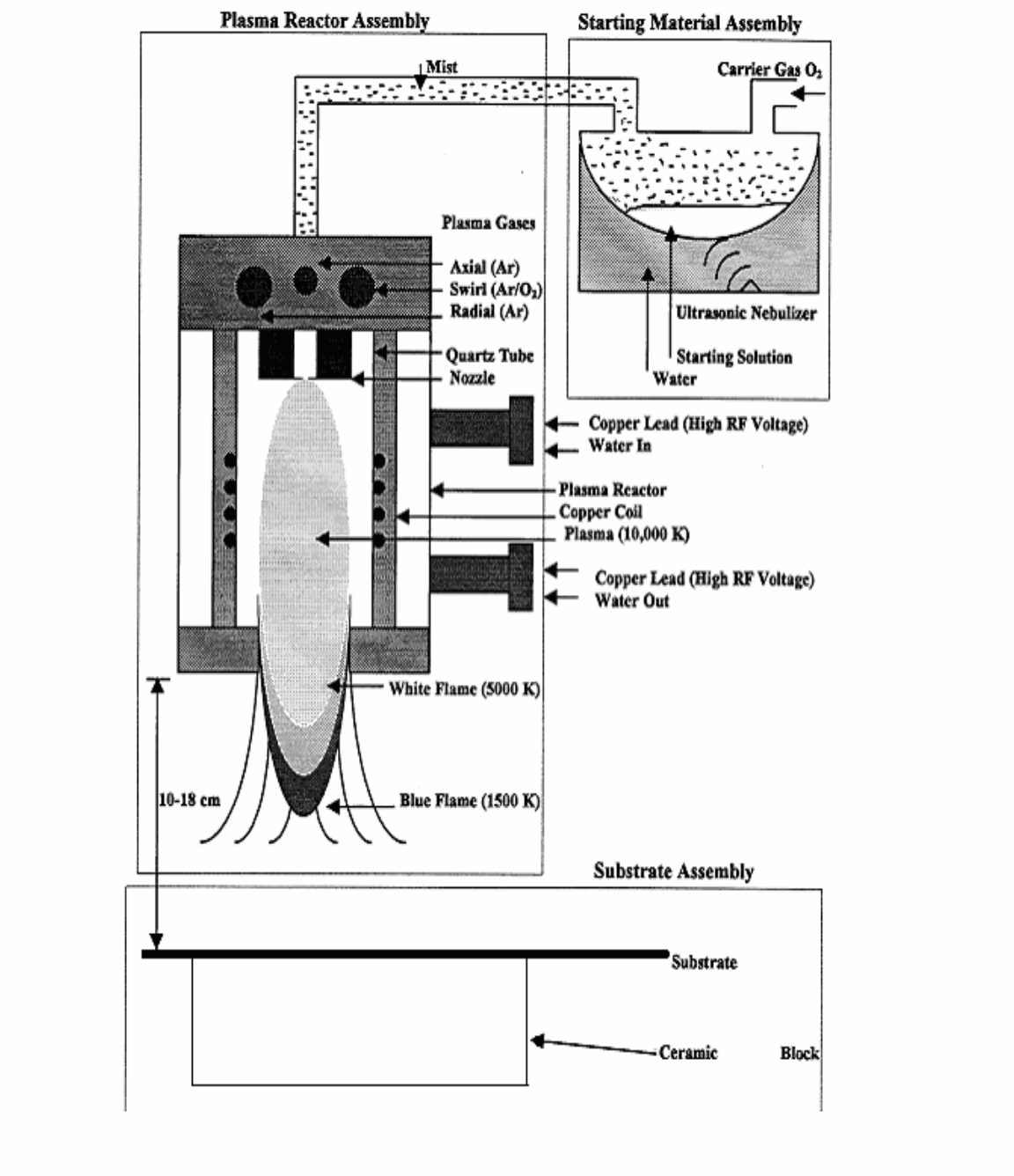

Figure II-8. Nebulizer, Plasma Torch, and Substrate Assemblies[1]

The Plasma torch and aerosol mist system are housed in a vented chamber next to the generator as can be seen in Figure II-9. This entire procedure occurs under atmospheric pressure.

Figure II-9. Aerosol mist delivery system

D. Gas Feed System

The gas feed system is demonstrated in Figure II-10. It begins with a tank of Ar gas that feeds into the gas flow controller. The Ar tank was adjusted to 80 psi for all atmospheric deposition runs. The gas flow controller used in this study was the TAFA model 47*10. Regular grade argon gas was used as the plasma gas and also as the carrier gas for all experiments. The axial, swirl, and radial lines were adjusted to generate and maintain a stable plasma region inside the Torch. The carrier gas was adjusted for desired levels for each run.

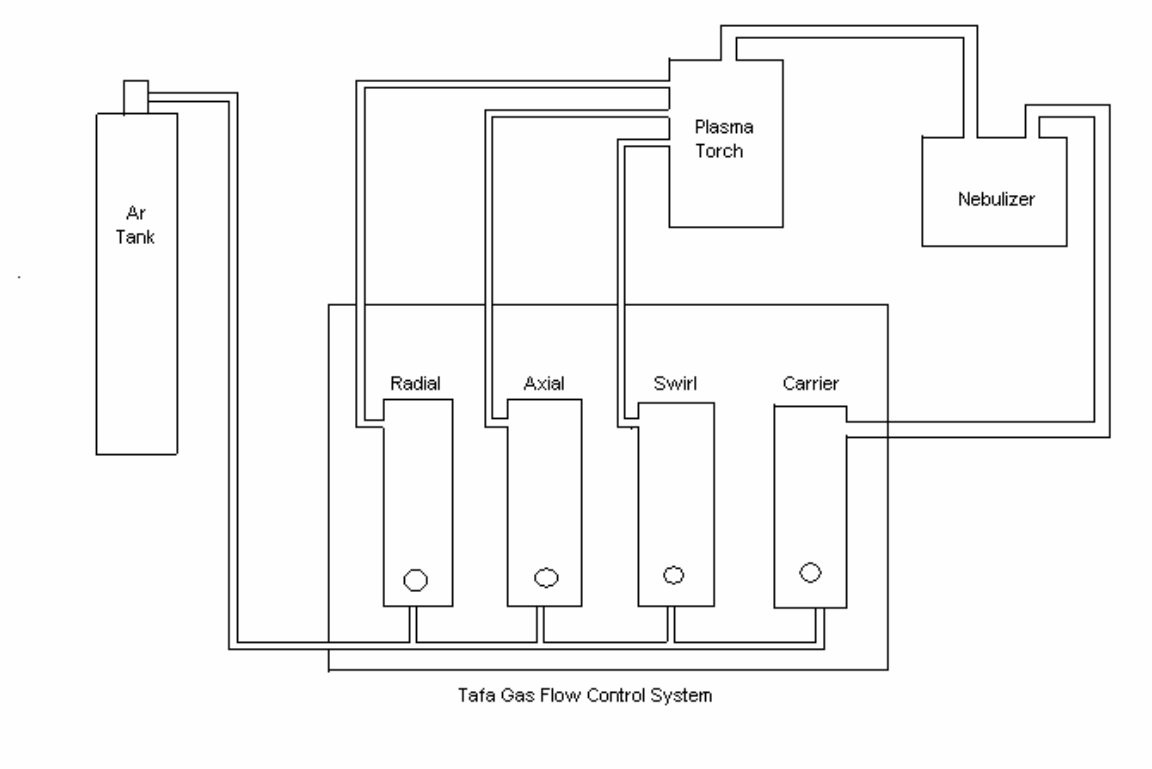

Figure II-10. Gas Feed System

E. Operation of the Atmospheric RF Plasma System

Proper operation of this system is crucial and the following procedures should be followed exactly to avoid any damage to the system or to any individuals operating the system. Before beginning, make sure that the system is cleaned and that there are no foreign objects in the way of any of the subsystems.

1. Preparation of the Aerosol Mist Delivery System

The nebulizer machine, along with the air filter, should be cleaned before operation. The nebulizer chamber should be filled with water up to the max fill line. Make sure that the metal shield is in place as it prevents radio frequency waves from interfering with the

operation of the transducer. For optimum operation of the nebulizer during deposition, it should be run for five to ten minutes prior to each use. Place one of the plastic covers over the water filled chamber and let it warm up. This warm up period will also add humidity to the deposition chamber which will enhance the ignition of the plasma torch. The reason for this is that plasmas conduct electricity and a more humid atmosphere helps ignition.

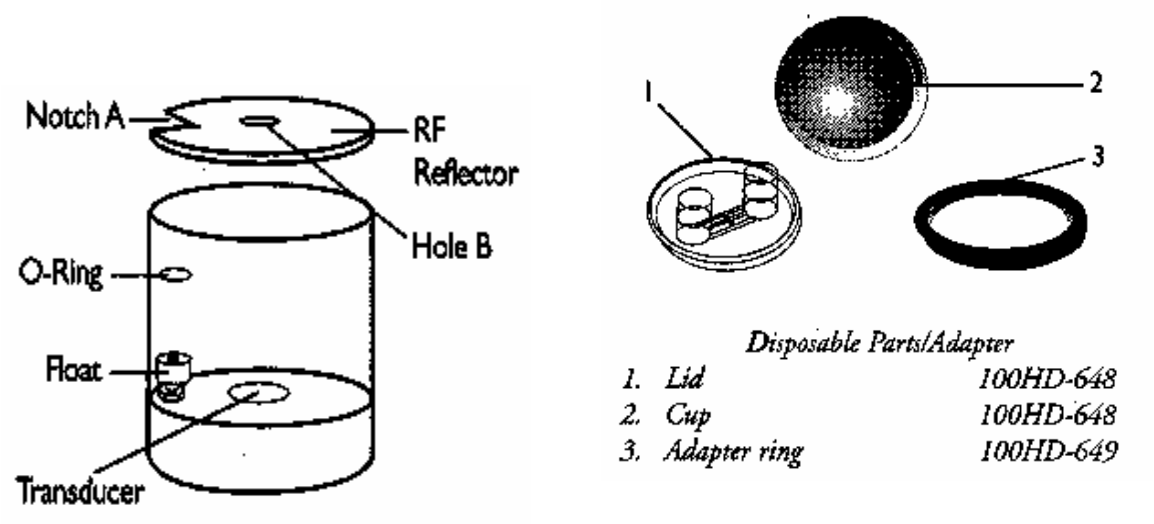

Figure II-11. Nebulizer Chamber Assembly (Devilbiss)[7]

Figure II-11 shows that a soft plastic precursor cup (part #2) fits in the top of the nebulizer chamber. Add the desired amount of precursor, put the plastic cover in place, and connect the incoming carrier gas line and the outgoing precursor delivery tube to the lid (part #1).

2. Precursor Preparation

A quantity of fumed silicon dioxide (SiO_2) was obtained from Alpha Aesar Chemical Company. This is in powder form with a particle size of seven nanometers. The desired quantity of SiO_2 is mixed with 100ml of de-ionized H_2O in a beaker and then placed on a

Thermix stirrer for ten minutes. The solution is then placed in the soft plastic cup and then into the nebulizer chamber.

Solutions of 10g/liter, 20g/liter, and 50g/liter were utilized for this study.

3. Preparation of the Plasma Torch

Operation of the plasma torch in this system causes a buildup of nano-sized particles on the interior of the quartz tube and also on the outlet structure. Therefore, the torch should be disassembled and cleaned after each use. A combination of soap and water or any light solvent such as isopropyl alcohol can be used. Disassemble the torch completely and clean all parts before reassembly. The high heat involved in operation of the generator also causes the o-rings to dry out. Therefore, they should be thoroughly cleaned and lightly coated with high vacuum grease before reassembly. This will keep them pliable and should help prevent any coolant water leaks.

The structure of the plasma torch is made of soft brass for the most part and great care should be taken not to over tighten the nuts and bolts during reassembly. This will prevent damage to the threads and o-rings.

The plasma torch fittings on the RF generator are encased in a ceramic insulation material which is quite brittle and easily damaged. Therefore, while attaching the plasma torch to the RF generator, care should be taken not to over-tighten the fittings. The couplings contain o-rings so over-tightening is not necessary to avoid coolant water leaks.

4. Preparation of the Substrate

Prepare the substrate to be used and adjust the assembly to the desired height below the plasma generator. For instance, Figure II-12 shows this procedure with the distance d equal to 18.73cm. The substrate should be cleaned thoroughly with isopropyl alcohol and then with de-ionized water.

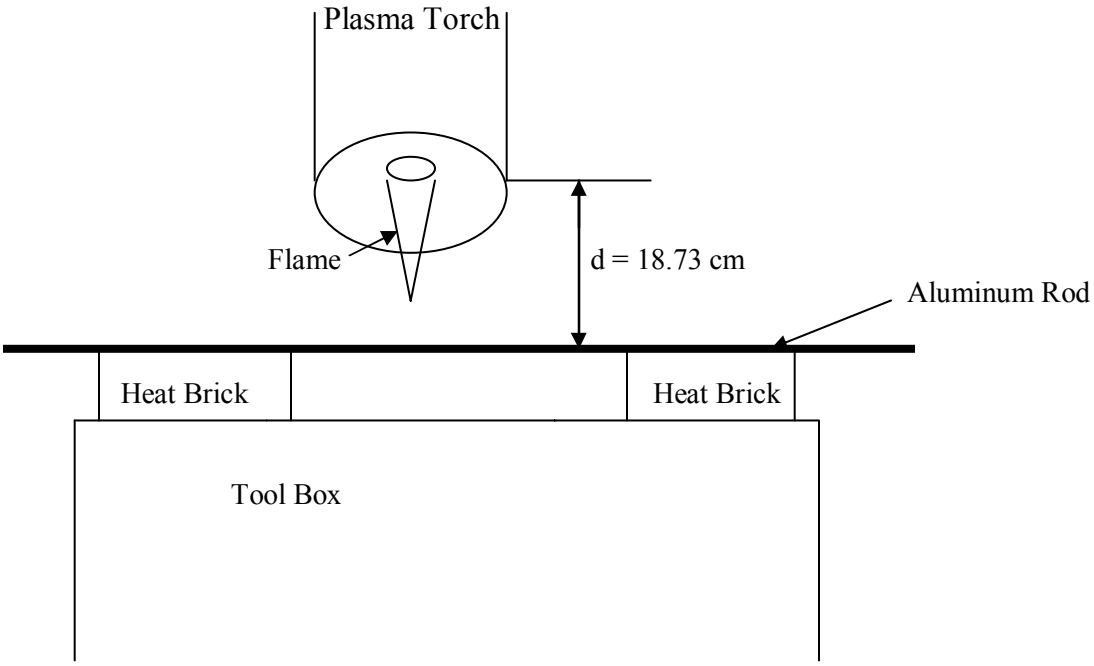

Figure II-12. Torch and Substrate Assembly

5. Starting the RF Generator

Before turning on any power to the RF generator, it is a good idea to activate the water cooling system. This step doesn't need to be done until just before the filament switch is turned on, but has to be done to avoid damage to the power tube. The sooner the cooling system is turned on the less likely one will forget and run the power tube without it. After turning on the water, go to the drain and make sure that the coolant is actually flowing.

Next, turn the power to the system on at the breaker box and then turn the power switch on the generator on. Allow the system to run at least three minutes before continuing.[6] While waiting for the system to warm up, prepare the plasma torch for operation.

After preparation of the torch, turn the argon gas tank on to 80psi and adjust the plasma gas lines at the gas flow controller. The axial, swirl, and radial gas lines should be adjusted as shown in Table 1. Leave the carrier gas line turned off at this time.

Table I. Plasma and Carrier Gas Flow Settings

Argon Gas Flow Line	Setting
Radial Gas Flow	8%
Axial Gas Flow	4%
Swirl Gas Flow	6%
Carrier Gas Flow	5%

Turn the green filament switch on. Just to the right of the filament switch, a red reset button will glow red for a period of time. After this period, its intensity will increase and it will glow a bright red. This means that the filament is warmed up and the system is ready for RF power. For the next step, refer to the ignition of the plasma torch section below.

6. Ignition of the Plasma Torch

A Ni80/Cr20 filament wire is used to enhance the ignition of the plasma torch. The filament should be formed in a ring with a straight piece approximately six inches long leading from this ring. An eighteen inch long piece of wood is used to remove the remainder of the filament after successful ignition of the torch. Insert the piece of wood in the ring and lift the filament out of the torch assembly. The wood is used because of the high heat generated in the wire and also because of the danger of high voltage associated with the electro-magnetic field. This process is demonstrated in Figure II-13.

Graphite rubbed on the interior of the quartz tube just prior to reassembling the torch will also enhance ignition. The most effective method is to use a combination of the filament and the graphite.

Make sure the substrate is not directly below the torch during the ignition procedure. This will avoid pieces of the nickel chromium filament from falling onto the substrate and contaminating the surface.

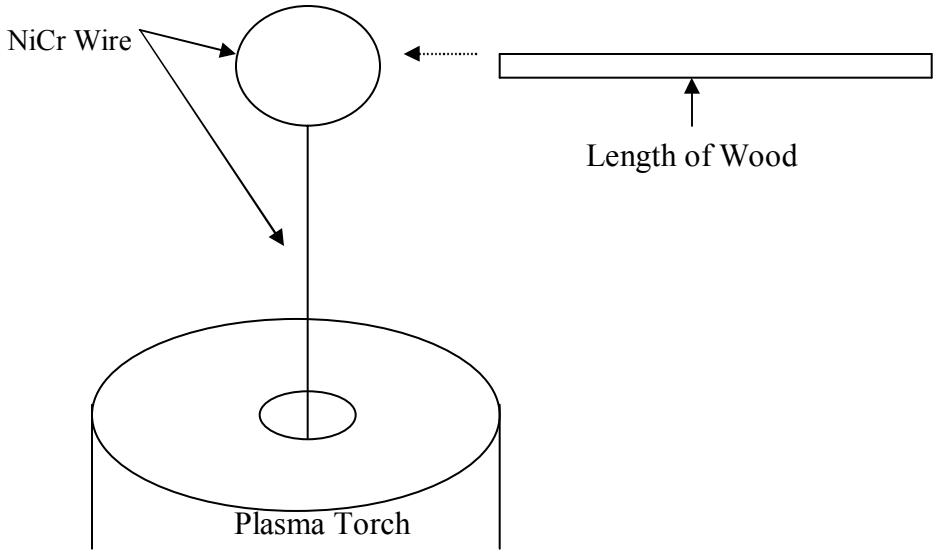

Figure II-13. Extraction of NiCr Filament

When the intensity of the reset light changes to bright red on the RF Generator, turn the RF power dial to 25% and push the green RF power button on. The nickel chromium wire inside the torch should begin to glow a bright red and produce a great deal of concentrated heat in the center of the quartz tube. This together with the power generated by the electro-magnetic field will begin to ionize the argon gas and form plasma. If successful, the torch will ignite and a cone shaped flame will appear exiting the base of the torch. If the torch does not ignite, the RF generator will reset with a loud noise. To make another attempt at ignition, press the reset button and turn the RF power button back on.

If the torch still doesn't ignite, turn the axial gas line off and repeat the above starting procedure. Turn the radial gas controller up high and then bring back down to the original setting of eight percent. Continue to manipulate the radial gas line control in this manner until the torch ignites. This procedure may have to be repeated numerous times before successful ignition is obtained.

After the torch is ignited, remove the NiCr filament with the long piece of wood taking extreme care not to touch the torch or the filament with your bare hands. Adjust the

carrier gas line to the desired setting and turn on the nebulizer power. Ensure that a mist is being created and that the carrier gas is carrying the precursor out of the end of the tube. Next, place the precursor delivery tube in the top of the plasma torch. This last step must be done slowly because the carrier gas is argon which will become ionized upon entering the torch. This will change the state of the plasma region and sometimes will result in quenching the system. If this occurs, repeat the entire ignition procedure.

Once successful starting of the system is achieved, check the voltage and current readings of the meters on the control panel. Typical settings are demonstrated in Table II.

Slide the substrate assembly into its position beneath the plasma torch. Take care to align the substrate beneath the plasma flame in the desired area for deposition.

Table II. Typical Voltage and Current Settings

RF Power	25%
DC Plate Voltage	4.7kv
Grid Amps	0.12A
Plate Amps	1.6A

7. Shutting Down the System

When deposition is complete, remove the substrate assembly from beneath the plasma torch. Remove the substrate and place it in a sample case or out of the way of the entire system. Turn the Rf power dial down to zero slowly and wait for the power readings to

reach a minimum before turning the RF Power button off. Because the controller for the RF generator is slow to react, this will avoid a surge in power when the machine is started again.[6] Turn the filament power button off, but leave the coolant water running for at least five minutes. Turn the nebulizer off. Turn the argon gas lines off at the flow controller and then turn the argon tank off. When the proper time has elapsed, turn the coolant water off.

F. Deposition on Glass Slides

Three types of substrates were used for the atmospheric pressure depositions. Film was deposited on microscope glass slides (soda lime silicate), an aluminum rod, and a cylindrical glass tube. Table III demonstrates the deposition parameters for a forty five minute deposition run where SiO_2 was deposited on a glass slide.

Table III. Deposition Parameters – Glass Slide

RF Power	25%
DC Plate Voltage	4.7K
Grid Amps	0.12
Plate Amps	1.6
Radial Gas Flow	8%
Axial Gas Flow	4%
Swirl Gas Flow	6%
Carrier Gas Flow	5%
Nebulizer Power	100% down to 20%

An examination of the table reveals nebulizer power settings ranging from 100% down to 20%. The mixture is not homogenous and some settling occurs because of the fact that silicon dioxide doesn't actually dissolve in water. Therefore, as the amount of precursor

decreases, the concentration of silicon dioxide increases. This increase in concentration causes a continual increase in loading of the plasma torch. To avoid quenching the torch the nebulizer power is periodically turned down.

This experiment was a forty five minute run with the substrate a distance of 14.6cm from the bottom of the plasma torch. The precursor solution concentration was 20g/liter.

G. Deposition on Aluminum Rod

Table IV demonstrates the run parameters for the first deposition of silicon dioxide on the surface of a 1/8 inch diameter aluminum rod. The target material used for this run was fumed silicon dioxide (SiO_2) with a 7nm particle size. A solution of 1 gram SiO_2 was mixed with 100ml of de-ionized H_2O (10g/liter). The aluminum rod was cleaned with isopropyl alcohol first, acetone next, and then with de-ionized water. The coating was deposited on the outside of this rod with its translational position fixed. The rod was manually rotated three times during the run in an attempt to form a uniform coating around the rod. Because of the danger of arcing, the distance from the substrate to the bottom of the torch was increased to 18.73cm.

Table IV. Deposition Parameters – Aluminum Rod

RF Power	25%
DC Plate Voltage	4.7K
Grid Amps	0.12
Plate Amps	1.6
Radial Gas Flow	8%
Axial Gas Flow	4%
Swirl Gas Flow	6%
Carrier Gas Flow	5%
Nebulizer Power	40%

1. After Sanding the Aluminum Rod

As is shown in the results and discussion section, the surface of the aluminum rod before deposition was very rough. Therefore, the first step in substrate preparation for this run involved smoothing its surface. This was accomplished by wet sanding the rod with a 600 grit automotive sand paper. Next the substrate was cleaned thoroughly with isopropyl alcohol and then with acetone to remove any contamination and then allowed to dry. The rod was then thoroughly washed, first with tap water and then with de-ionized H_2O. In an attempt to evenly distribute the coating around the rod, it was rotated three times by hand during the run. The deposition time for each turn was fifteen minutes for a total of 45 minutes for the entire run. The distance (d) from the substrate to the bottom of the torch was 18.73cm. Table 1 demonstrates the run parameters for this deposition. A solution of 10g/liter was used.

Table V. Deposition Parameters – Aluminum Rod #2

RF Power	20%
DC Plate Voltage	4.3K
Grid Amps	0.11
Plate Amps	1.8
Radial Gas Flow	8%
Axial Gas Flow	4%
Swirl Gas Flow	6%
Carrier Gas Flow	5%
Nebulizer Power	40%

H. Deposition on Glass Tube

The substrate used in this experiment was a one inch diameter glass tube four foot in length. This tube was provided by Osram Sylvania and is used in the manufacture of

fluorescent light bulbs. The coating was deposited on the outside of this tube with its translational position fixed. The tube was rotated three times manually in an attempt to form a uniform coating around the tube. A metal rod was inserted inside the tube so that it could be manipulated during the run without touching the hot glass. The deposition parameters for this run are noted in Table VI. The distance d was 11.59cm and a precursor solution of 10g/liter was used. This was a forty five minute run.

Table VI. Deposition Parameters – Glass Tube

RF Power	20%
DC Plate Voltage	4.3K
Grid Amps	0.11
Plate Amps	1.8
Radial Gas Flow	8%
Axial Gas Flow	4%
Swirl Gas Flow	6%
Carrier Gas Flow	5%
Nebulizer Power	40%

I. Analysis

Thin films deposited with the atmospheric system were analyzed with scanning electron microscopy (SEM) and also with energy dispersive spectroscopy (EDS).

1. SEM

The thin films deposited with this system are in the nanometer range in thickness and are not visible to the naked eye. Therefore, a scanning electron microscope is necessary to analyze these films. SEM's are made up of a column which houses an electron gun, lenses, a scanning coil, and various control devices. At the bottom of the column is a sample chamber with a motorized stage to insert and remove samples. Because an electron beam is extremely unstable it cannot be generated and maintained in a gas filled environment.[8] This results in the necessity to operate this system in a vacuum.

A beam of electrons is generated by the electron gun at the top of the column and directed to the sample.[9] An electro- magnetic field is created by the scan coils deflecting the beam in a controlled pattern. This pattern of deflection is then displayed as an image on a cathode ray tube.

a. Sample Preparation

The coatings for this study are deposited on glass slides, cylindrical glass tubing, and cylindrical aluminum rods. The samples analyzed are SiO_2 and therefore are not conductive. Therefore, these samples have to be coated with a conductive material so that the electrons in the SEM have an electrical path to follow. This conductive coating is applied in a small sputter chamber where the samples are coated with a gold palladium film. This film consists of 70 % Au and 30 % Pd.

The glass samples have to be broken so as to obtain a small enough piece to fit on the sample holder. A sample is obtained and glued to the surface of the holder and placed in a drying oven for five minutes. A piece of the sample is glued parallel to the holder so as to obtain a top view and a piece is also glued perpendicular to the holder to obtain a cross sectional view. The top view can be used to examine the topography of the film and a comparison of large and small particles can be made. The particle size can also be determined with the top view. The cross sectional view can be used to determine the thickness of the film.

The cylindrical aluminum rod samples are merely cut to size and glued to the substrate holder. After drying in the oven, all samples are coated with AuPd in the small sputter chamber and are then ready for examination in the SEM.

2. EDS

Energy dispersive spectroscopy was also used to analyze the deposited films. EDS is used to test the elemental composition of a specimen that is being imaged in a SEM.[10] When samples in a SEM are bombarded with an electron beam, electrons are emitted from the atoms that make up the surface of the sample. When electrons from higher shells fill the resulting vacancies, x-rays are emitted. Each element emits x-rays that have identifiable energy characteristics. An EDS detector evaluates the quantity of x-rays in relation to their energy. A spectrum is then produced displaying the elements present in the specimen.

Samples are prepared in the same manner as those being prepared for SEM analysis. In this study EDS analysis was completed immediately following SEM analysis.

III RESULTS AND DISCUSSION – ATMOSPHERIC PRESSURE FILMS

SEM analysis of the deposited coatings revealed spherical particles with sizes ranging from one micrometer to less than fifty nanometers in diameter. The majority of the substrates were coated with small particles with a scattering of large particles throughout. The small particles are mainly spherical in shape while the large particles appeared either spherical or in the shape of a snowflake. These snowflake shaped particles appear to be small particles clustered together which is known as agglomeration.

EDS analysis demonstrated the elemental content of the deposited films. Analysis of the substrates with and without a coating was performed for comparison purposes.

A. Glass Slide Substrate

Figure III-1 demonstrates SEM analysis (top view) of SiO_2 deposited on a soda lime silicate glass slide. Table III on page 21 shows the deposition parameters for this run. This was a forty five minute run with the substrate a distance of 14.6cm from the bottom of the torch. An examination of the micrograph reveals that the majority of the small particles are in the range of 50 to 100nm in diameter. The large particles on the substrate are on the order of one micrometer in diameter. There are some areas where there are clumps of large and small particles demonstrating a film that is not very homogenous. This is probably caused by the fact that SiO_2 does not actually dissolve in water but due to the small 7nm particle size of the precursor it is suspended in the water. Larger quantities could be suspended in one area of the liquid as opposed to another area. The slide does show some areas that are fairly homogenous.

Figure III-2 shows the clumping problem from a different angle. The gray area to the left is the substrate showing the edge of the glass going diagonally across the micrograph. The parallel lines in the gray area are fracture lines. This is the side view of the substrate and demonstrates thicknesses from between 125nm to about 250nm. This view

demonstrates the agglomeration that is occurring during deposition. This view also demonstrates the roughness of the deposited film.

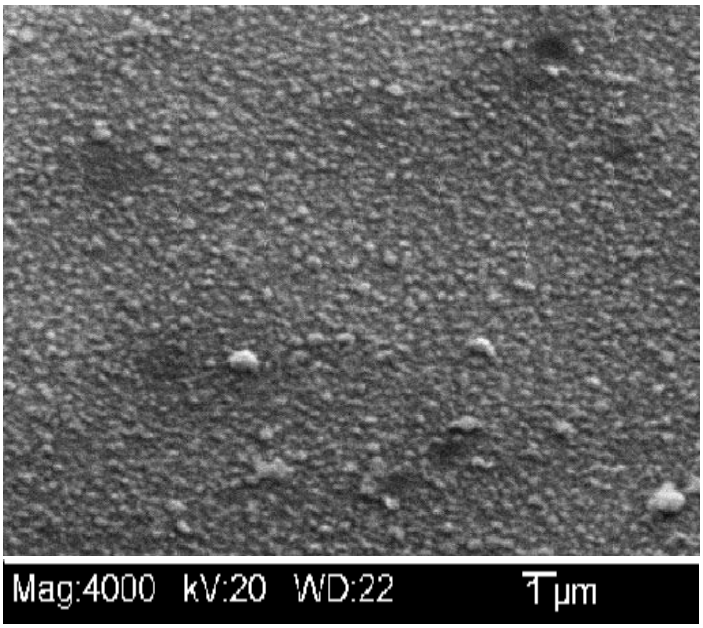

Figure III-1. Top View - Glass Slide With SiO_2

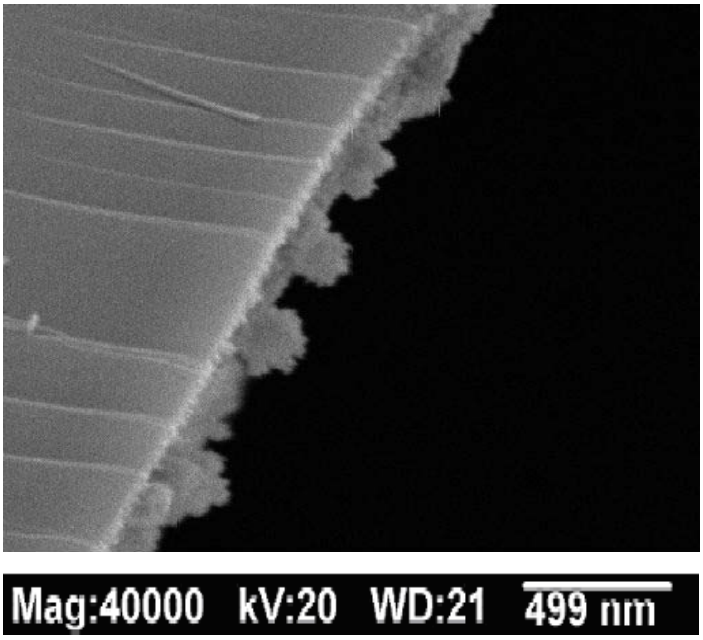

Figure III-2. Side View – Glass Slide With SiO_2

Figure III-3 demonstrates EDS analysis of the thin film on the glass slide. The presence of silicon and oxygen is demonstrated, but because silicon dioxide was deposited on silicon, these results are inconclusive.

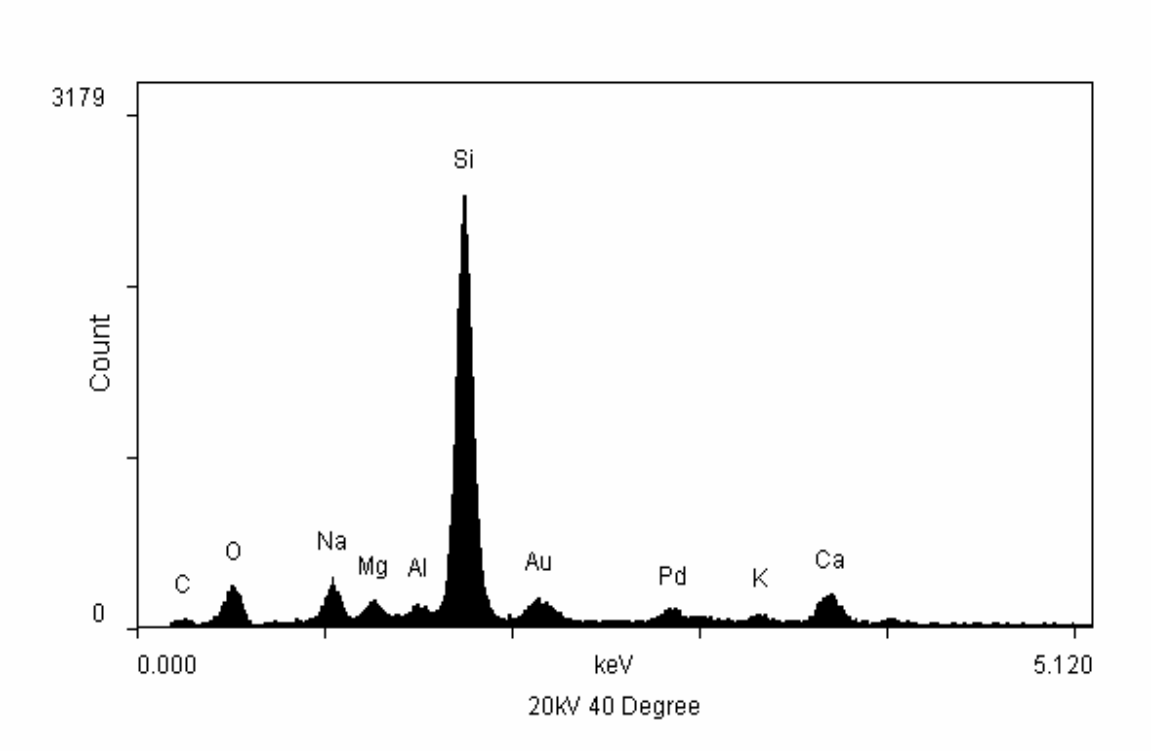

Figure III-3. EDS Analysis of Coated Glass Slide

B. Aluminum Rod Substrate

Figure III-4 demonstrates SEM analysis (top view) of SiO_2 deposited on a 1/8 inch diameter aluminum rod. Refer to Table IV on page 22 for the deposition parameters. The distance d was 18.73cm and a solution of 10g/liter of precursor was used.

The coated sample was cut into three segments and three random surface points around the aluminum rod were examined with SEM at 40,000x magnification. Figure III-4 demonstrates the results of the first surface point examined.

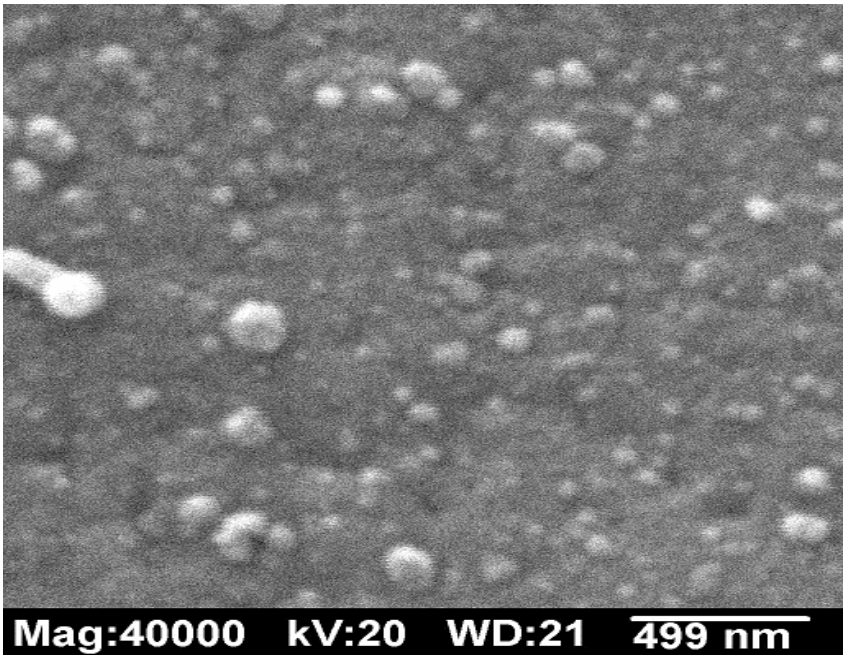

Figure III-4. Top View – Aluminum Rod Surface Point #1

The next surface point (#2) examined is shown in Figure III-5. A comparison of the first two points shows a mixture of large and small sized particles evenly distributed about the examination area. Under such great magnification, the substrate appears to be quite rough. This would indicate that the substrate for future runs should be smoothed with a fine grit sandpaper or very fine steel wool. Point #2 seems to be denser and contains more small particles than point #1. The micrographs at both points one and two demonstrate films that are not continuous.

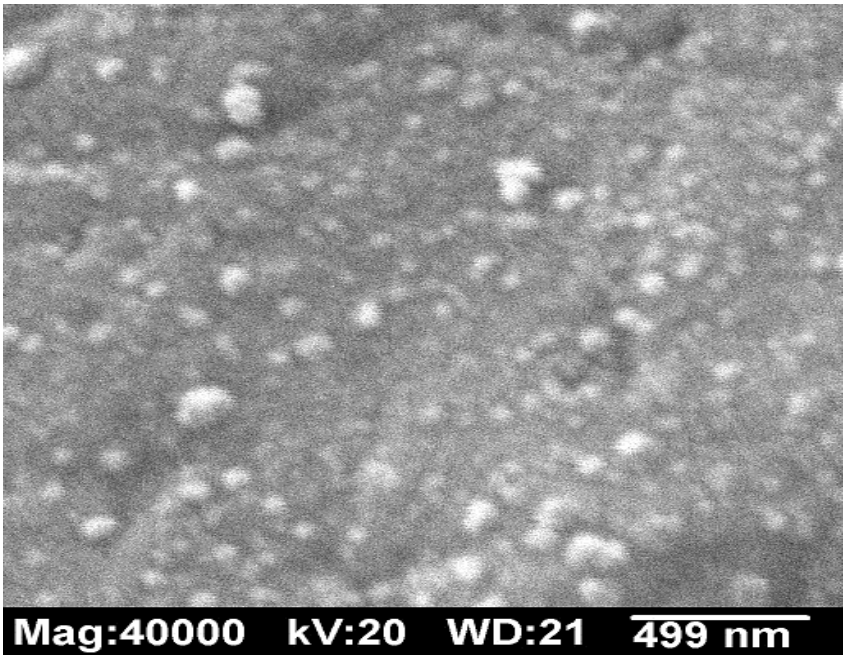

Figure III-5. Top View – Aluminum Rod Surface Point #2

The results for surface point #3 are shown in Figure III-6. Some small and large particles can be detected, but these are fewer in number than the first two points. Also, this section of the substrate is very rough confirming the need for better substrate preparation.

For reference purposes and to show that a film was actually deposited, the substrate was examined with no coating. Figure III-7 demonstrates the uncoated surface of the aluminum rod. Although the specimen was thoroughly cleaned with alcohol and acetone, a few small particles can be detected. These are probably due to contamination from particles in the air settling on the substrate. This rod was never exposed to silicon dioxide which will be demonstrated with EDS analysis.

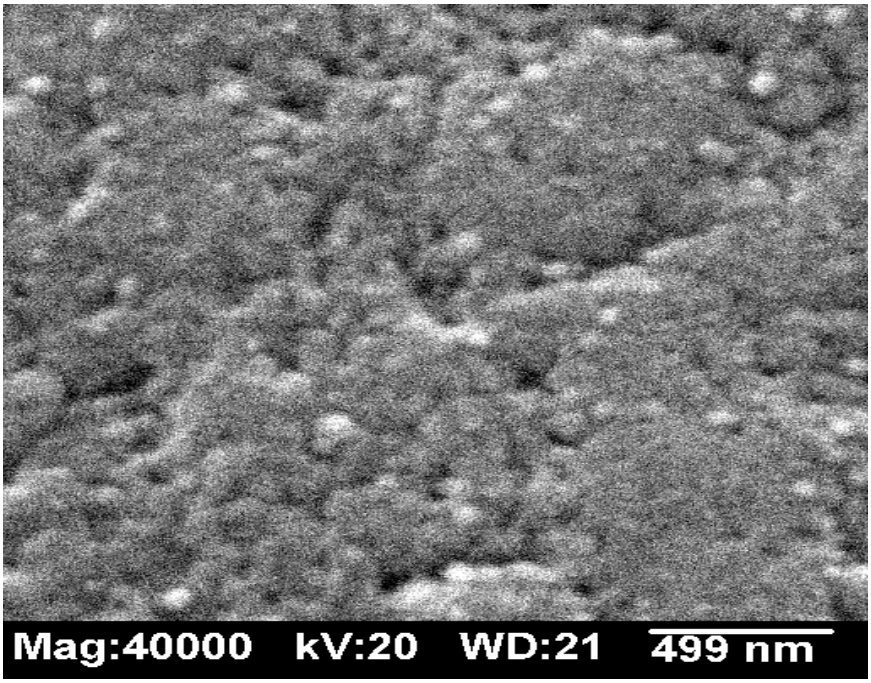

Figure III-6. Top View – Aluminum Rod Surface Point #3

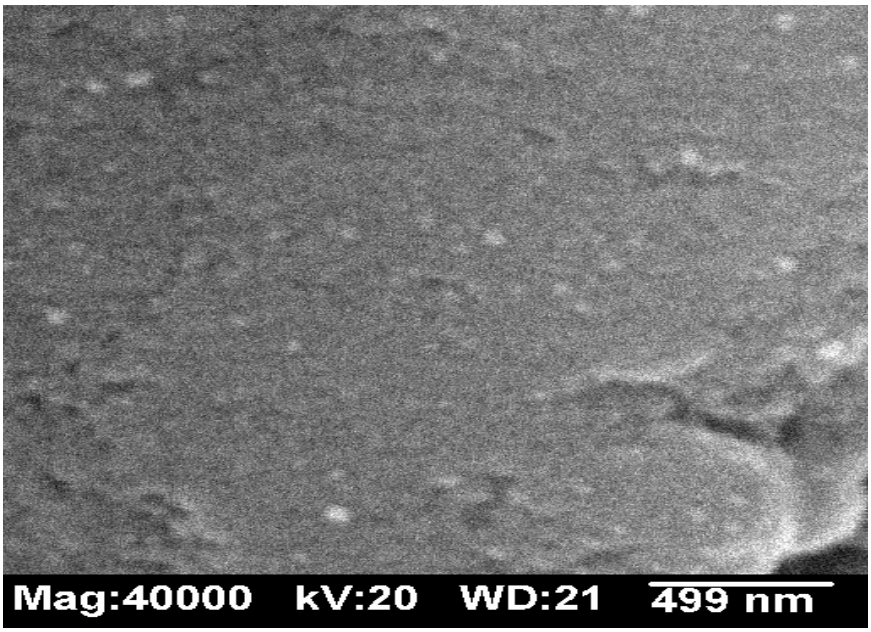

Figure III-7. Top View – Aluminum Rod Without Coating

A sample of the uncoated surface was examined with EDS and the results are shown in Figure III-8. The results show the presence of aluminum, gold, and palladium. The presence of gold and palladium is a result of sample preparation for SEM and EDS.

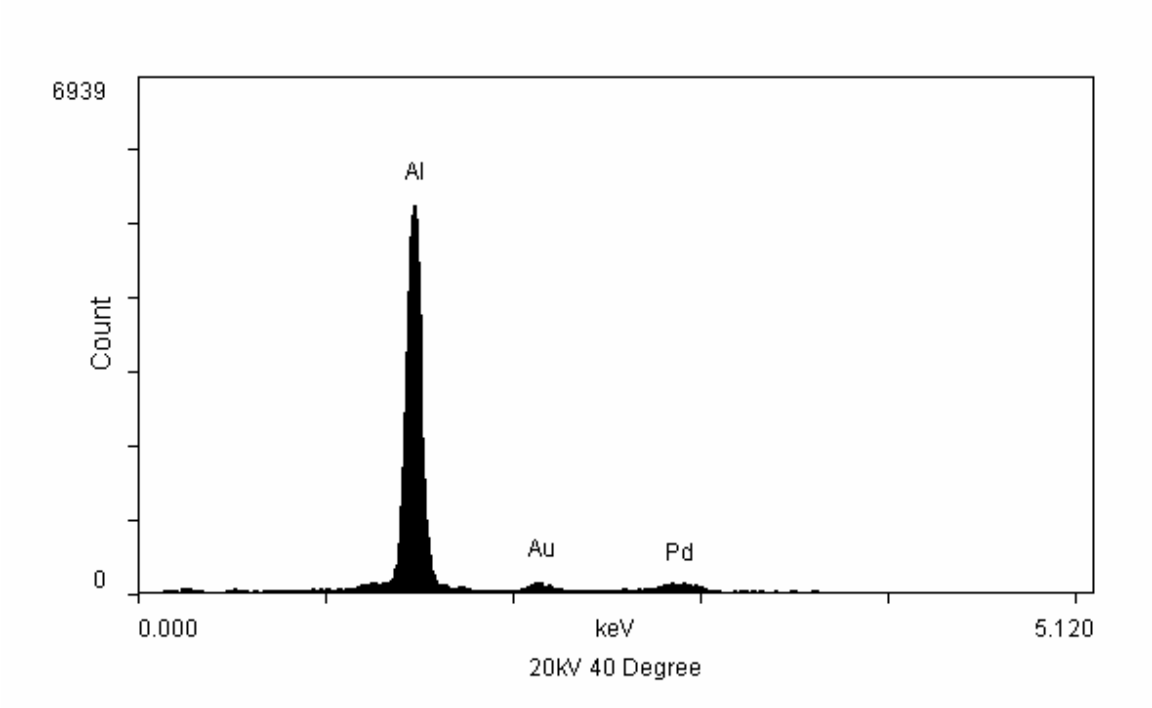

Figure III-8. EDS Analysis - Uncoated Aluminum Rod

Figure III-9 shows the results of EDS testing of the coated surface. As can be seen, silicon and oxygen are now present confirming that a SiO_2 coating was actually deposited. The presence of magnesium is contamination and is a result of using the same nalgene tubing that was used in previous studies.

1. After Sanding the Aluminum Rod.

Figure III-10 demonstrates SEM analysis of a random area on the aluminum rod. Large and small particles of SiO_2 can be observed. The striations on the image are a result of preparing the surface with the automotive sandpaper. It is apparent that the 600 grit paper

was too rough and the desired smoothness was not achieved. Actually, the opposite was achieved. In future runs, a polish should be tried instead of the sandpaper. The coating appeared very similar on two other surface points around the rod.

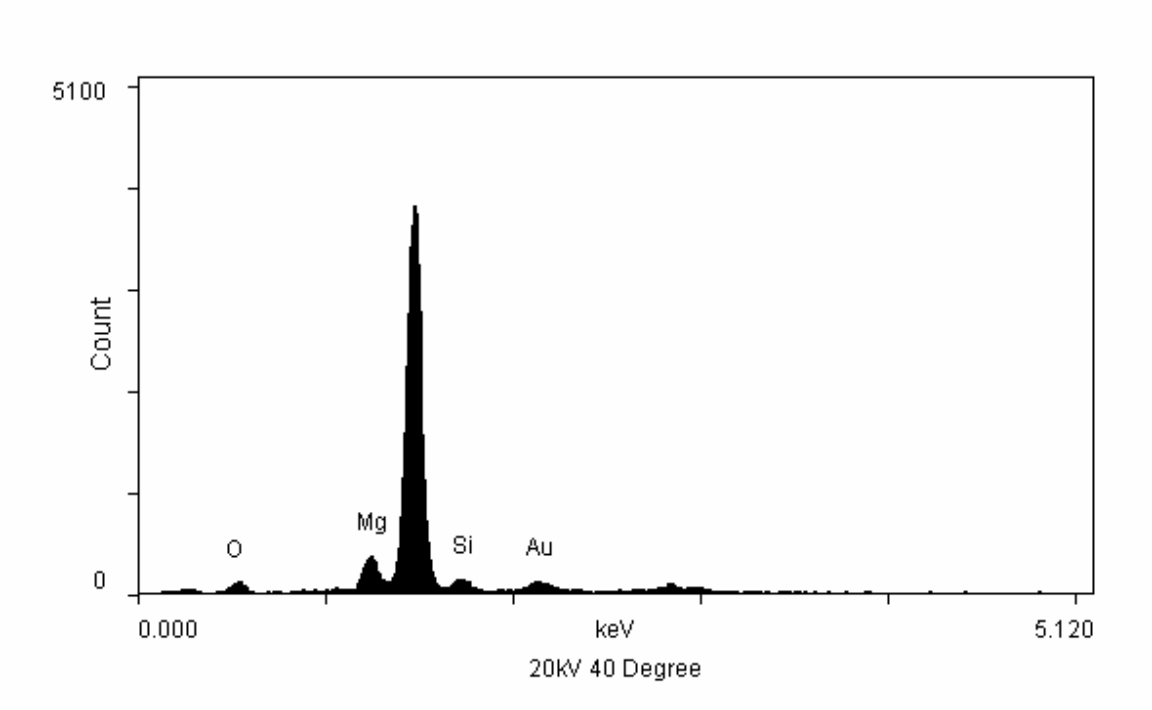

Figure III-9. EDS Analysis - Coated Aluminum Rod

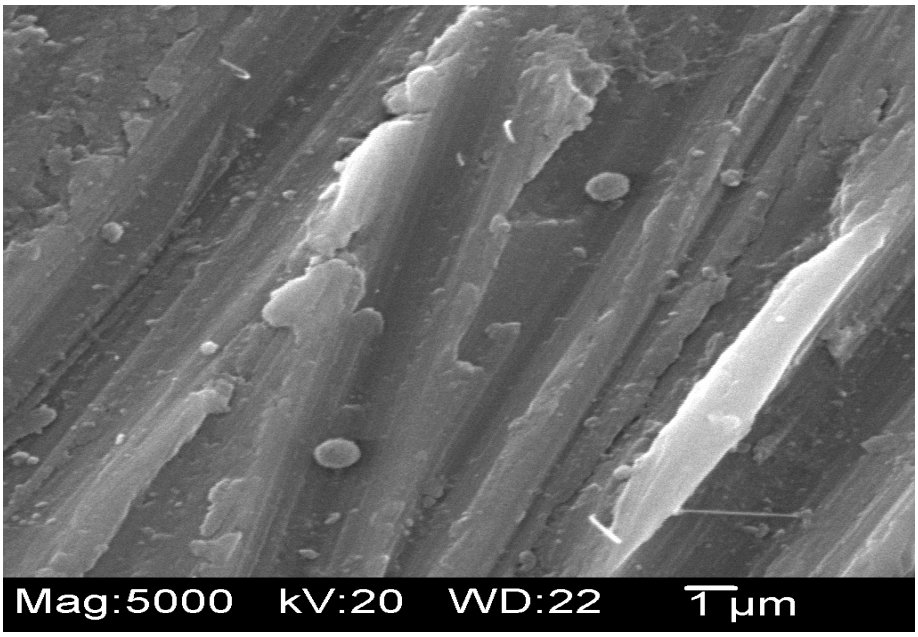

Figure III-10. Surface of Sanded Aluminum Rod

C. Glass Tube Substrate

Table VI on page 24 lists the deposition parameters for a forty five minute run using a precursor solution concentration of 10g/liter. Figure III-11 demonstrates the SEM analysis of a random point on the surface of the glass tube. It shows the presence of a few large and small particles, but it also demonstrates that a continuous thin film is not present. The larger particles are approximately 0.8μm to 1 μm in diameter. The smaller particles range from 0.3 to 0.5 μm in diameter.

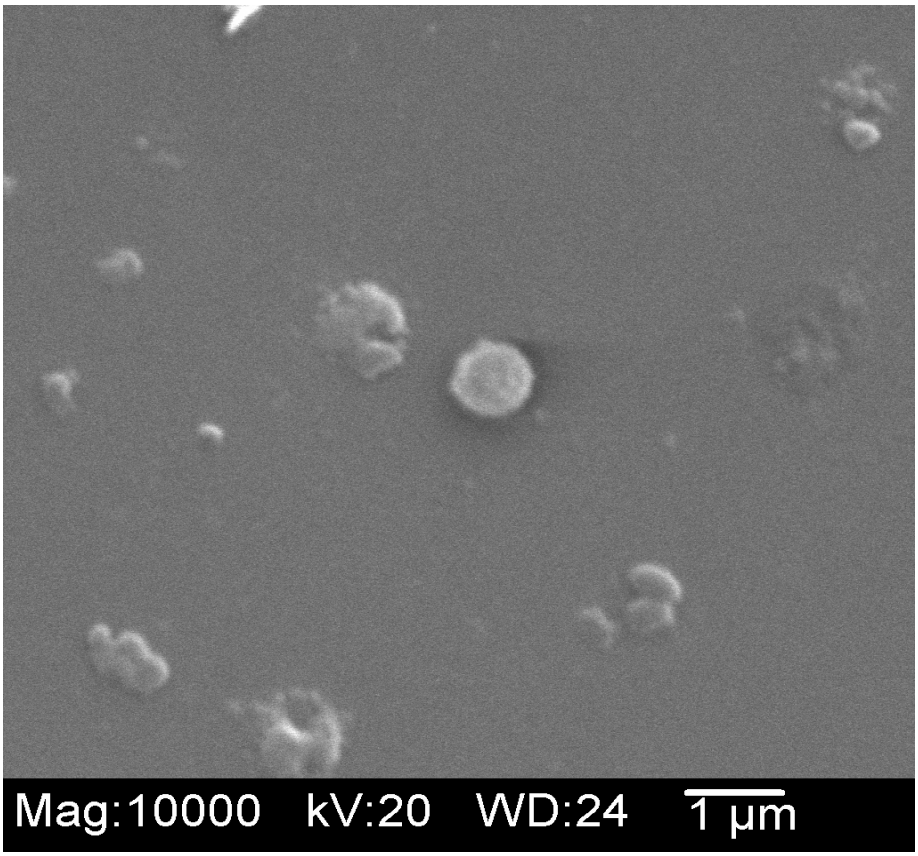

Figure III-11. Surface of Glass Tube

Figure III-12 shows the SEM analysis of the edge of the substrate. The gray area to the left is the substrate. The area to the right of the edge shows a few small particles and also demonstrates the absence of a continuous coating.

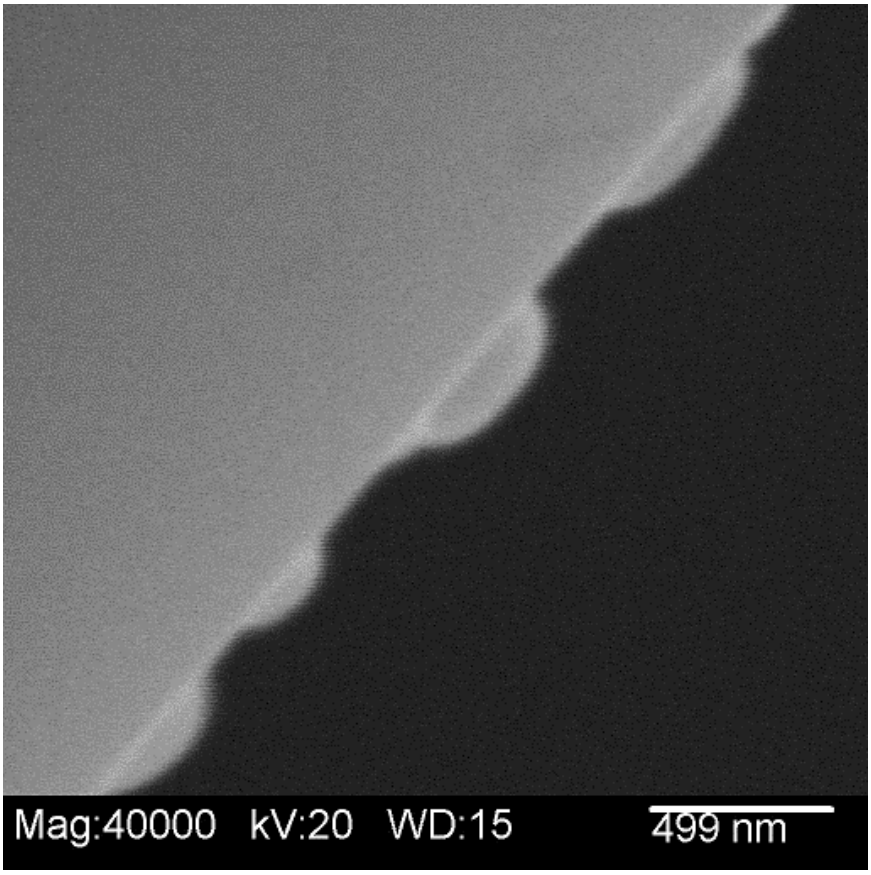

Figure III-12. Edge of Glass Tube

Figure III-13 shows the EDS analysis of a single particle on the surface of the substrate. It shows the presence of silicon and oxygen, and also the AuPd preparation coating. It also shows Ca and Na which are part of the chemical makeup of the substrate. The problem with this analysis is that silicon containing material is deposited on silicon containing material. Also present is the Mg contamination from the nalgene tubing.

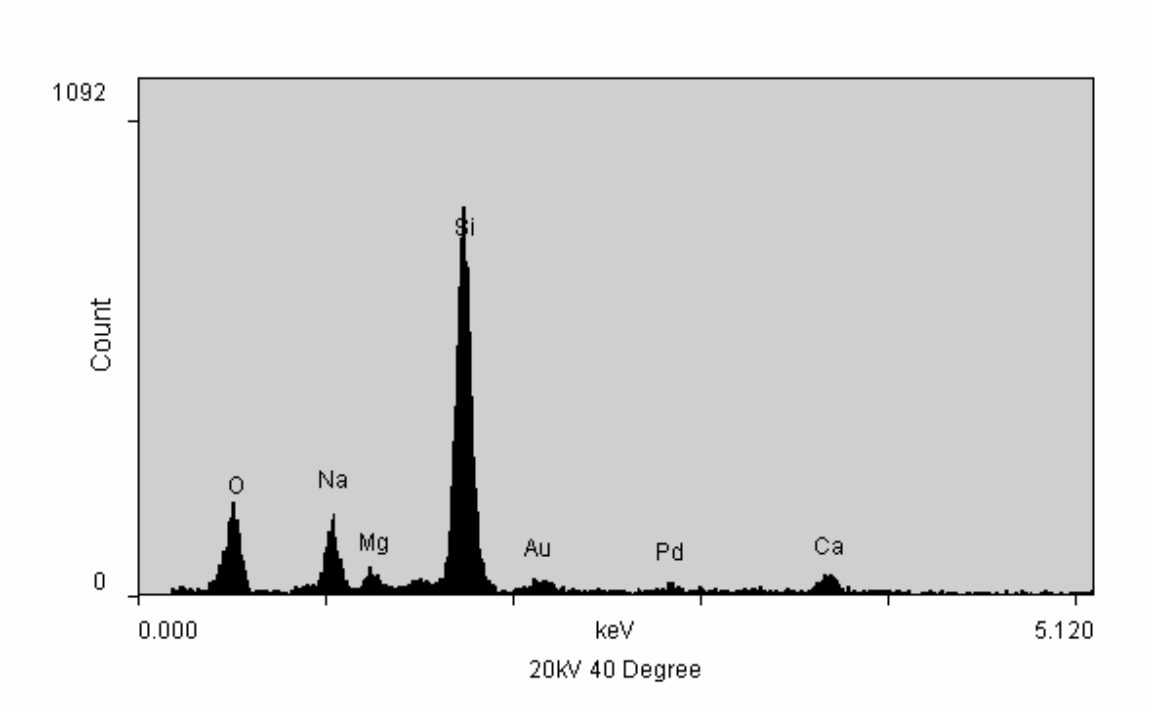

Figure III-13. EDS Analysis – Surface of Glass Tube with Coating

Figure III-14 shows the EDS analysis of the surface of the glass tube without a coating. A comparison of the two graphs shows that the silicon content is almost the same, but the oxygen content for the particle is higher than the surface of the glass. This would tend to confirm that the particle on the surface of the tube is indeed SiO_2, but because silicon dioxide was deposited on silicon, these results are inconclusive.

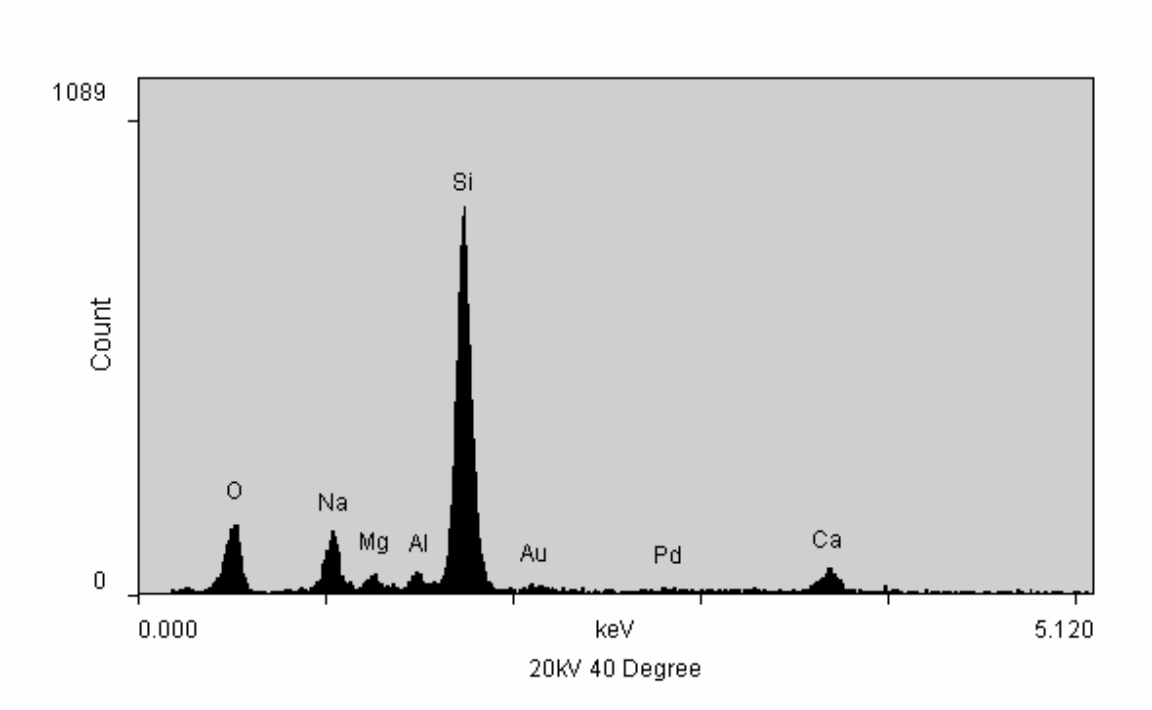

Figure III-14. EDS Analysis – Surface of Glass Tube without Coating

IV EXPERIMENTAL PROCEDURE – VACUUM SYSTEM

The RF plasma aerosol mist thin film deposition system at Alfred University has been traditionally used to deposit thin film coatings on the exterior of substrates under atmospheric pressure conditions. Because of an interest in depositing thin films on the inside of glass tubes, a vacuum deposition system needed to be developed. This vacuum system would involve forming a vacuum inside a glass tube, generating glow discharge plasma in this vacuum, and then introducing a precursor. The precursor would then be vaporized by the plasma and subsequently condense onto the interior surface of the tube.

Some of the same equipment used in the atmospheric system could be used in the new vacuum system. The RF generator, the nebulizer, the gas flow controller, and the deposition chamber could be utilized with little or no modifications. The plasma torch would not be adequate. Therefore, an alternative method of forming plasma would have to be developed.

A. Vacuum Deposition System Design

The system depicted in Figure IV-1 was the accepted design for the new RF plasma vacuum thin film deposition system. An open air inductive coil would have to be developed that would provide power in the form of an electro-magnetic field. The glass tube would have to fit inside of the coil so that the energy from the electro-magnetic field could disassociate the plasma gas. Fittings had to be found or manufactured that would connect the plasma gas line, the precursor carrier line, and the vacuum pump line to the ends of the glass tube. These fittings would have to form a tight seal with the glass tube so that a vacuum could be formed inside the system.

The plasma gas would be delivered to the system from a gas tank through the Tafa gas flow controller. The precursor material would be delivered to the glass tube from the mist

chamber of the DeVilbiss nebulizer. The precursor carrier gas would be delivered to the nebulizer mist chamber from the Tafa gas flow controller. Because the nebulizer mist chamber would have to be open to the vacuum system, a way of sealing the plastic precursor cup and lid would have to be developed. Also, because the plasma and carrier gas lines would be open to the vacuum system, modifications to the gas flow controller and gas line fittings would have to be performed. The Tafa gas flow controller was designed to operate under the pressure provided by gas tanks, not under the pressure provided by a mechanical vacuum pump. Therefore, its performance in this new vacuum system was in question.

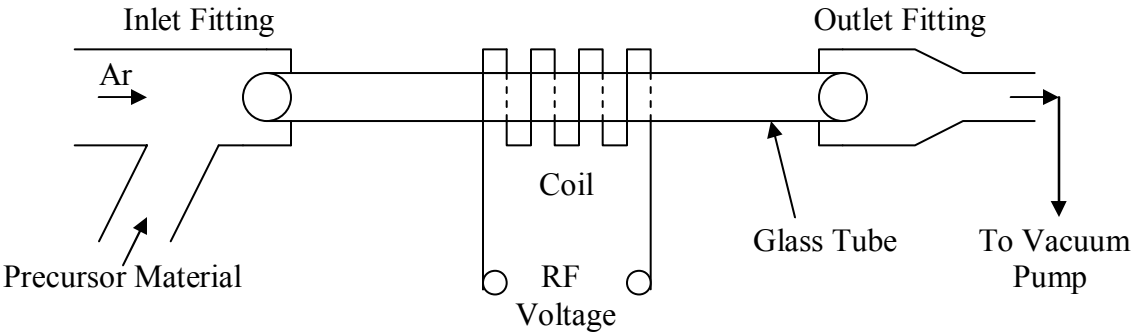

Figure IV-1. Vacuum System Design

1. Glass Tubes

The glass tubes used in this experiment were obtained from Osram Sylvania. These tubes are 1.23m or four feet in length and have an outer diameter of 2.54cm. The ends of the tubes taper down to a lip and it was observed that this lip accommodates an o-ring. The glass used in the manufacture of these tubes has a much higher melting point than the soda lime silicate glass used as substrates in the atmospheric system. The melting point of these tubes is 1100º C and the glass becomes pliable at a temperature of approximately 700º C.

Figure IV-2 demonstrates the end of one off the glass tubes complete with an o-ring attached.

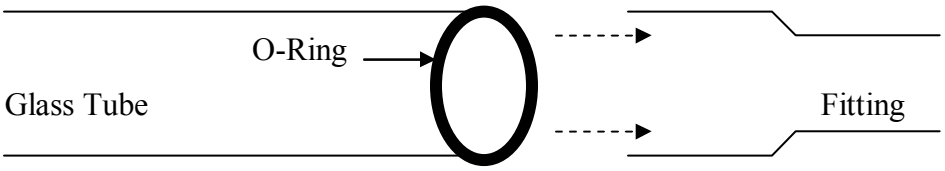

Figure IV-2. Glass Tube with O-ring

2. Plasma Gas

The plasma gas used in this experiment is regular grade argon (Ar) delivered from free standing gas tanks. Argon was chosen because it requires less energy to disassociate it's atoms than other plasma gases. Also, argon is a very inert gas and therefore does not react with the precursor target material.

Nitrogen, on the other hand, requires much more energy for disassociation of atoms to form plasma. Nitrogen may react with precursors to form nitrides such as aluminum nitride, a quality that is not desired with this system.

3. Gas Flow Controller

The Tafa gas flow controller was modified to be used in the new vacuum system. The same carrier gas line used in the atmospheric system can be used in the vacuum system, but because it utilized soft plastic tubing, this line would not maintain its integrity in a vacuum. Therefore, it would have to be redesigned.

The plasma gas line was made of hard plastic tubing and it was believed that this tubing would maintain its integrity in a vacuum system. Therefore, only the fitting which attaches to the intake of the glass tube would have to be redesigned.

a. Carrier Gas Line

The soft plastic carrier gas line was replaced with a hard plastic line. The fitting that attaches to the nebulizer mist chamber had to be redesigned to work in a pressurized system. It was observed that a standard three quarter inch CPVC fitting would fit very tightly over the plastic lid intake to the mist chamber. After this observation, it was just a matter of obtaining standard fittings that would adapt to the gas line fittings. Figure IV-3 demonstrates the carrier gas flow fitting design.

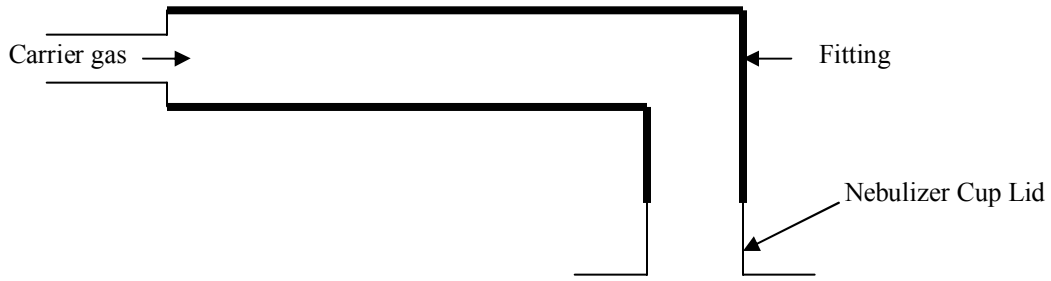

Figure IV-3. Carrier Gas Line Fitting

b. Plasma Gas Line

The radial gas line used in the atmospheric system was redesigned to be used as the plasma gas line for the new vacuum system. This line is made of hard plastic so the only modification necessary was to the fitting. This fitting had to be redesigned to attach to the glass tube inlet fitting. This was just a matter of finding the correct standard fittings

that would work. Figure IV-4 demonstrates the carrier gas flow fitting design as well as the glass tube inlet fitting design. The glass tube inlet fitting was designed such that the plasma gas line and the carrier gas line come together at the inlet to the glass tube. Because the glass tube has an outer diameter of one inch, a standard one inch copper fitting could be used in conjunction with an o-ring to form a tight seal between the fitting and the glass tube. As Figure IV-4 illustratrates, the chosen fitting was a one inch to three quarter inch reduction fitting.

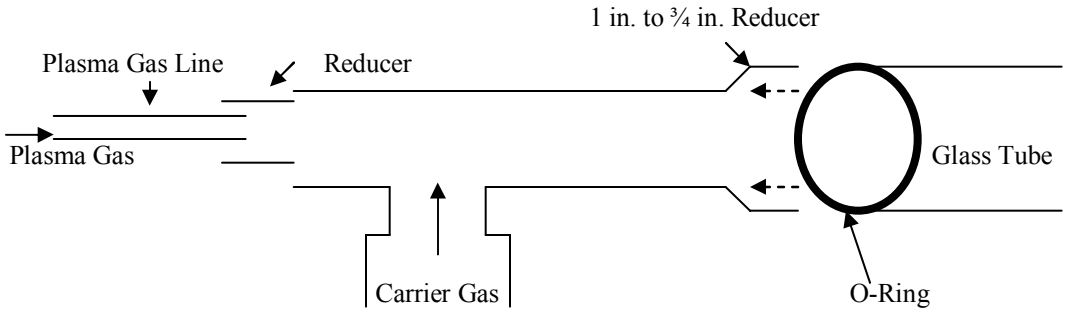

Figure IV-4. Plasma Gas Line Fitting

4. Vacuum Line and Fittings

A Duo Seal model number 1402 mechanical vacuum pump was available and it was decided to use this in the newly designed system. The pressure obtained by this pump as measured in another system was in the range of twenty millitorr. The available vacuum line coming from the pump was utilized and the vacuum line coming from the outlet of the glass tube had to be designed so that it would adapt to the existing line. This was just a matter of finding the correct reducing fittings that adapted the glass tube outlet fitting to one half inch copper water line. This one half inch copper water line fit inside the existing vacuum line and clamps were used to form a tight seal.

5. System Test #1

At this point a test of the vacuum system was performed to determine if a vacuum could be produced inside the system without the nebulizer connected and without RF power. The precursor inlet was capped and the system was assembled. The inlet and outlet fittings were connected using o-rings. Due to the weight of the metal fitting assemblies, they had to be supported. This was accomplished by using metal stands that were available. When the vacuum pump was turned on the test revealed no apparent vacuum leaks.

6. Coil Design

An open air inductive coil had to be designed that would accommodate the size of the glass tube through its center. This coil would need to have fittings that would adapt to the radio frequency generator. Because the fittings for the plasma torch serve as both water cooling lines and as electrical contacts, the new coil would have to have the same qualities. Therefore, the newly designed coil would have to be made of some type of conductive water line. Also, because this coil would replace the plasma torch, it had to be impedance matched with the generator. The inductance of the plasma torch was measured at 0.9μH. The inductance of a coil is given as:

$$L\ (\mu H) = (\ 0.04\ \mu\ r^2\ N^2\ )\ /\ l$$

where: $\mu = 1$ (air)
r = radius of the coil
N = # of turns
l = length of the coil

The inductance of the coil inside the plasma torch was calculated to be 3.5 μH.

Because of the complexity of the design of this new coil, it was decided to find a commercial company to manufacture one using the measured value of inductance. Figure IV-5 and Figure IV-6 on the next page were sent to Mr. Eric Bouchard, the

director of production for Tekna Systèmes Plasma, a firm in Montreal, Canada. The coil was manufactured and shipped within a week. The inductance of the new coil was 0.5μH. The loading that occurs when the glass tube is placed in the core of the inductor should alter this value of inductance. When received, the coil was installed and an inspection of the coolant system revealed no leaks. Figure IV-7 shows a picture of this coil.

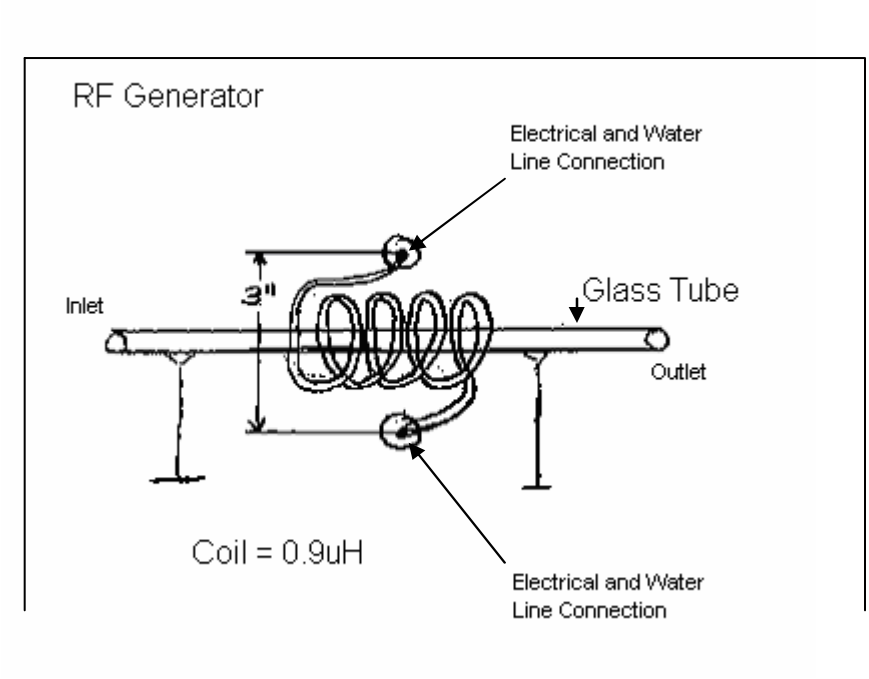

Figure IV-5. RF Generator with Coil Attached – Front View

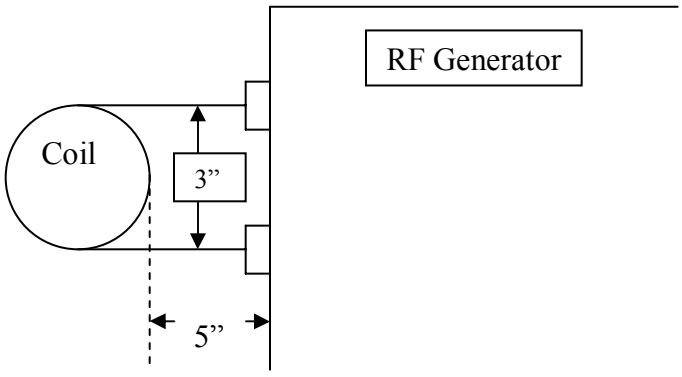

Figure IV-6. RF Generator with Coil Attached – Side View

7. System Test #2

At this point it was decided to test the system without connecting the nebulizer. The purpose of this test was to see if plasma could be generated in the vacuum inside the glass tube. The precursor inlet was capped and the system was assembled. The tube was inserted into the core of the coil and the inlet and outlet fittings were connected using o-rings. The vacuum pump was turned on and allowed to run for five minutes. The coolant water was turned on and then the RF generator was turned on and allowed to warm up for three minutes. The filament power was turned on and when it was warmed up, the RF Power was turned on. The argon gas pressure was set to eighty pounds per square inch and the flow control was set to one percent. The RF power dial was then turned to ten percent. When the argon finally reached the coil area inside the glass tube, the first glow discharge for this system was established and is demonstrated in Figure IV-7.

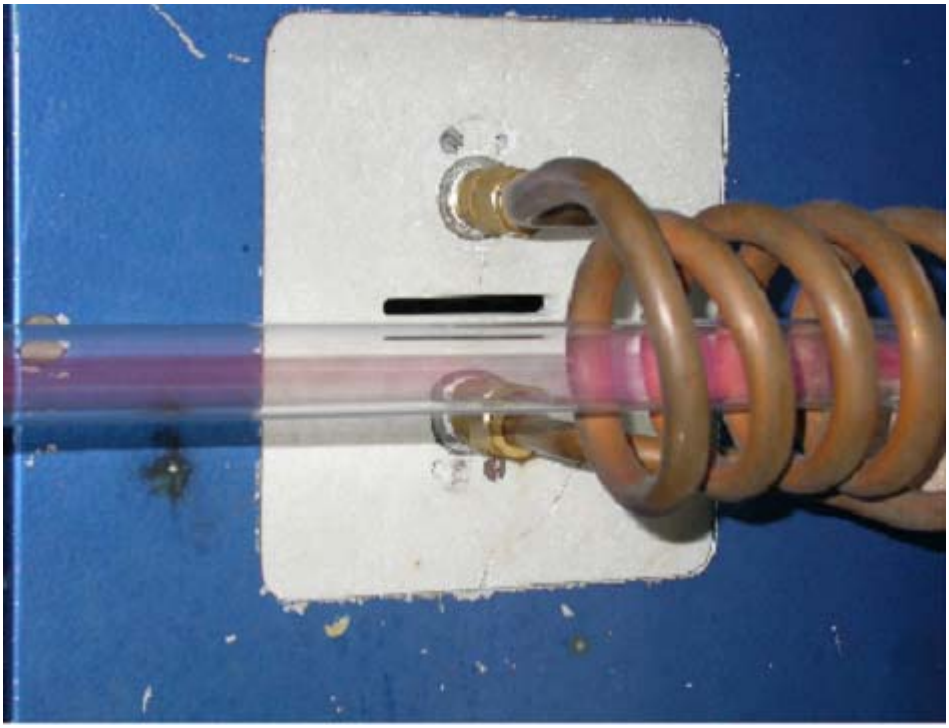

Figure IV-7. First Glow Discharge

8. Gas Flow Rate Optimization

The plasma region in the glass tube did not appear very complete and did not fill the entire tube. To improve this glow discharge region would require optimal settings for gas flow and the best vacuum possible. In an attempt to establish a plasma gas flow rate for the system, different argon tank pressures were experimented with. From this experimentation it was found that a setting of about four pounds per square inch was the optimal setting for the tank. The results of this optimization can be observed in Figure IV-8.

This process also revealed that the valves in the Tafa flow controller were definitely not designed for use in a vacuum. The flow controller for the plasma gas line was turned completely off and the pressure of the vacuum pump still forced argon through the valve.

Figure IV-8. Second Glow Discharge

9. Temperature Profile

At this point it was decided to optimize the power setting. This would involve finding a maximum power setting that would not result in the failure of the glass tube. The heat generated by the plasma increases with power setting increases. The manufacturer of the glass tubes provided the chemical and physical properties of these tubes. These specifications can be found in the appendix on page 103. The melting point of the glass used in the manufacture of the tubes was given at 1100º C and the glass becomes pliable at 700º C. Because of the constant pressure provided by the vacuum, it was estimated that the tubes would fail at a temperature less than the pliability temperature.

A thermocouple thermometer was used to measure the heat generated at various RF power settings. This test showed that the highest power setting was 14%. Anything higher resulted in failure of the tubes. The graphical results of this test can be found in the results and discussion section on page 66. Figure IV-9 demonstrates what happened when the RF power dial was raised above 14%. The section of the tube in the coil area holds up for about three seconds under the intense heat from the plasma and then it becomes pliable. At this point the forces from the vacuum cause the tube to fail. One of these failed tubes can be seen in Figure IV-10.

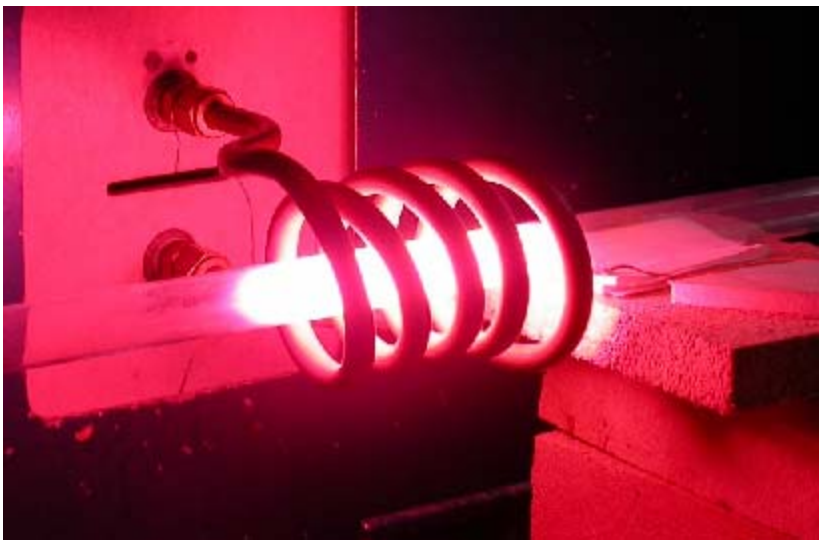

Figure IV-9. Coil Area Plasma

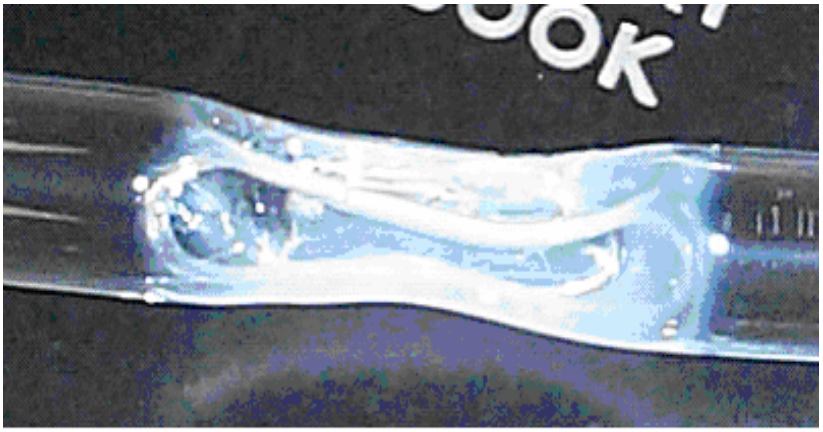

Figure IV-10. Failed Tube

10. Nebulizer Mist Chamber Design

The nebulizer mist chamber was not designed to work in any type of pressurized system and would have to be redesigned. It was desired to use the soft plastic disposable precursor cups that fit inside the mist chamber. This would allow the use of different types of precursor with the same mist chamber and cross contamination would not occur.

The outlet of the mist chamber is the same physical shape as the inlet, so a standard three quarter inch CPVC fitting would work. This fitting was connected to three quarter inch CPVC tubing and connected to the precursor inlet of the glass tube. At this point the entire system was assembled and another system vacuum test was performed.

This vacuum test revealed that the disposable precursor cups were not adequate for use in a vacuum system. They collapsed under the pressure from the vacuum. In an attempt to solve this problem, a series of metal stays was manufactured which conformed to the shape of the interior of the cups. The metal stays ensured the integrity of the disposable cups, but a new weak point was discovered when the system was placed in a vacuum. The disposable plastic lids that fit the disposable plastic cups would not maintain their integrity and failed when a vacuum was produced. After several attempts and several broken lids, the idea of using the disposable plastic cups and lids was abandoned.

At this point it was decided to try using the hard plastic mist chamber without the disposable cups. Instead of filling the mist chamber with water, the precursor would be placed directly into the mist chamber. The mist chamber comes with a hard plastic lid. Several mist chambers were available and two were chosen to be used with the two types of precursor. This would avoid the chance of contamination from using the same chamber for different precursors.

Another system vacuum test revealed a leak between the mist chamber lid and the chamber itself. Therefore work still needed to be done if a strong vacuum was to be established. The problem was solved by adding a thin o-ring between the lid and mist chamber. Another vacuum test revealed no major leaks and a vacuum in the milltorr range was established. Again, the system doesn't contain a vacuum gauge and the vacuum pressure value is estimated from measurements using this pump on another system.

11. System Test #3

At this point, another complete system test was performed. Now the entire system, including the nebulizer mist chamber, was open to the vacuum system. For this test, the mist chamber was filled with just de-ionized water. When the system was fully assembled the vacuum pump was turned on and the usual start up procedure for the RF generator was followed. When the system was energized a plasma region could not be established. An examination of the system revealed that the water in the mist chamber appeared to be bubbling rapidly. This continued for about twenty minutes and then the bubbling effect became less rapid and finally stopped. The outside of the mist chamber was found to be cold to the touch. A test of the nebulizer revealed proper operation. It was believed at this time that the cold mist might be responsible for the inability to establish a plasma region.

12. Liquids in a Vacuum

An investigation into the theory of liquids under pressure revealed why the water in the mist chamber was bubbling. Water mist was escaping as it does during evaporation. In other words, the water in the mist chamber was undergoing a very rapid evaporation. In a vacuum, the atmospheric pressure that keeps water molecules from escaping is changed. In order to adjust to the new pressure, water mist escapes from the water until the pressure between the liquid and air is equalized. This explains the bubbling effect and also why a plasma region could not be established. Water mist was freely entering the inside of the glass tube preventing the formation of plasma.

In addition to the water mist problem, the freezing rate of the water was raised because of the vacuum. When liquids are placed under vacuum pressure, the boiling and freezing temperatures of that liquid are changed.[11] This was confirmed by the experiment. After about thirty minutes ice was forming in the mist chamber. Instead of the normal 32ºF freezing temperature, the water was freezing at room temperature. It was believed that a combination of the cold and the water mist was preventing the formation of plasma in the glass tube.

13. Redesign of Precursor Carrier Tube

In an attempt to address the water mist problem, it was decided to restrict the flow of the precursor carrier tube. A three quarter inch CPVC valve was added to the tubing. This would allow some control over the amount of precursor allowed to enter the plasma region. Another system test showed that a plasma region could now be established inside the glass tube. This system test also demonstrated that the plasma region was not nearly as complete as that produced without the nebulizer chamber connected to the system. It was necessary to set the precursor flow valve so that the smallest possible amount of flow was achieved.

Another problem with the system was that the rapid evaporation experienced during

the first few minutes also caused some of the liquid to enter the glass tube. This would result in loss of the plasma region. The nebulizer was lowered and the precursor delivery tube was changed so that the precursor chamber was about six inches below the level of the glass tube. This effectively solved the problem as was demonstrated by another system test.

This last system test also revealed that much higher power settings have to be used when the nebulizer chamber is open to the vacuum chamber. Previously, a maximum RF power setting of fourteen percent could be achieved without melting the glass tubes. With the nebulizer chamber connected RF power settings as high as thirty to thirty five percent could be used for short periods of time without compromising the integrity of the glass tubes.

Consequently, the higher power settings created another problem. Because of the fact that plasmas are conductive, the higher power settings were causing enough of an increase in current to cause it to arc through the glass tube and into the metal stands that were supporting the tubes. This arcing put a small hole in the glass tubes and caused failure of the vacuum system. These metal stands were on a metal toolbox in the metal deposition chamber which was grounded to the system. This provided a convenient path for the electrical current. This problem was solved by replacing the metal stands with ceramic bricks. Because of the danger of arcing, a great deal of care was taken not to touch the metal fittings while the system was in operation.

14. Deposition Attempt #1

For the first run it was decided to try to deposit silicon dioxide on a small substrate placed inside the glass tube. A small black carbon substrate was chosen for both its availability and its color. The black color would contrast with the white film and the naked eye might detect the presence of a deposit. The complete vacuum deposition procedure was followed. Table VII demonstrates the deposition parameters used for this run.

The carbon substrate was placed in the middle of the tube for the first attempt. When the system was energized it was noticed that the carbon substrate began to glow red hot. The system was shut down and the position of the substrate was changed to midway between the center of the tube and the vacuum end.

A thirty minute run produced certain results. An examination of the carbon substrate demonstrated a white deposit scattered about the substrate. This demonstrated that the precursor was indeed entering the plasma region and that it was vaporized by the plasma. The vapor then condensed onto the carbon substrate. SEM and EDS analyses confirmed the presence of a silicon dioxide deposit on the substrate as is shown in the results and discussion section on page 67.

Table VII. Deposition Parameters – Carbon Substrate

RF Power	25%
DC Plate Voltage	8.5K
Grid Amps	0.44
Plate Amps	1.5
Carrier Gas Flow	Less Than 5%
Nebulizer Power	70%
SiO_2 Concentration	5 grams per liter of de-ionized H_2O

15. Deposition Attempt #2

The second attempt at deposition just involved the interior of the glass tube as a substrate. The same deposition parameters as outlined in Table VII were used. It was decided to turn the plasma gas line completely off during this run. This was an attempt to determine if the line was needed. A plasma region was established with just the carrier gas line connected.

This thirty minute run also produced certain results. A film appeared to be present on the interior of the glass tube near its outlet. SEM and EDS analyses confirmed the presence of a silicon dioxide deposit on the substrate as is shown in the results and discussion section on page 70.

16. System Redesign

At this point it was decided that the system should be redesigned to address several problems. The metal fittings on the ends of the glass tube were very heavy and seemed to inhibit the generation of a vacuum inside the tube. Their weight would sometimes make it quite difficult to create a vacuum inside the tube. The danger of electrical current arcing through the metal was also a problem that should be addressed. In addition, if homogenous thin films were to be deposited on the entire interior of a tube, then the entire tube would need to be translated back and forth through the coil area during deposition runs.

It was decided to try CPVC fittings and tubing because of their light weight. Standard fittings were used that adapted to the end of the glass tube with the o-ring. A much better fit was attained with the CPVC than that of the metal. If successful, this would solve both the weight and the arcing problem.

The inlet translation problem was solved by using an old chair base with casters as the platform for the ultrasonic nebulizer. The old chair was removed from the base and a wood platform was attached. This would allow the nebulizer to be translated manually while the system was in operation. The nebulizer, glass tube, and the outlet assembly would all be in a straight line with the pressure from the vacuum pump holding everything together. Soft high heat ceramic insulation material was used on top of the ceramic brick supports so the tube could slide easily. Figure IV-11 demonstrates the inlet translation design.

The outlet translation assembly was designed using a T shape at the end of the outlet tube. Both sides of the T could then slide on a wooden track. The flexible vacuum line

was attached to a line extending perpendicularly from the outlet assembly. Figure IV-12 demonstrates the inlet translation design.

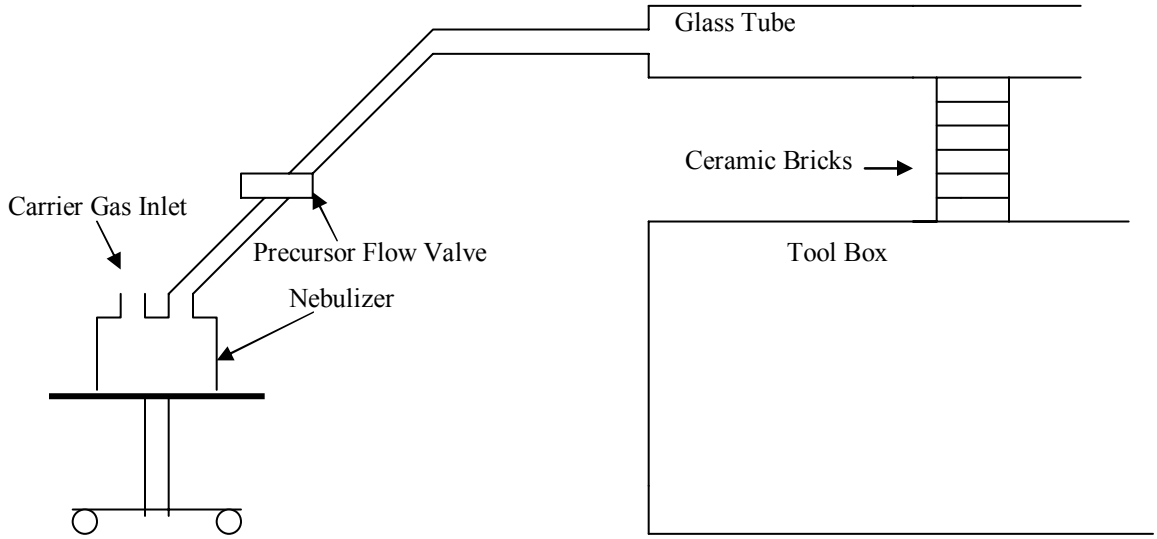

Figure IV-11. Inlet Translation Design

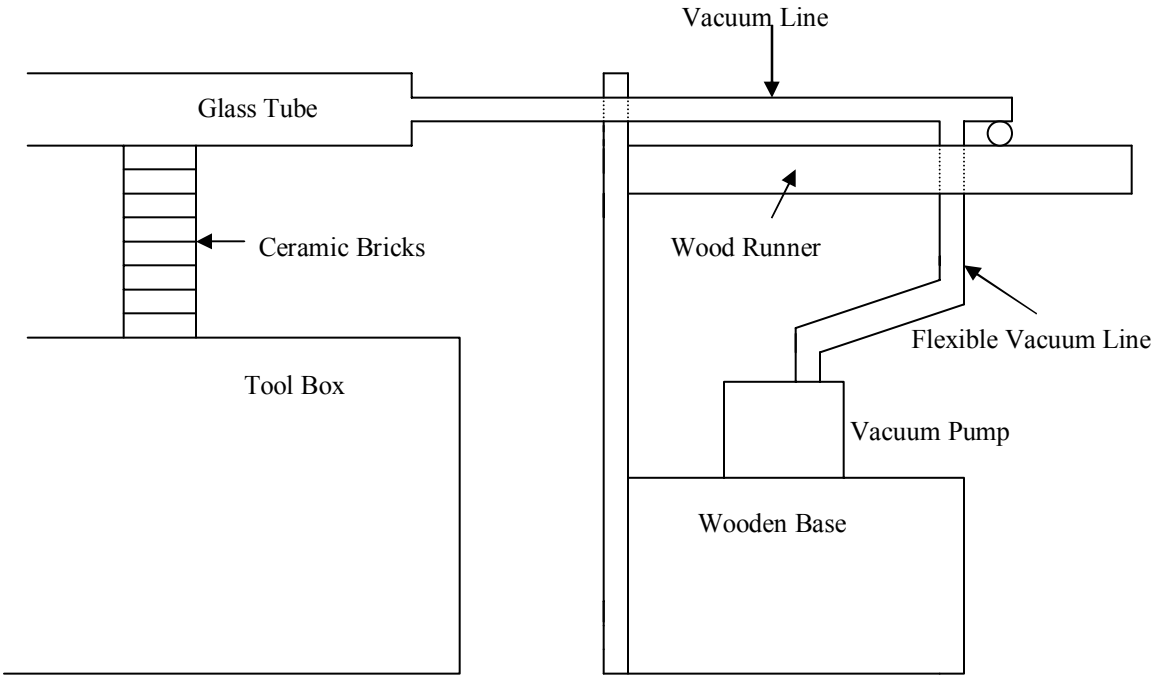

Figure IV-12. Outlet Translation Design

The only gas line needed in this redesigned system would be the carrier gas line. The last deposition run demonstrated that a plasma region could be formed using only the carrier gas line. Figure IV-13 demonstrates the newly designed system.

The entire system was assembled and tested with just water in the nebulizer and the nebulizer running. The results of this test demonstrated the effectiveness of the newly designed system. A strong plasma region was established by controlling the precursor inlet valve. Opening the valve completely resulted in no plasma and restricting the flow to the minimum possible rate resulted in the optimum plasma region. The entire system could be manually translated by moving the nebulizer platform along the floor. The position of the glass tube in relation to the coil could now be adjusted without danger of electricity arcing through the metal fittings.

Figure IV-13. Redesigned System

17. Yttrium Containing Films

It was decided to use yttrium nitrate, $Y(NO_3)_3 \cdot xH_2O$, as the precursor to test the operation of the new system. The deposition parameters for this run are listed in Table VIII.

The plan was for a thirty minute deposition run. The tube would be manually translated three times during the deposition. The positions of the coil in relation to the glass tube would be three equidistant places along the tube. Refer to Figure IV-14 for the relative positions of the coil in relation to the glass tube. The coil positions are measured from the center of the coil.

Table VIII. Deposition Parameters – Yttrium Nitrate as Precursor

RF Power	30%
DC Plate Voltage	8.9K
Grid Amps	0.47
Plate Amps	2.0
Carrier Gas Flow	Less Than 5%
Nebulizer Power	60%
Yttrium Concentration	25 grams per liter of de-ionized H_2O

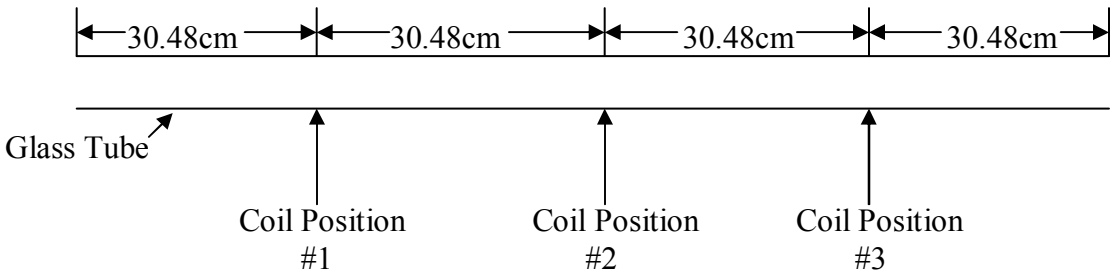

Figure IV-14. Coil Positions for Translation

Yttrium nitrate powder, which has a solubility limit of 1347 g/liter, was obtained from Alfa Aesar chemical company.[12] The desired amount of this powder was mixed with de-ionized water in a beaker and placed on a model 220T Thermix stirrer for thirty minutes. The solution was then poured into the nebulizer chamber and the complete deposition procedure was followed.

When starting the system the coil was oriented in coil position number two. When the system was fully operational and plasma was formed, the glass tube was translated to coil position number one for the first part of the deposition. The plasma region extended into the CPVC tubing and after approximately thirty seconds the inlet tube connector failed. This failure was due to the intense heat of the plasma which caused a portion of the CPVC fitting to become pliable. The force on the fitting from the vacuum caused the fitting to deform and loss of the vacuum resulted.

A supply of new fittings was obtained and the deformed fitting was replaced. The system was reassembled and experimentation to determine maximum translation distance was performed. From this experimentation it was determined that the system could not be translated at all using the CPVC fittings and tubing. Any translation at all resulted in deformed fittings or tubing and failure of the vacuum plasma system. The optimum position of the tube with regards to the coil was determined and is demonstrated in Figure IV-15. The system flow direction causes more heat to be carried to the outlet which accounts for the longer distance towards the outlet end of the tube.

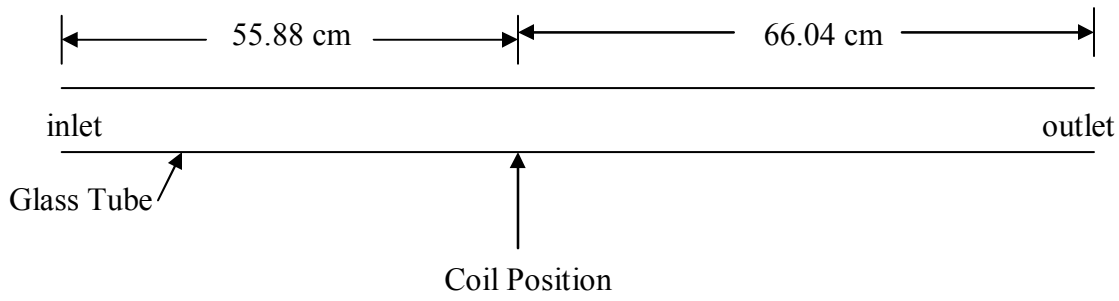

Figure IV-15. Coil Position without Translation

a. Second Yttrium Deposition Run

The second attempt at depositing an yttrium oxide film was conducted. The same deposition parameters as outlined in Table VIII were used. The optimized coil position was used but after ten minutes the system failed due to overheating of the inlet fitting. The thirty percent power setting was too high and caused too much heat in the system. The intense heat from the plasma caused the glass to cloud over in one particular section of the glass tube. An analysis of this tube demonstrated the presence of a coating as is discussed in the results and discussion section on page 72.

Experimentation to optimize RF power settings for the system with the nebulizer chamber in operation was performed at this time. The experimentation demonstrated that for runs less than ten minutes in duration, power settings up to thirty percent could be utilized. RF power settings in excess of thirty percent caused too much heat and either the inlet or outlet fitting failed.

For runs longer than ten minutes in duration it was observed that power settings up to twenty five percent could be used. Several runs of over thirty minutes were tried at twenty five percent RF power and the fittings were not compromised.

18. Temperature Profile of Redesigned System

An attempt was made to use the thermocouple thermometer to determine the temperature profile of the redesigned system. It was soon observed that the new system with its robust plasma region contained too much power to use a thermocouple probe. All attempts to place the probe on the exterior of the glass tube resulted in arcing of current through the glass tube and into the probe. This resulted in a small hole in the glass tube which compromised the vacuum system.

It was decided to obtain an optical pyrometer and use it in the temperature profile procedure. The only one available was a Raytek model RAYMA2SCSF infrared pyrometer with a minimum reading potential of five hundred degrees Celsius. This instrument was not capable of profiling the system because of this minimum. However,

the pyrometer could be used to measure the exterior surface temperature of a glass tube at the point of tube failure. This is the point when the coil area plasma glows white hot and results in implosion of the tube. Refer to Figure IV-9 on page 48 and Figure IV-10 on page 49. It was found that the temperature of the exterior of the glass tube at the point of failure was 593º C.

An Ultimax model UX-40P optical pyrometer was used to determine the exterior surface temperature of a glass tube during a deposition run. This pyrometer has a range of -50º C to 1000º with a spectral range of eight to thirteen micrometers. Figure IV-16 demonstrates the areas of the tube tested with this pyrometer. Point number one is to the left of the coil, point number two is inside the coil region, and point number three is to the right of the coil. This test was performed during a deposition run with aluminum nitrate as the precursor. The RF power was set to twenty five percent and then raised to thirty percent half way through the run. The results of this test are discussed in the results and discussion section on page 67.

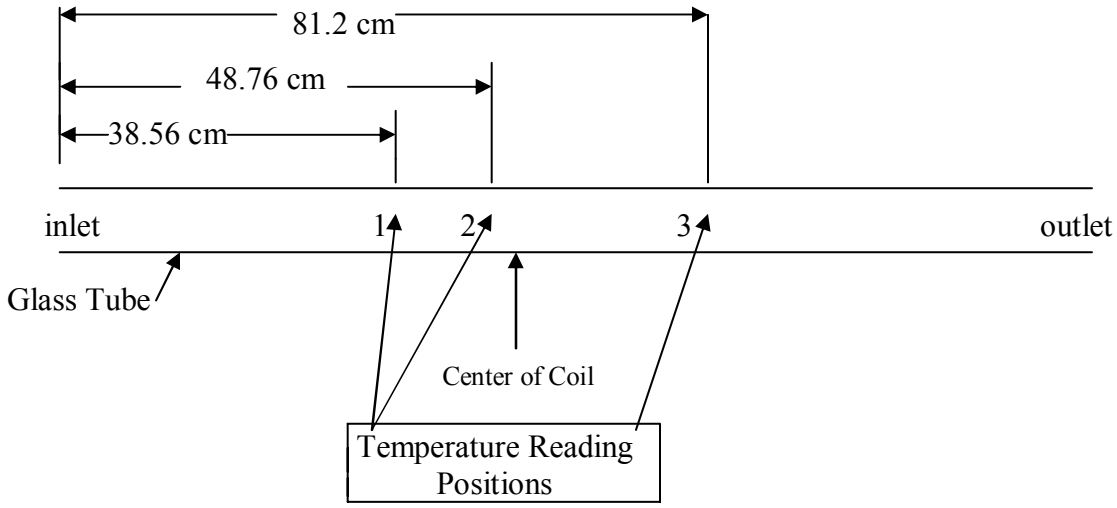

Figure IV-16. Temperature Reading Positions

19. Aluminum Containing Films

Aluminum nitrate powder, which has a solubility limit[12] of 637 g/liter, was obtained from Alfa Aesar chemical company. The desired amount of this powder was mixed with de-ionized water in a beaker and placed on a model 220T Thermix stirrer for thirty minutes. The solution was then poured into the nebulizer chamber and the complete deposition procedure was followed. For the results regarding these coatings refer to the results and discussion section on page 90.

Table IX. Deposition Parameters – Aluminum Nitrate

RF Power	20%
DC Plate Voltage	8.4K
Grid Amps	0.4
Plate Amps	1.2
Carrier Gas Flow	Less Than 5%
Nebulizer Power	100%
Aluminum Nitrate Concentration	25 grams per liter of de-ionized H_2O

20. Glass Filter Paper

A glass filter paper was placed in the outlet connector assembly in an attempt to determine the amount of precursor entering the tube during a deposition. To determine the weight of the filtered precursor, the filter paper would have to be weighed before and after the run. The filter paper had to be kept in place using a small screen to avoid it being sucked into the vacuum pump. After several attempts it was observed that a part of the paper stuck to the screen and the weight of the filter would not be accurate after a run. Therefore, this test only showed that precursor was entering the plasma region.

This experiment demonstrated that a large amount of water mist was escaping from the liquid precursor. The decreased flow resulted in the water vapor reforming into liquid and collecting on the bottom of the glass tube. This water mist was probably causing a decrease in the power of the plasma. Subsequent runs will require eliminating the escaped water mist problem.

It was necessary to run the vacuum pump until the liquid in the nebulizer chamber stopped bubbling. Experiments demonstrated that placing the precursor under a vacuum for twenty minutes allowed the pressures to equalize and the maximum amount of water mist to escape.

21. Optimization of Solution Concentration

Another problem encountered was the inability of the nebulizer to form an aerosol mist from high concentrated solutions of yttrium nitrate and water. The nebulizer would form a mist with solutions as high as five hundred grams per liter of aluminum nitrate powder and water, but when this same concentration was tried with yttrium nitrate a mist would not form. An investigation into the reason for this revealed that yttrium has an atomic weight of 88.91amu and aluminum has an atomic weight of 26.98amu. It was realized that the weight of the yttrium nitrate precursor was the problem. The yttrium was so heavy that the nebulizer was unable to create a mist. It therefore became necessary to optimize the precursor solutions for both yttrium nitrate and aluminum nitrate. This was done experimentally by misting different solution concentrations and observing the cloudiness of the resulting mist. That is, observing the mist by eye to determine which one appeared to contain the highest concentration.

a. Aluminum Nitrate

Table X demonstrates the results of solution concentration testing for aluminum nitrate. Further testing is required to determine the optimum concentration to use.

Table X. Aluminum Nitrate Concentration

Aluminum Nitrate Nebulizer Power (100%)	25 g/l	most dense
	50 g/l	most dense
	100 g/l	dense
	200 g/l	dense
	500 g/l	least dense

b. Yttrium Nitrate

Table XI demonstrates the results of solution concentration testing for Yttrium nitrate. The optimum concentration to use is twenty five grams per liter.

Table XI. Aluminum Nitrate Concentration

Ytrium Nitrate Nebulizer Power (100%)	25 g/l	most dense
	50 g/l	dense
	100 g/l	dense
	200 g/l	least dense
	500 g/l	no mist

V RESULTS AND DISCUSSION – VACUUM FILMS

An attempt was made to make a temperature profile this newly designed system. This was performed to determine the actual temperature of the exterior surface of the glass tubes while they are under the influence of plasma. The original system was examined with a thermocouple thermometer and the second system was examined with a pyrometer.

An experiment was also performed to determine the effects of plasma on the surface chemical composition of the glass tubes. Samples were obtained by exposing the glass tubes to plasma while varying exposure time and radio frequency power. These samples were analyzed by Electron Spectroscopy for Chemical Analysis or ESCA. ESCA is a test where a sample is bombarded with x-rays. The interaction between the x-rays and the sample surface causes electrons from the top five to ten atomic layers to be ejected. The analysis of the ejected electrons gives the atomic composition of the coating.

Another experiment was to deposit SiO_2 with the vacuum system. This experiment demonstrated the ability of this system to actually deposit a coating. These coatings are not continuous thin films at the time. These films will be examined using SEM and EDS analyses.

Yttrium and aluminum containing films on the interior surfaces of the glass tubes will be analyzed with SEM, EDS, ESCA, and SNMS analyses techniques. SNMS, or Sputtered Neutral Mass Spectrometry, uses a mass spectrometer to analyze the intensity of each element present. Glass filter papers will be analyzed in a similar manner.

Analysis of the glass filter papers used to determine precursor flow was done at Alfred University with EDS and SEM. A sample was also sent to Osram Sylvania for analysis.

A. First Temperature Profile

Figure V-I demonstrates the position of the thermocouple probe during the temperature profile procedure. The probe was placed at the edge of the coil towards the outlet end of

the tube and the RF power was varied with time. For instance, a power setting of eleven percent was initially used and it took two minutes for the temperature at this level to stabilize at 143º C. At this point the power setting was raised to twelve percent and the temperature was allowed to stabilize. This was repeated for thirteen and fourteen percent power settings.

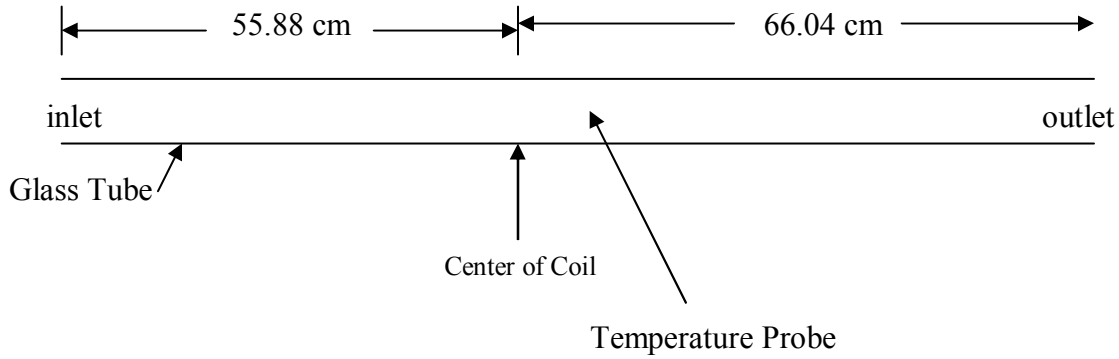

Figure V-1. Thermocouple Temperature Probe

The graph of temperature vs time on the next page demonstrates that the amount of heat generated by the plasma region increases with time and also with increases in RF power. The graph also indicates a less incremental temperature with each increase in RF power. At each point when the RF power is increased, a smaller increase in temperature is observed. This demonstrates that the radio frequency waves emitted by the generator momentarily interfere with the operation of the thermocouple thermometer. This first profile was done on the originally designed system.

1. Temperature Profile – Second System Design

The temperature of the surface of the glass during a deposition run was measured with an optical pyrometer as demonstrated in Figure IV-16 on page 60. Three different

locations of the glass tube were examined with two different power settings. The results of this test are summarized in Table XII.

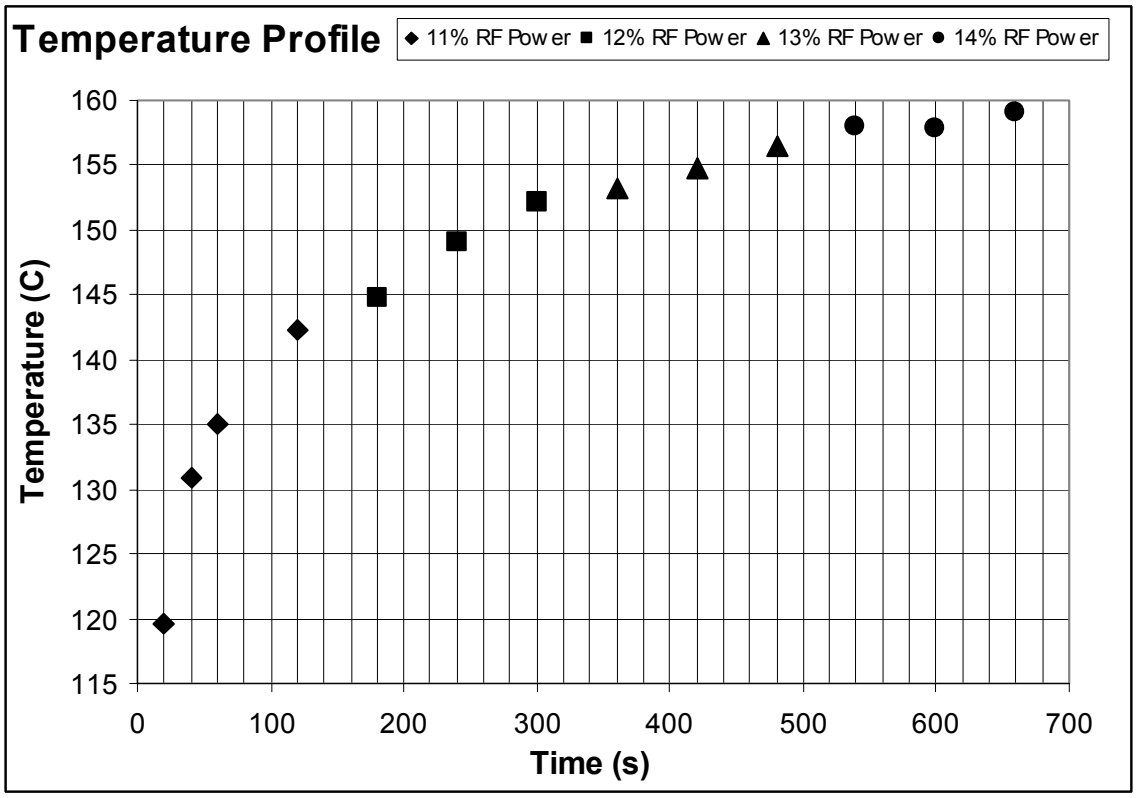

Figure V-2. Temperature Profile – First System

Table XII. Temperature Readings

Position of Temperature Reading	Temperature (25% RF Power)	Temperature (30% RF Power)
Point #1	207ºC	224ºC
Point #2	270ºC	288ºC
Point #3	189ºC	208ºC

The graph of temperature vs distance demonstrates that the surface temperature of the glass tube during a deposition run is dependant upon the position of the coil with respect

to the glass tube. The best fitted trend lines on the graph show how the temperature of the tube decreases as the distance from the coil increases. Point number two is a point on the surface of the tube inside the coil area. As expected, the temperature at point number two is higher than that at the other two points and this temperature increases with an increase in RF power. The temperature at points one and three also increase with an increase in RF power. A best fitted curve was applied among the three points for each of the RF power settings.

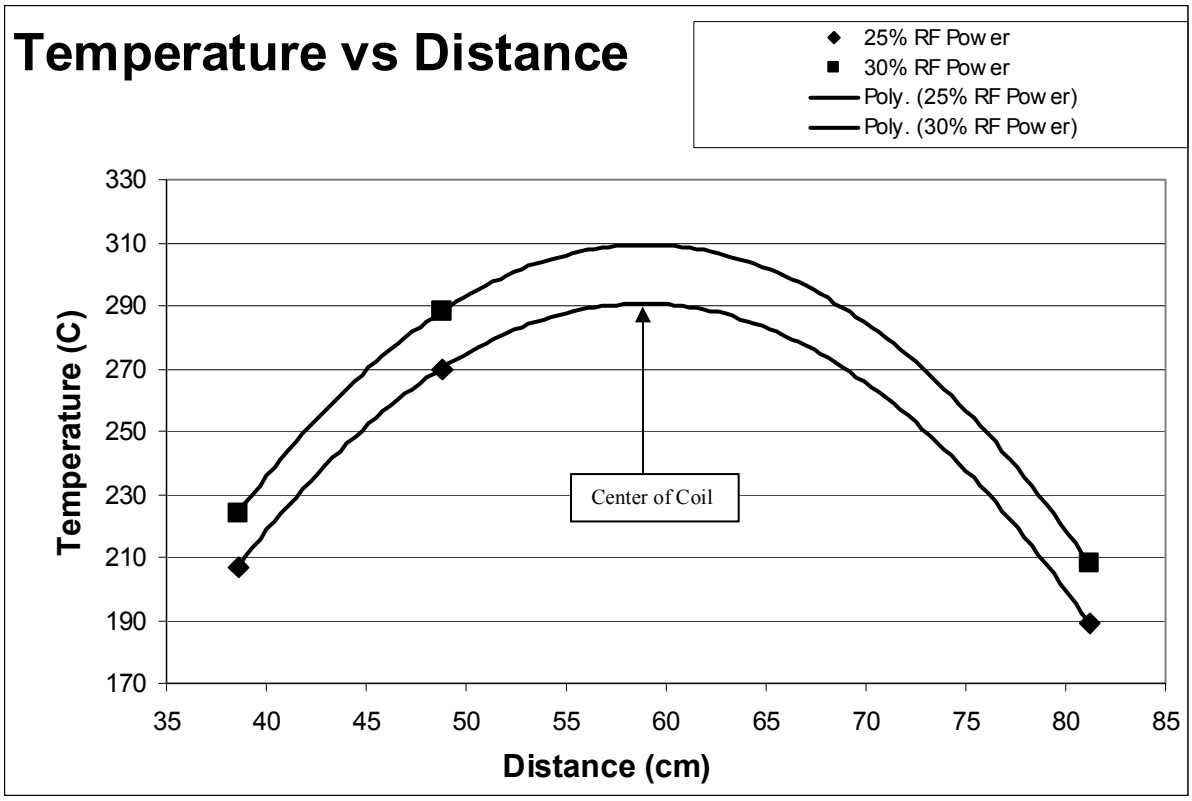

Figure V-3. Temperature vs Distance

B. Carbon Substrate

The SEM micrograph depicted in Figure V-4 demonstrates a SiO_2 deposit which is not continuous. The dark area at the top right shows the surface of the black substrate. Large and small particles ranging in size from about one hundred nanometers to almost one micrometer can be observed.

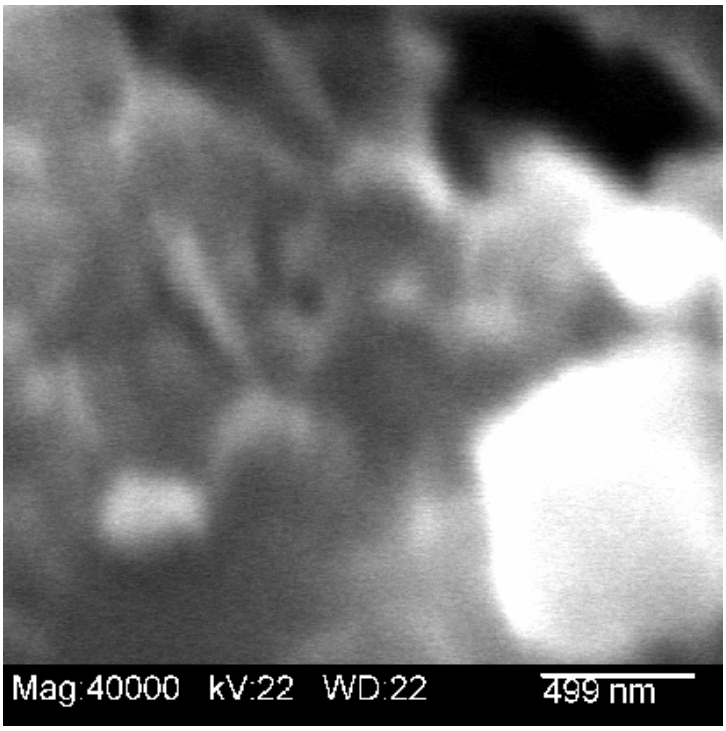

Figure V-4. Carbon Substrate with SiO_2 Coating

EDS analysis of the carbon substrate without a coating is demonstrated in Figure V-5. It demonstrates only the presence of carbon on the uncoated surface.

EDS analysis of the carbon substrate with a coating is demonstrated in Figure V-6. It shows that a silicon rich deposit is present on the surface of the substrate. Also demonstrated is high oxygen content. This indicates that the deposited coating contains both silicon and oxygen.

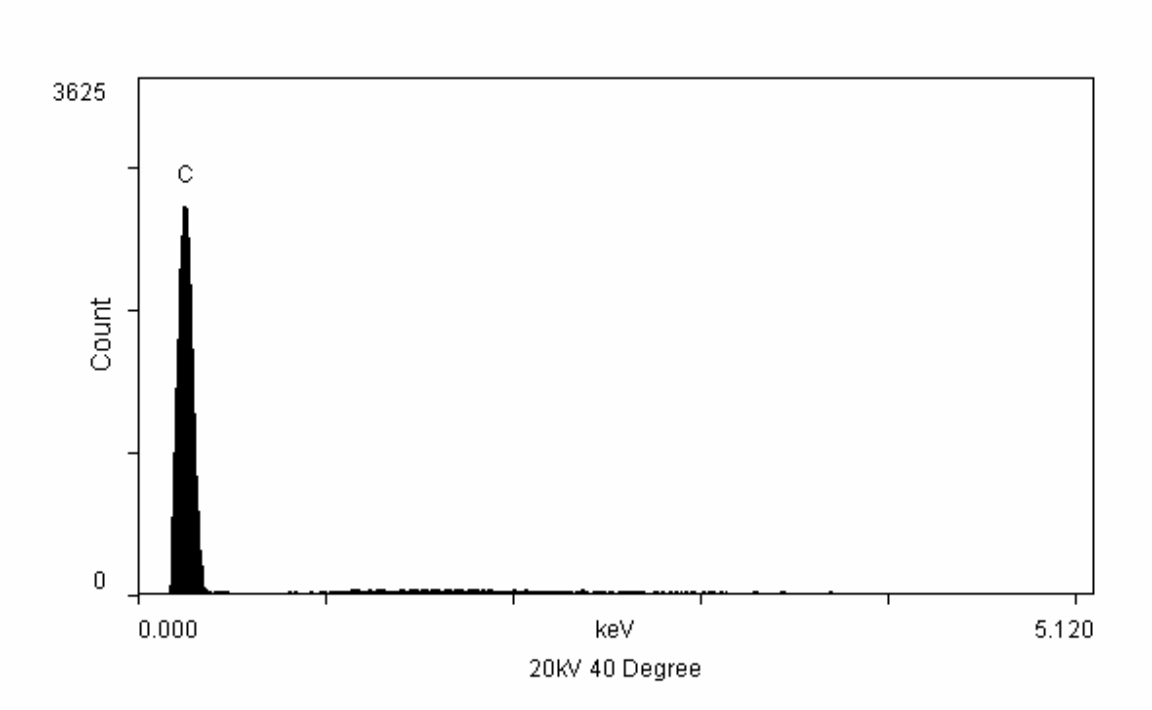

Figure V-5. Carbon Substrate without Coating

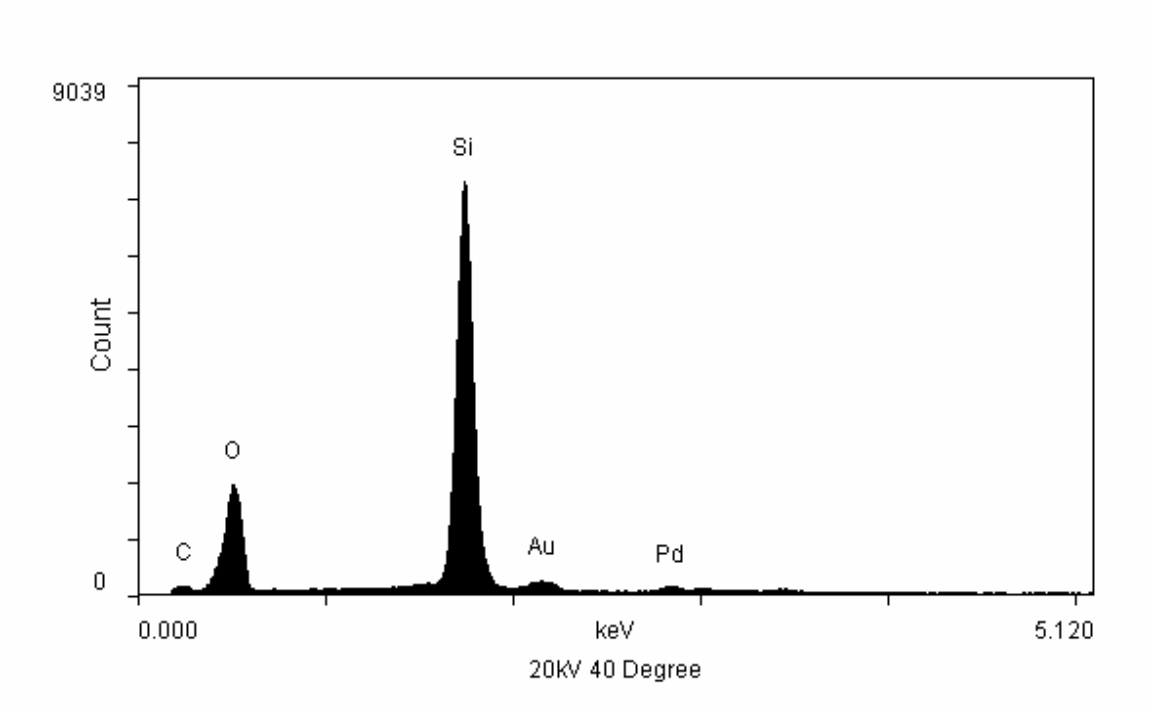

Figure V-6. Carbon Substrate with Coating

C. Silicon Dioxide on Interior Surface of Tube

Figure V-7 demonstrates the SEM analysis of a silicon dioxide coating on the interior surface of a glass tube. This is a top view looking straight down on the coating and shows the presence of large and small particles. The smallest particle is two to three hundred nanometers in diameter while the largest particle measures about six hundred nanometers in diameter. This micrograph illustrates the deposition of SiO_2 particles as opposed to a continuous thin film.

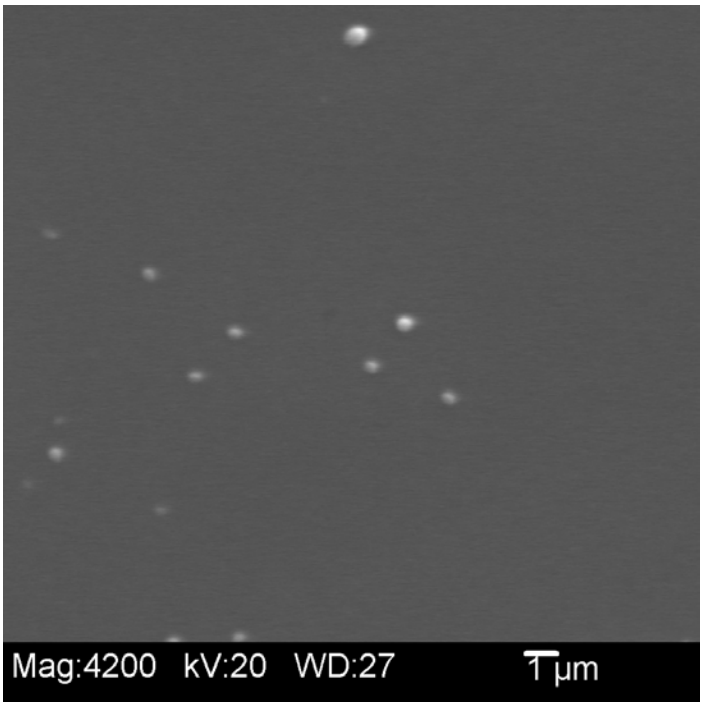

Figure V-7. Silicon Dioxide - Surface

Figure V-8 shows an edge view of the same coating. The gray area at lower right is the glass substrate and the diagonal white area is the SiO_2 coating. This micrograph demonstrates the thickness of the coating which ranges from about 1.5µm to 3µm in thickness. Also demonstrated is the fact that the film is not very uniform.

Figure V-9 demonstrates EDS spectrum of the interior surface of the glass tube without a coating present. This graph shows the presence of all the elements used to manufacture

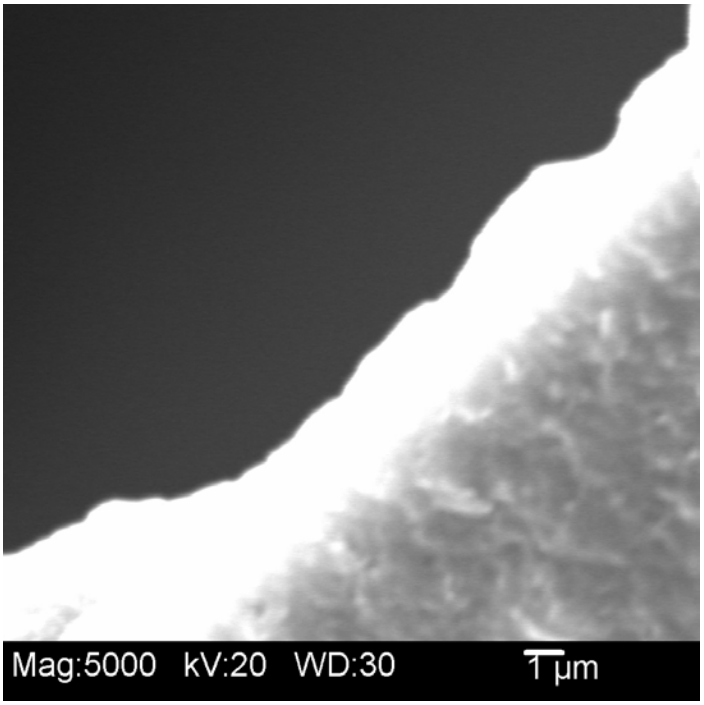

Figure V-8. Silicon Dioxide - Edge

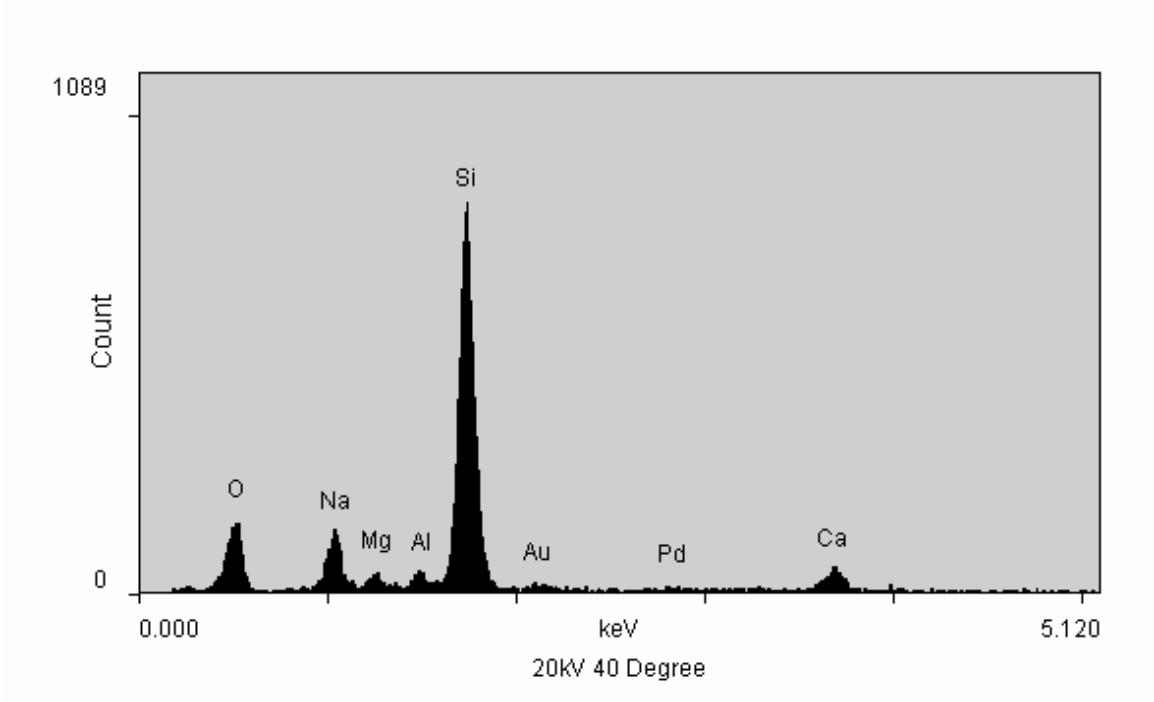

Figure V-9. Glass Tube without Coating

the glass tubes. Also shown is the gold and palladium used to prepare the sample for SEM/EDS analyses. Figure V-10 is the analysis of the tube with the coating present.

A comparison of Figures V-9 and V-10 demonstrates that the silicon content is almost identical. The oxygen content of the coated surface appears to be higher than the uncoated surface. The analysis problem lies with the fact that this is a silicon containing coating on a silicon containing substrate.

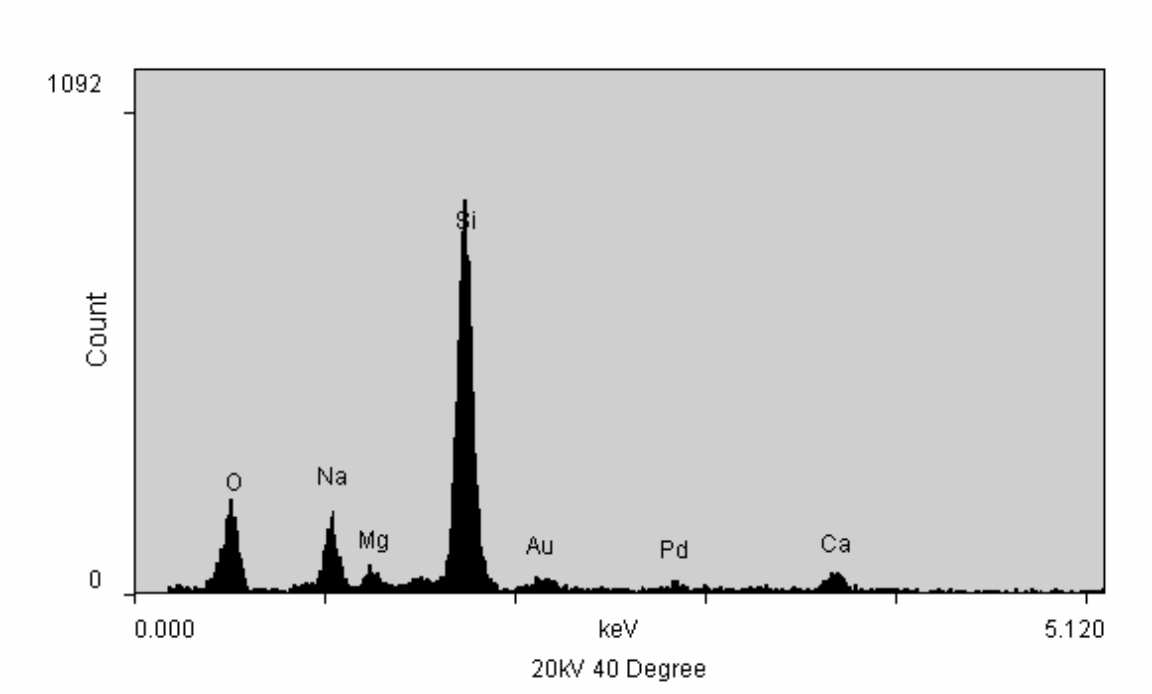

Figure V-10. Glass Tube with SiO_2 Coating

D. Yttrium Containing Films

Attempts to deposit yttrium and aluminum containing films on the interior of the glass tubes resulted in formation of cloudy sections of the glass. The cloudiness of the glass may be caused by the intense heat of the plasma and is an undesirable effect. The RF power level has to be optimized such that enough heat is present to form a film, but not too much so as to cloud the glass. Both cloudy and clear sections of the glass tubes were examined.

1. Cloudy Section of Glass Tube Y1

Figure V-11 demonstrates an SEM micrograph of an yttrium containing coating on a cloudy section of the interior surface of glass tube number Y1. This analysis shows the presence of large and small spherical particles. Figure V-12 shows that the diameters of these particles range from about fifty nanometers to approximately one micrometer. Both Figures V-11 and V-12 demonstrate a thin film that is not continuous.

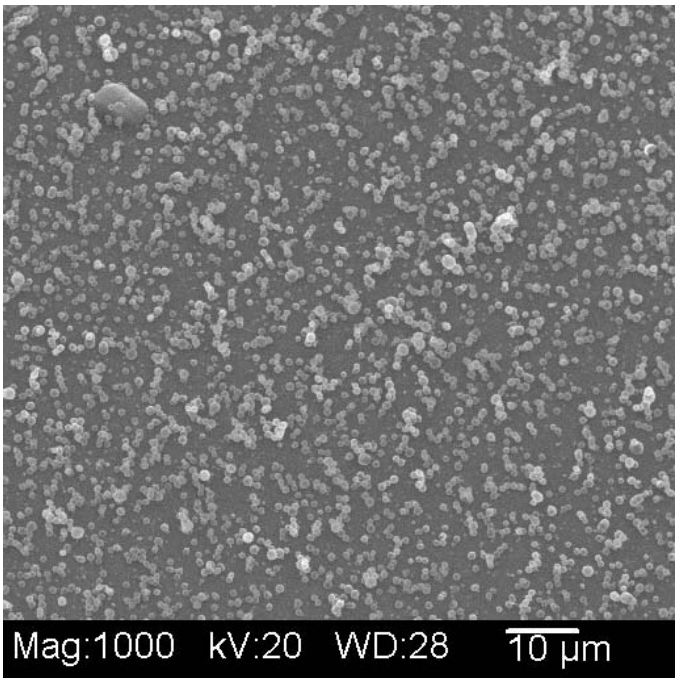

Figure V-11. Glass Tube with Yttrium Containing Coating (Magnified 1000X)

The inside surface of sample Y1 was also examined by EDS analysis. The small spherical particles were yttrium rich as is demonstrated in Figure V-13. The silicon, aluminum, and calcium peaks are observed due to the interaction of the electron beam with the glass tube.

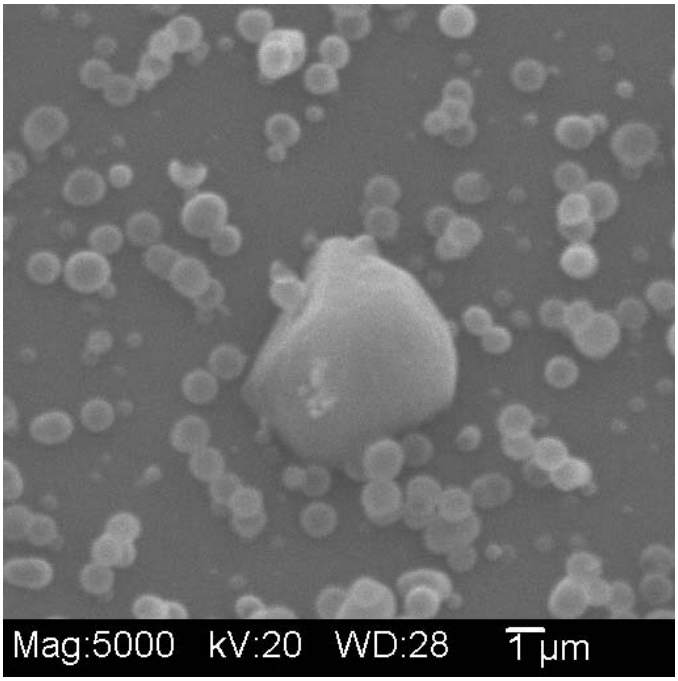

Figure V-12. Glass Tube with Yttrium Containing Coating (Magnified 5000X)

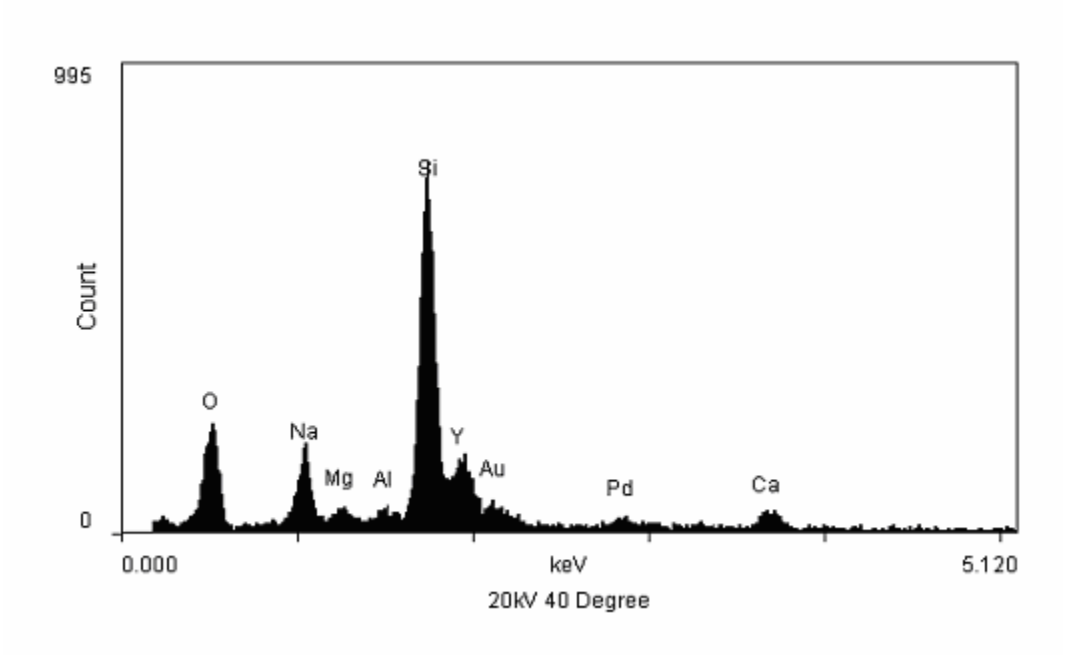

Figure V-13. Glass Tube with Yttrium Containing Coating - Small Sphere

Also shown in Figure V-12 is a larger particle measuring almost four micrometers across. When this large particle was analyzed with EDS, the absence of yttrium and the presence of titanium were demonstrated. Refer to figure V-14 for the EDS analysis graph. The titanium is a contamination the source of which can't be explained at this time.

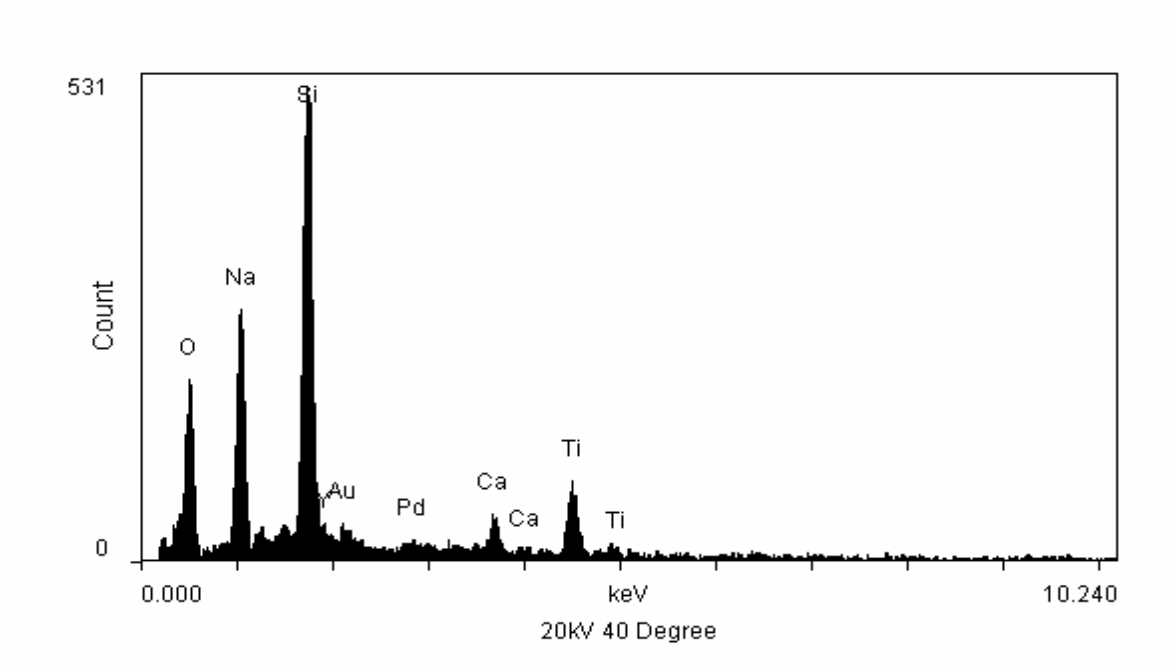

Figure V-14. Glass Tube with Yttrium Containing Coating - Large Sphere

Table XIII demonstrates the atomic composition of the interior surface of tube Y1 obtained with ESCA analysis. An examination of this table reveals that a cloudy section of Y1 contained twelve percent yttrium. Also demonstrated is the presence of seventy-four percent oxygen. This is an increase in oxygen over the sixty three percent content of the control sample. The increase in oxygen along with the presence of yttrium demonstrates the presence of an yttrium containg film. This confirms the results obtained with EDS analysis at Alfred University.

Table XIII. ESCA Analysis - Interior Surface of Y1

Sample	Y	Si	O	Na	Mg	Ca	Al
Y1C - Cloudy	12	9.1	74	3.5	0.6	0.7	0.2
Y1C - Clear	4.1	11	63	19	1.4	0.8	0.3
Y1E1	ND	14	58	26	2.0	0.9	0.2
Y1E2	ND	16	58	23	1.6	0.9	0.3
Control	N/A	19	63	14	1.3	1.1	0.4

The SNMS graph of Intensity (cps) vs. Depth (nm) depicted in Figure V-15 demonstrates that the intensity of yttrium is about ten thousand cps at the surface of the film. The intensity curve then decreases in a gradual slope demonstrating a non continuous film. The graph demonstrates that the thickness of the film is approximately sixty nanometers.

2. Clear Section of Glass Tube Y1

A clear section in the center of sample Y1 was also analyzed with SNMS at the labs of Osram Sylvania. The results as demonstrated in Figure V-16 show that the intensity of yttrium is about one thousand cps at the surface of the film. The intensity curve then decreases in a gradual slope demonstrating a non continuous film. The graph demonstrates that the thickness of the film is approximately forty nanometers.

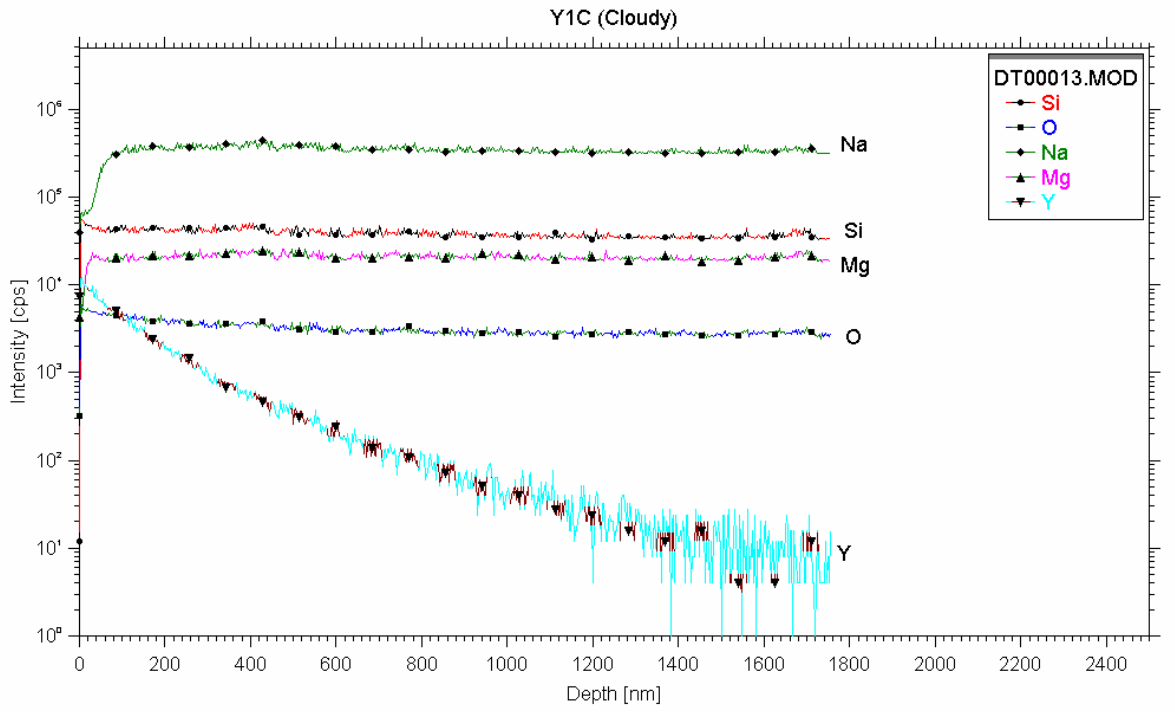

Figure V-15. Glass Tube Y1 – Cloudy Section

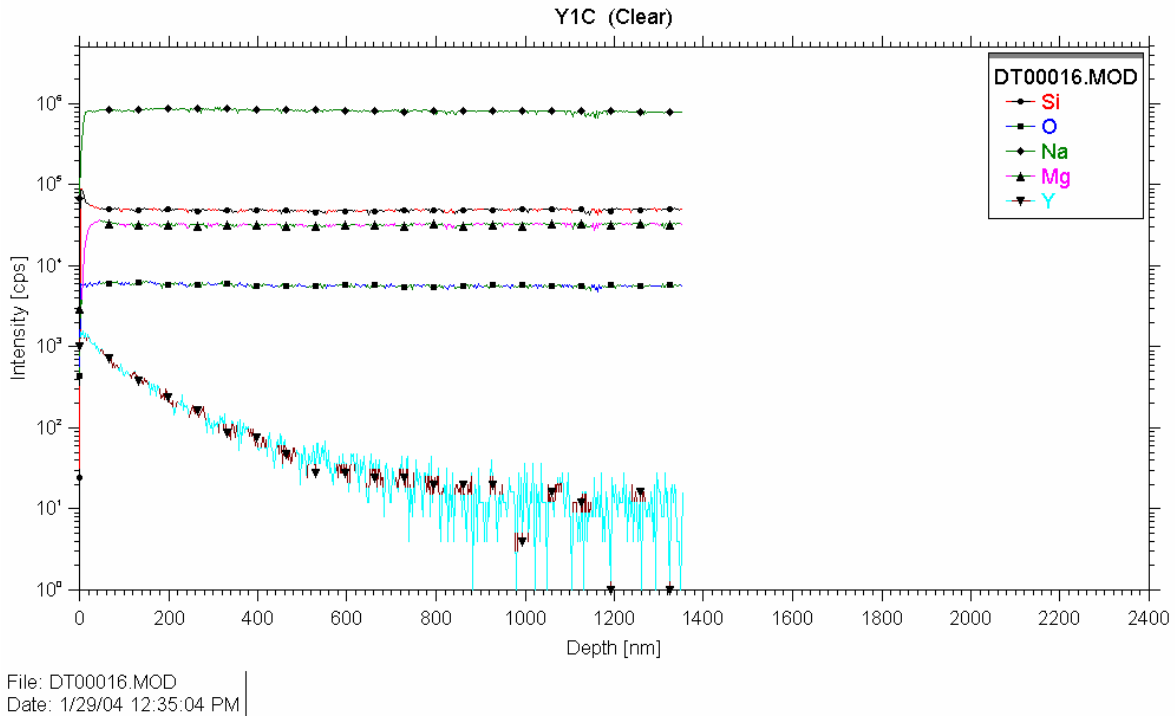

Figure V-16. Glass Tube Y1 – Clear Section

3. Tubes Y2 – Y19

No coatings were produced for experiments Y2 through Y19. Table XIV demonstrates ESCA analysis of tubes Y10 through Y13. As can be seen, no yttrium coating was detected. Analysis of tubes Y2 through Y9 (Table XVI) and tubes Y14 through Y19 demonstrated similar results.

Atomic Composition of Surface (%)

Sample	Y	Si	O	Na	Mg	Ca	Al
Y10C	ND	24	64	8.6	1.0	1.2	0.5
Y10E	ND	18	54	22	3.6	1.4	0.3
Y11C	ND	26	67	4.6	0.6	1.0	0.4
Y11E	ND	14	59	25	1.5	0.9	0.3
Y12C	ND	27	67	4.6	0.5	1.1	0.4
Y12E	ND	13	58	25	1.8	0.8	0.3
Y13C	ND	27	67	4.7	0.4	1.0	0.3
Y13E	ND	14	58	25	1.7	0.9	0.3

Table X1V. ESCA Analysis – Tubes Y10 through Y13

4. Filter Paper Results

The EDS analysis of a glass filter paper placed in the outlet line during deposition demonstrated the presence of Yttrium. The complete analysis can be found in the appendix on page 123. ESCA analysis of a similar sample showed a twelve percent yttrium content. This demonstrates that precursor material is entering the glass tubes during deposition.

5. Tubes Y20 – Y25

When the major problems with the system were solved, consistent results were obtained with the next series of experiments. That is, thin films were deposited on all tubes. For all six of these tubes, the precursor solution concentration was twenty five grams of yttrium nitrate per one liter of de-ionized water and the nebulizer power was set at one hundred percent. The precursor delivery was manually changed by manipulating the precursor delivery valve throughout the deposition time. This was done in an attempt to ensure that an adequate amount of precursor was entering the plasma region. Turning the valve completely off during deposition accomplishes two things. First, removal of the nebulizer chamber and gas feed lines from the vacuum sub-system decreases the number of vacuum leaks and therefore creates a better vacuum. This leads to a much stronger plasma region with which to heat the glass and vaporize the precursor. Second, closing the valve stops the flow of precursor and allows a heavy concentration of such to accumulate in the nebulizer chamber. This heavy accumulation of aerosol mist was then dumped into the plasma region by opening the valve. This procedure was followed throughout the deposition runs.

Table XIII demonstrates the ESCA analysis of tubes Y20 through Y25. Deposition runs involving tubes Y20 through Y22 were conducted for five minutes at twenty five percent RF power. Runs involving Y23 and Y24 were conducted for eight minutes at twenty five percent RF power. For tube Y25, twenty percent RF power was used and the run lasted eight minutes. Each tube was analyzed at four different locations as indicated in the table.

The results show that the highest composition of yttrium was found in the center section of each tube. This was expected as the center of the tube is where the high energy coil region is located. There was little or no yttrium present at the beginning of each tube. Only tube Y23 showed the presence of yttrium at the beginning of the tube in the amount of 0.6 percent. There was no consistency in composition from tube to tube, but there was no consistency in the delivery of the precursor either.

6. Tube Y21

Figures V-17 and V-18 show the ESCA analysis of clear and cloudy sections of tube Y21. The sample areas were sixteen and one half inches from the beginning of the tube and located in the coil region. The curves showing the intensity of yttrium are consistent with those of tube Y1 in that they decrease in gradual slopes indicating non-continuous films. The intensity of yttrium at the surface of the film for tube Y21 (cloudy) is higher than that of tube Y21 (clear). This is also consistent with the results for tube Y1.

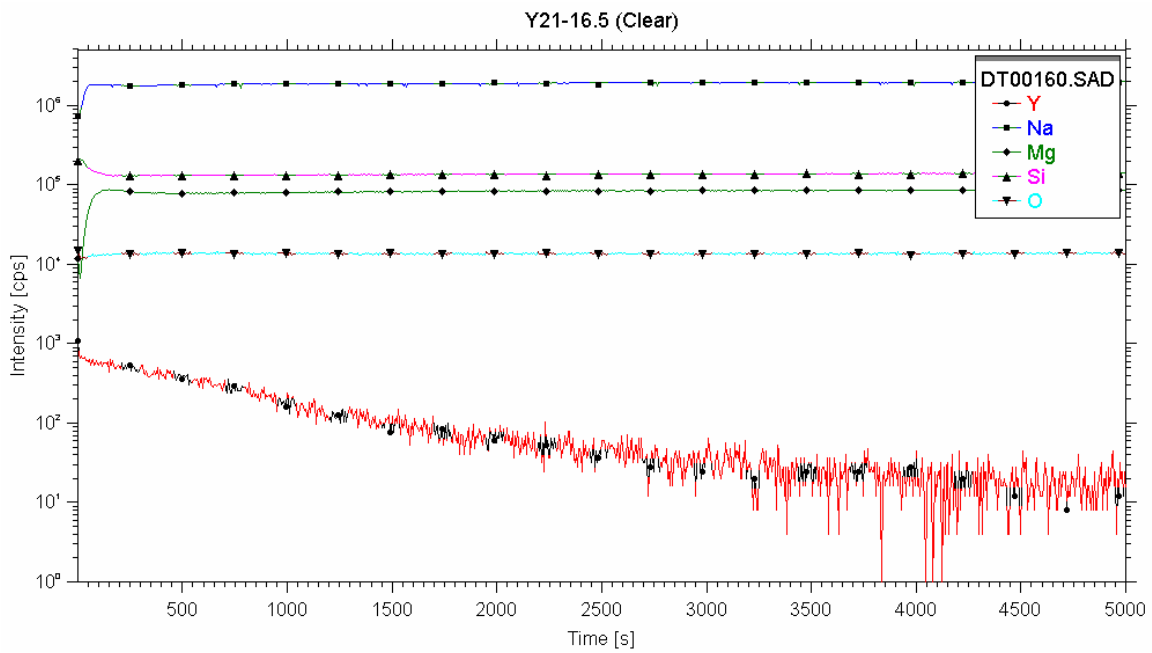

Figure V-17. Center of Tube Y21 (Clear Region)

7. Tube Y22

Figure V-19 demonstrates the SNMS analysis of the center of tube Y22. The yttrium curve depicted in this figure is consistent with those of non-homogenous films in that the profile shows a gradual slope change. This graph confirms the presence of a non-homogenous yttrium containing thin film on the interior surface of the glass tube.

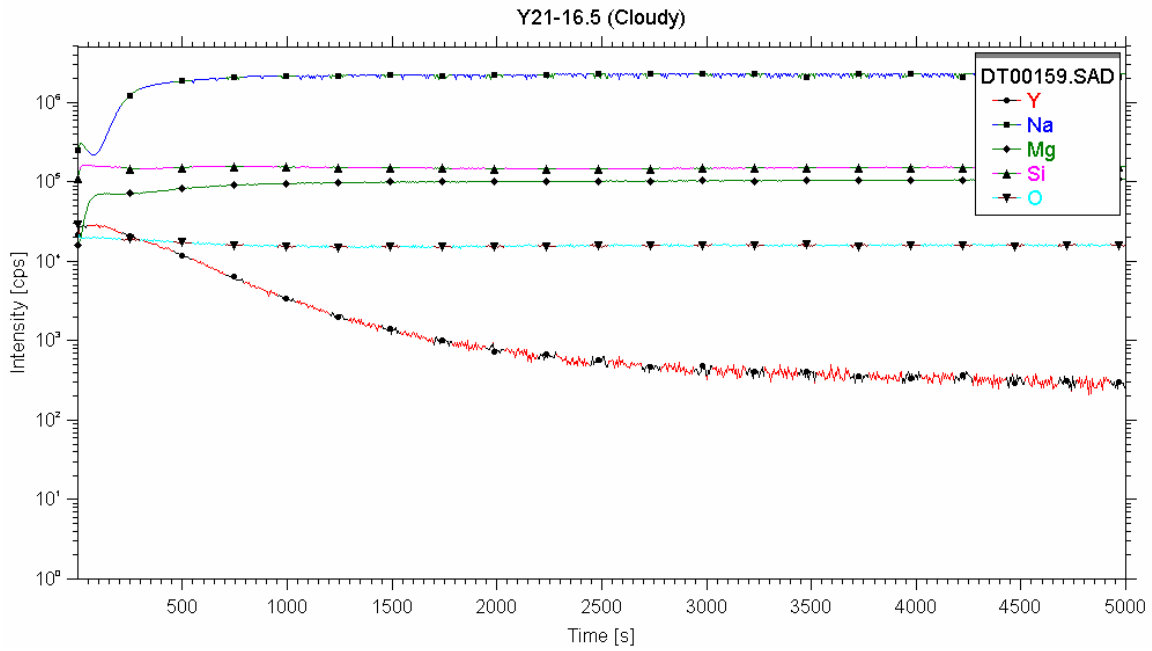

Figure V-18. Center of Tube Y21 (Cloudy Region)

Figure V-20 shows the SEM analysis of a center section of tube Y22. The micrograph illustrates the presence of a non-homogenous coating.

Five areas of the sample shown in Figure V-20 were analyzed with EDS. Figures V-21 through V-25 show the results of this analysis. The graphs of spectrum 1, 2, 4, and 5 demonstrate the presence of yttrium. These graphs further confirm the presence of an yttrium containing thin film on the interior surface of the glass tube.

Figure V-23 demonstrates the absence of yttrium for spectrum 3. This confirms that the coating is not continuous.

Table XV. ESCA Analysis – Tubes Y20 through Y25

Atomic Composition of Surface (%)

Sample	Na	Mg	Ca	Si	O	Al	Y
Y20-2" (B)	13	2.0	1.2	24	60	ND	ND
Y20-18" (C)	5.3	0.5	0.3	5.7	72	ND	16
Y20-34"	9.5	1.1	1.1	18	64	ND	5.5
Y20-44" (E)	14	1.3	1.1	17	62	0.4	4.1
Y21-2" (B)	12	0.8	1.1	25	60	0.4	ND
Y21-18" (C)	3.0	0.5	0.8	13	69	ND	14
Y21-34"	12	1.3	1.3	24	61	ND	0.2
Y21-44" (E)	16	2.0	1.1	21	59	0.4	0.4
Y22-2" (B)	17	1.9	0.6	19	62	0.3	ND
Y22-21" (C)	0.5	ND	ND	2.7	72	ND	25
Y22-34"	4.3	0.6	0.6	17	69	ND	8.3
Y22-44" (E)	18	1.7	1.0	19	59	0.4	0.1
Y23-2" (B)	16	1.9	0.8	20	61	0.2	0.6
Y23-25" (C)	4.3	0.6	0.3	18	66	ND	11
Y23-34"	11	0.4	0.5	11	66	ND	12
Y23-44" (E)	15	1.8	1.2	17	61	0.3	3.2
Y24-2" (B)	18	1.7	0.8	19	60	0.4	ND
Y24-23" (C)	8.9	0.2	0.6	9.8	68	ND	12
Y24-34"	1.7	ND	ND	29	68	ND	2.0
Y24-44" (E)	14	1.5	1.0	17	62	0.2	4.1
Y25-2" (B)	18	1.8	1.2	19	60	0.4	ND
Y25 20" (C)	1.2	0.7	ND	0.9	77	ND	20
Y25-34"	8.1	0.7	0.9	20	65	0.4	4.7
Y25-44" (E)	14	1.7	1.1	21	61	0.3	0.7

Note: ND indicates that the element was scanned but was not detectable.

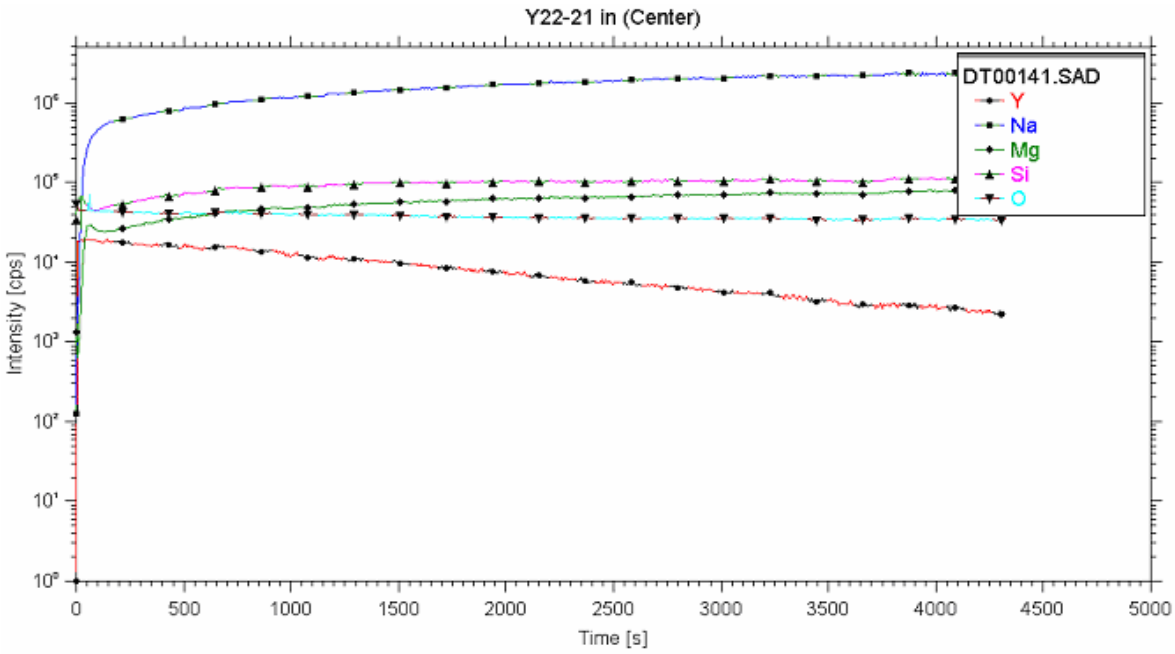

Figure V-19. Center of Tube Y22

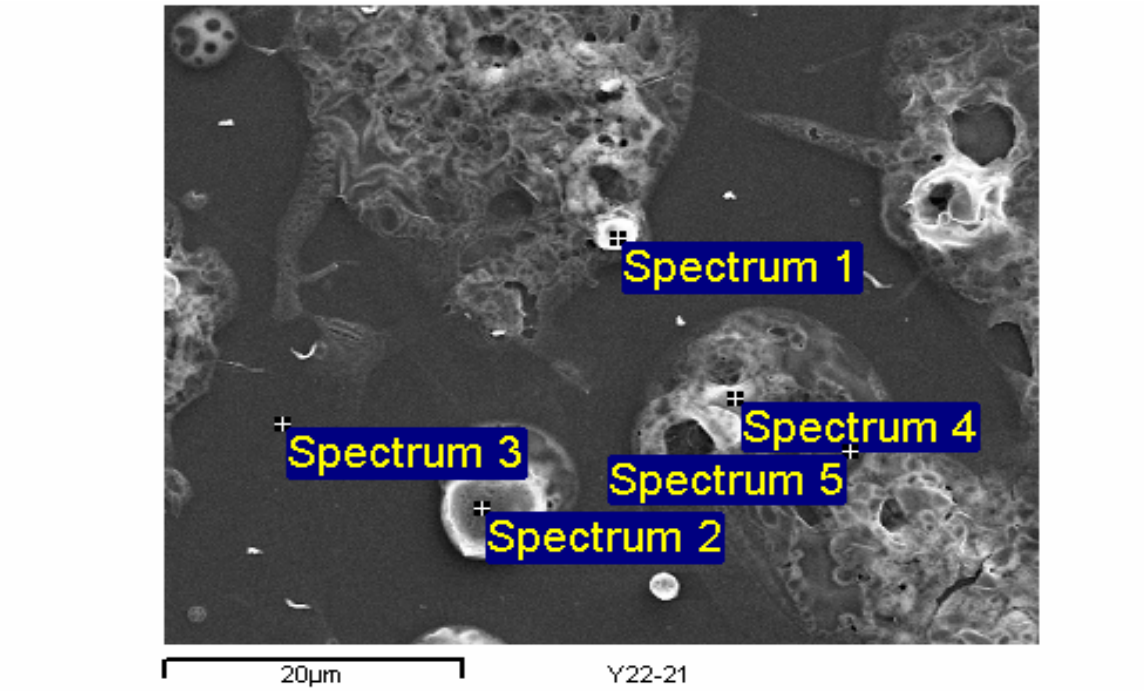

Figure V-20. SEM Analysis of Tube Y22

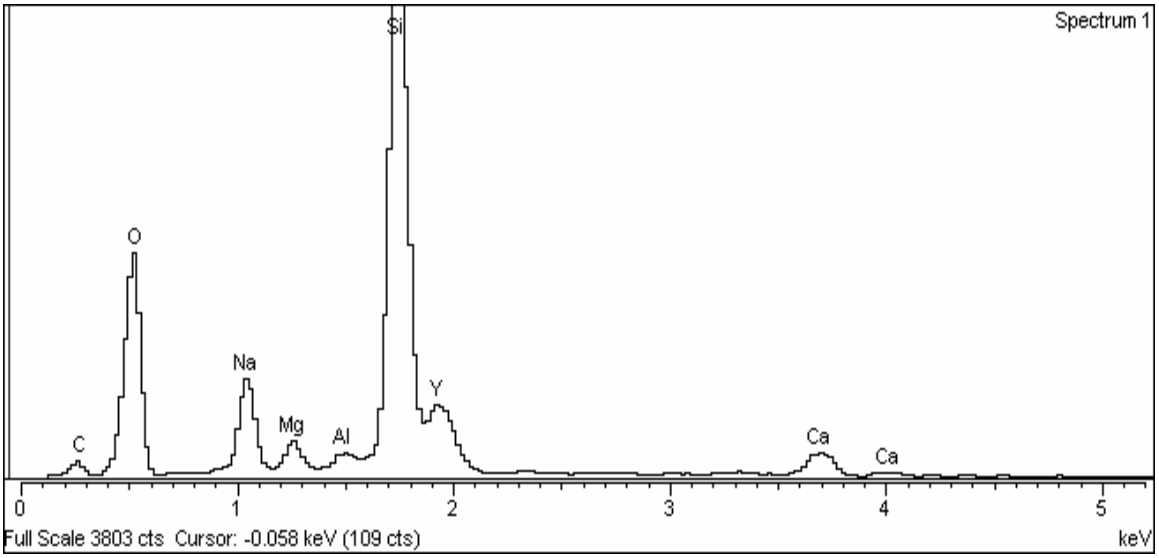

Figure V-21. EDS Analysis of Tube Y22 – Spectrum 1

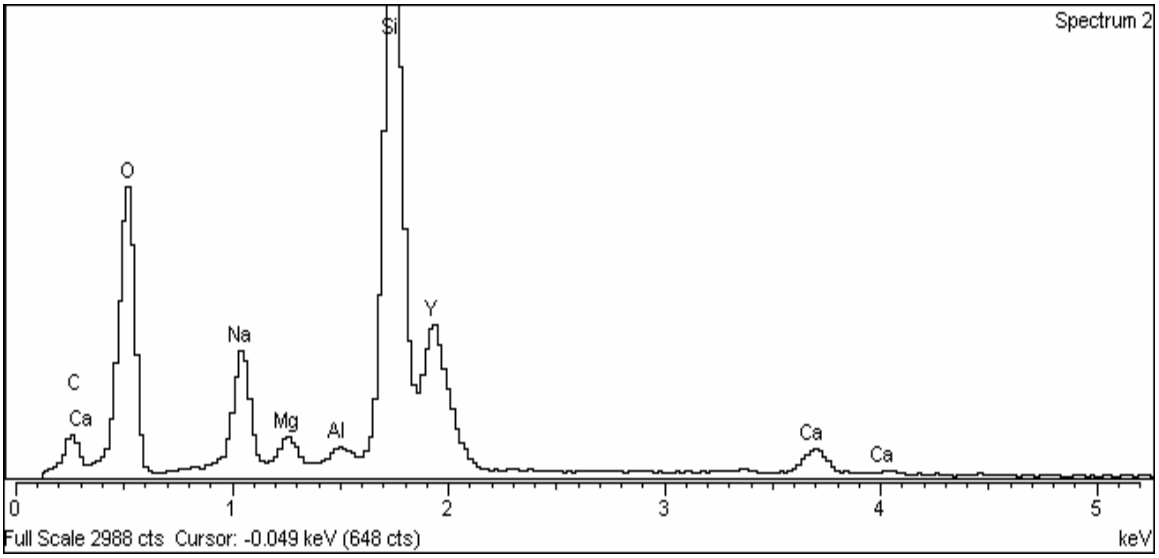

Figure V-22. EDS Analysis of Tube Y22 – Spectrum 2

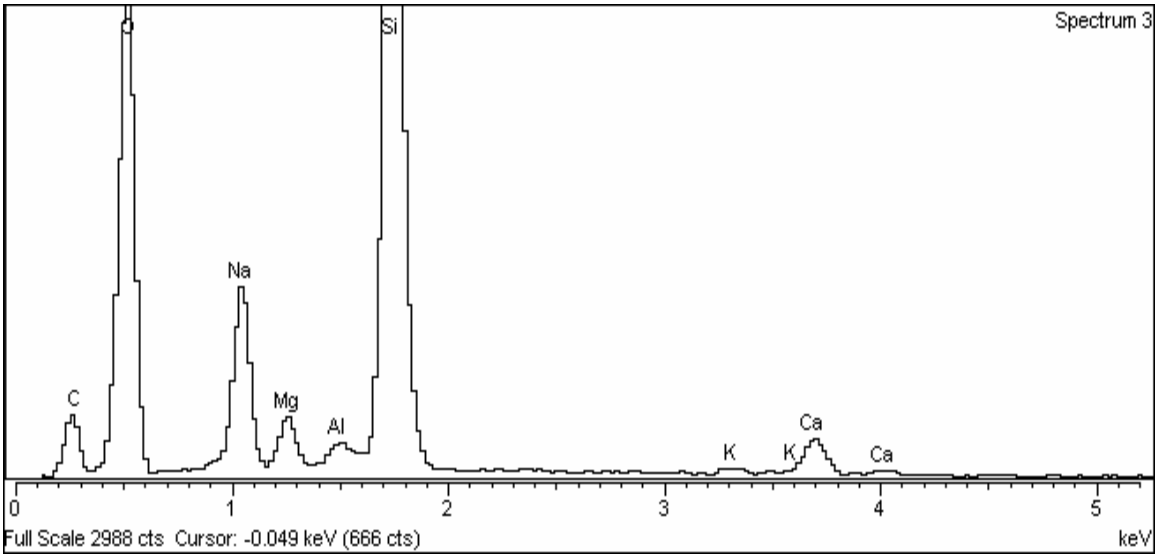

Figure V-23. EDS Analysis of Tube Y22 – Spectrum 3

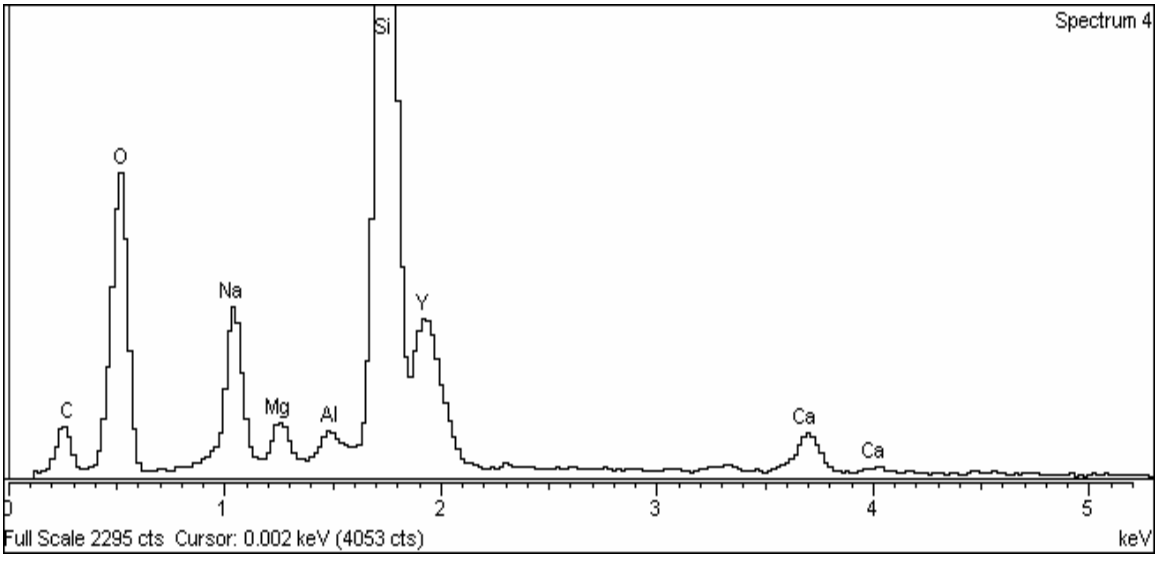

Figure V-24. EDS Analysis of Tube Y22 – Spectrum 4

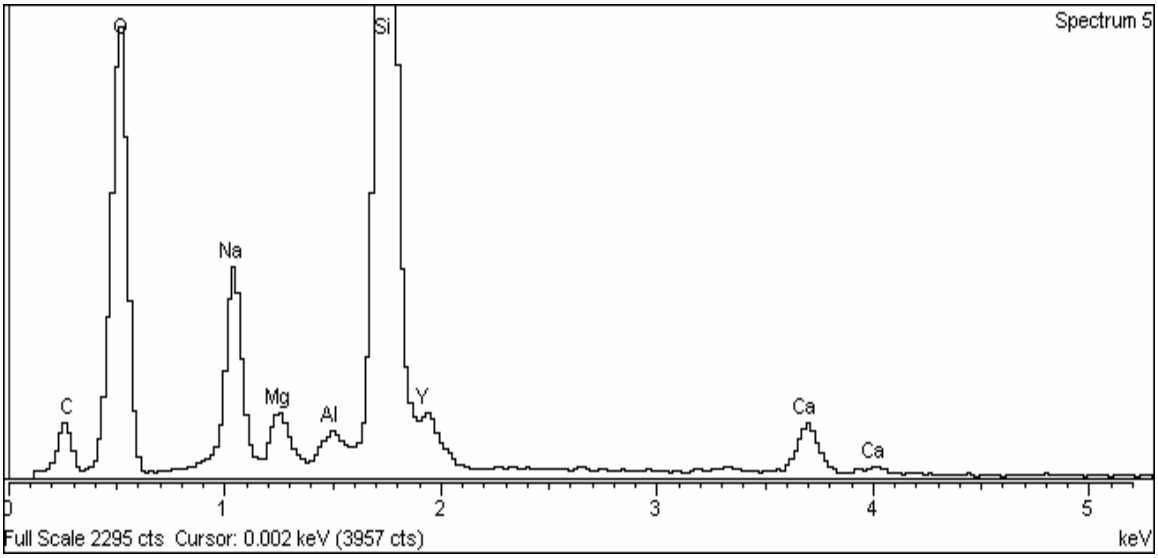

Figure V-25. EDS Analysis of Tube Y22 – Spectrum 5

8. Clear versus Cloudy Regions

The clouded sections of the post deposition tubes appear either before (to the left of) or within the coil region. No clouded sections have been detected after (or to the right of) the coil area.

Figures V-26 and V27 demonstrate SEM analysis of clear and cloudy sections of the interior of tube Y22. Both sample areas are located at twenty one inches from the beginning of the tube and are within the coil region. These two sample locations are right next to each other. The morphology of the clear and cloudy areas appears different. The clear area film is more continuous while the cloudy area film seems to be cracked. Both areas exhibit particulates that don't appear to be part of the film.

Figure V-26 confirms that an yttrium containing thin film can be deposited on the interior surface of a glass tube without clouding the glass.

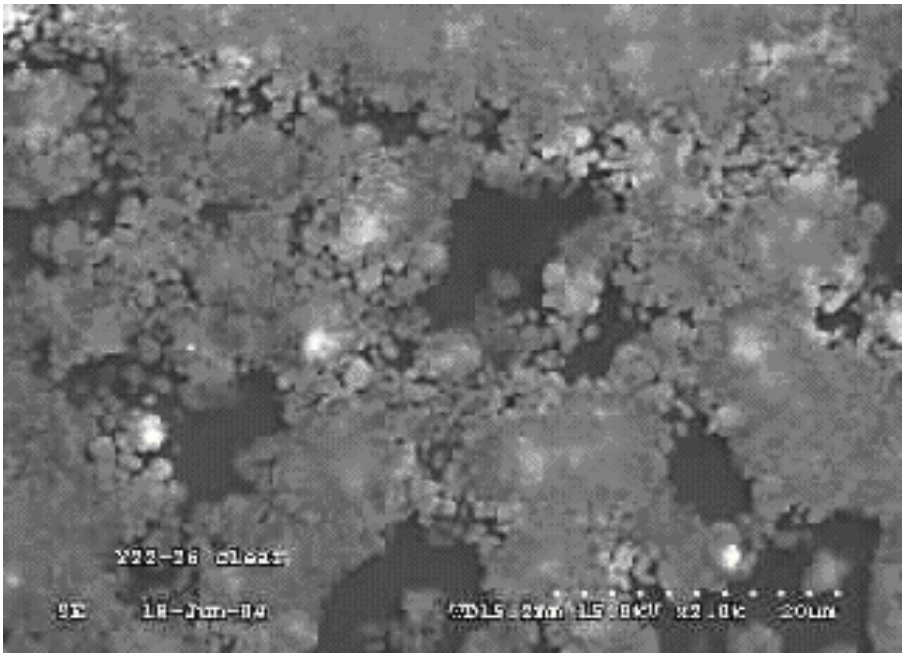

Figure V-26. Clear Section of Y22

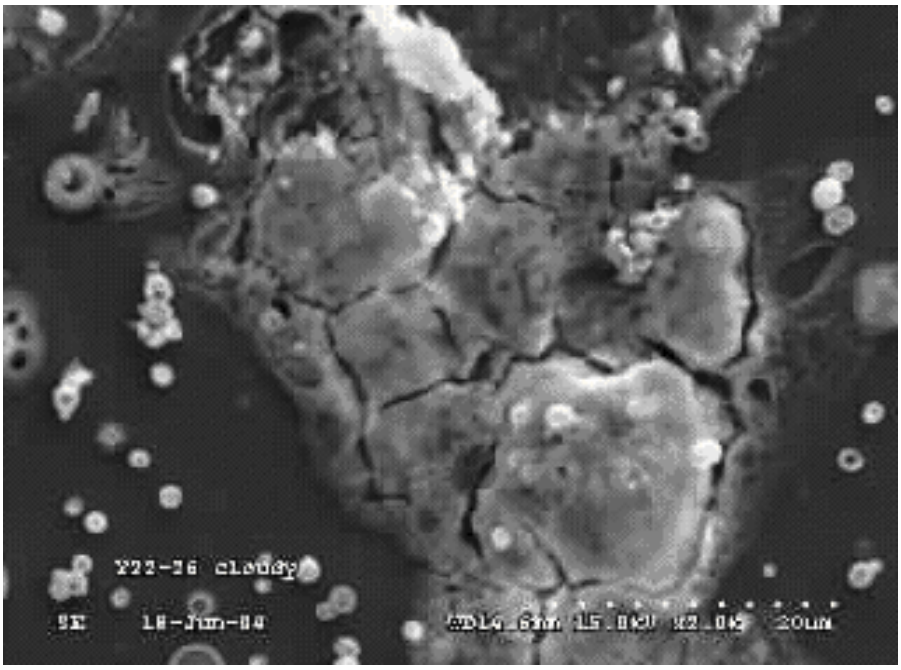

Figure V-27. Cloudy Section of Y22

9. FTIR Analysis

Since the coatings for each tube displayed cloudy regions and clear regions, FTIR analysis was conducted for representative regions, i.e., cloudy and clear. The designations of the samples are such that the number after the Y# is the distance measured from one end of the tube. For example, Y22 has two regions and three samples. Y22-2 (Clear) indicates that the sample was taken from a portion of the tube which is two inches away from the specified end and is clear by visual inspection. Y22-21 (Clear) indicates that the sample was taken from another portion of the tube which is twenty one inches from the specified end and is clear. Y22-17 (Cloudy) indicates that the sample was taken from another portion of the tube which is seventeen inches from the specified end and is cloudy.

FTIR analysis of tubes Y20 through Y24 was performed to determine the chemical bonding. In this study the main interest is to see if yttrium nitrate is present in the coatings. FTIR-ATR spectroscopy is a technique that can measure individual components in a mixture.[13] FTIR-ATR spectra were obtained for Y20-24 samples, as well as a control sample without any coatings, by using an ATR cell on the yttrium coated glass along with the uncoated glass to investigate the structural change near the surface of the glass.[14]

In Figure V-28 a spectrum for Y22-17 (Cloudy) is shown. The peaks between 1500 and 1700 cm^{-1} correspond to nitrate peaks. Presumably, the deposits are not completely reacted in the plasma. The ultimate goal would be to eliminate nitrate precursor material in the coatings. In the same figure, Y22-2 (Clear) spectrum is also shown and the peaks are not visible. The desired result is a chemical reaction that eliminates nitrogen from the precursor $Y(NO_3)_3$ leaving only yttrium and oxygen present in a yttrium oxide film. If nitrogen is present then the coatings would be the precursor deposited without the chemical reaction or with little reaction.

Figure V-28 demonstrates the FTIR analysis of tube Y22 at two different locations. Both ESCA and FTIR analysis detected no coating at the two inch location (Y22-2 Clear) so it can be used as a control. The Y22-17 (Cloudy) curve shows the presence of nitrate indicating no conversion to oxide. ESCA analysis of the same area detected no nitrate.

This suggests that the top surface layers were converted to oxide. The manner in which the precursor was delivered to the plasma region is probably the reason for this. Refer to the Process Control section on page 95. A large amount of precursor was first dumped into the plasma region resulting in deposition of nitrate without conversion to oxide. The precursor flow valve was then shut almost completely off allowing the intensity of the plasma to increase. It is at this time that the top surface layers of the deposit were probably converted to oxide.

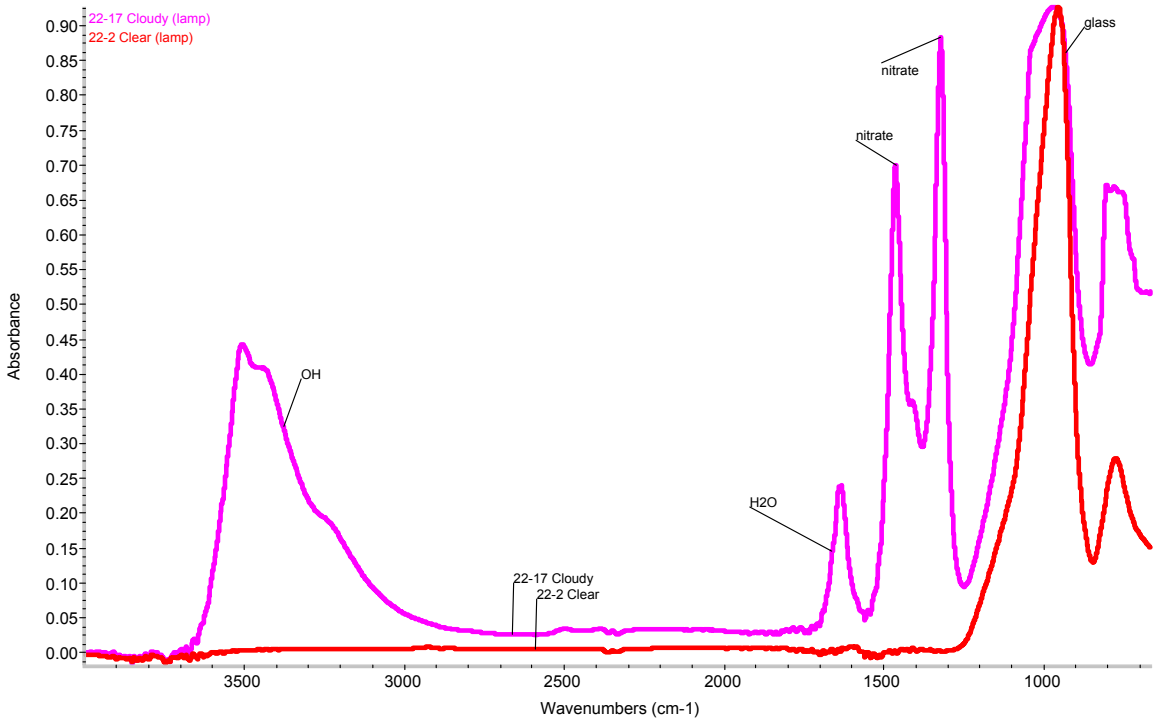

Figure V-28. FTIR (ATR Mode) Results of Tube Y22

Figure V-29 illustrates the difference among several coatings. The nitrate peaks for Y21, Y23, and Y24 are less visible. For the Y22 (Clear) sample, the nitrate peaks are not visible. Presumably, the Y22 (Clear) sample has a very thin layer of yttrium oxide. The postulation would be that the plasma is able to convert the precursor nitrate into the oxide. Although the ESCA analysis of tube Y22-21 (Clear) showed a small amount of

yttrium, FTIR analysis showed no evidence of a coating. The two analysis techniques have different sampling depths which is most likely the reason for the discrepancy.

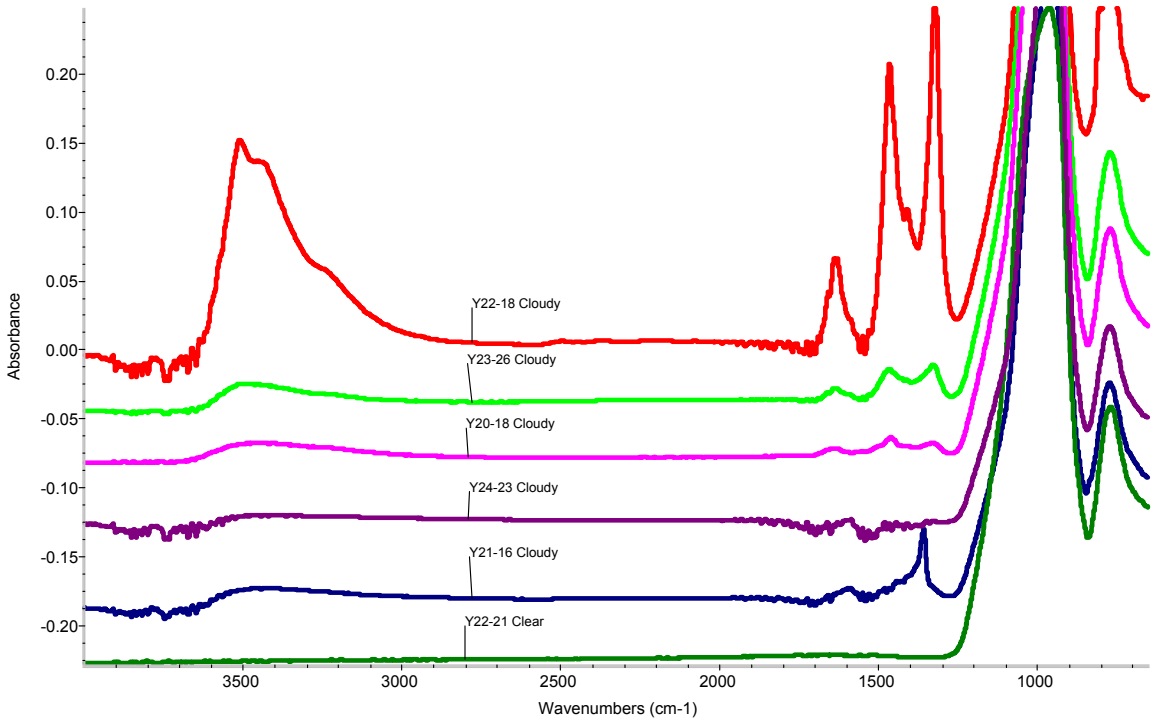

Figure V-29. FTIR (ATR Mode) Results of Other Tubes

E. Aluminum Containing Films

The high content of aluminum in the chemical makeup of the glass makes analysis of aluminum oxide films difficult. SEM micrographs show the presence of a deposit but this analysis is inconclusive.

Table XIV demonstrates that the aluminum content of a cloudy section of tube number Al1 is four percent. This increase is ten times that of the four tenths of a percent content in the control sample. Table XIV also reveals a slight increase in oxygen content which is larger than the sixty three percent content of the control sample. This would tend to indicate the presence of an aluminum containing film.

An examination of the plasma treated glass tubes in Table XII reveals that exposing the glass to plasma (without a precursor) results in as much as a sixty eight percent oxygen content. Therefore, the increase in oxygen content for Al1 could be caused by either the plasma or the formation of an aluminum containing film. Therefore, the presence of an aluminum containing film on the interior surface of Al1 can't be confirmed.

F. Plasma Treated Glass Tubes

In an attempt to determine the effects of plasma on the atomic composition of the glass tubes, experiments were run without introducing a precursor to the plasma area. Table XV11 demonstrates the ESCA analysis of six tubes exposed to plasma for various time periods. These experiments were performed using both ten and fifteen percent RF power. A comparison of these results and the control sample demonstrates that the composition of the glass changes after exposure to plasma.

Figures V-30 and V-31 demonstrate the change in the silicon content of a glass tube exposed to plasma for thirty minutes at ten and fifteen percent RF power respectively. The control value is nineteen percent silicon.

Figures A-1 through A-10 beginning on page 105 in the appendix demonstrate the effect of plasma on the other elements in the chemical makeup of the glass tubes.

Table XVI. ESCA Analysis - Interior Surface of Various Samples

Analysis Method: ESCA \ SNMS

				ESCA- Atomic Composition of Surface(%)						
Sample	**RF Power (%)**	**Precursor**	**Deposition Time**	**Si**	**O**	**Na**	**Mg**	**Ca**	**Al**	**Y**
Control	N/A			19	63	14	1.3	1.1	0.4	ND
Y2	14	25g Y-nitrate/l	30 min	26	68	5	1			ND
Y3	20	25g Y-nitrate/l	30 min	27	72	1.2	ND			ND
Y4	25	25g Y-nitrate/l	30 min	28	71	0.9	ND			ND
Y5	25	25g Y-nitrate/l	30 min	27	69	2.8	0.6	0.9		ND
Y6	20	25g Y-nitrate/l	30 min	23	63	11	1.5	1.1		ND
Y7	30	25g Y-nitrate/l	30 min	24	64	9.2	1.3	1.3		ND
Y8	20	50g Y-nitrate/l	30 min	24	65	8.1	1.2	1.2	0.5	ND
Y9	25	50g Y-nitrate/l	30 min	22	65	10	1.3	1.2	0.5	ND
Y10	15	50g Y-nitrate/l	30 min	23	66	8.3	1	1.1	0.5	ND
Al1 Cloudy	30	25g Al-nitrate/l	30 min	18	67	5	1.5	1.2	4	ND
Al1 Clear	30	25g Al-nitrate/l	30 min	21	62	11	1.1	0.7	0.6	ND
Al2	25	25g Al-nitrate/l	30 min	25	66	6.1	1.1	1	0.4	ND
Al3	20	25g Al-nitrate/l	30 min	24	63	9.7	1.5	1.3	0.4	ND
A14	15	50g Al-nitrate/l	15 min	23	64	9.3	1.5	1.1	0.4	ND
A14 Cloudy	15	50g Al nitrate/l	15 min	27	69	2.1	0.7	0.9	0.3	ND
A15	20	50g Al nitrate/l	15 min	23	65	9.5	1.2	1.2	0.5	ND
A16	25	50g Al nitrate/l	15 min	23	65	9.3	1.2	1.2	0.4	ND
A17	25	50g Al nitrate/l	30 min	24	65	7.2	0.6	1	0.4	ND
A18	20	50g Al nitrate/l	30 min	23	66	8.1	0.8	1.1	0.3	ND
A19	15	50g Al nitrate/l	30 min	24	68	5.2	0.9	1.1	0.4	ND

Table XVII. Plasma Treated Glass Tubes

Atomic Composition of Interior Surface (%)

Sample	Si	O	Na	Mg	Ca	Al
P1 10% RF,10 Min	24	66	8.0	0.7	0.9	0.2
P2 10% RF,20 Min	24	65	8.5	1.2	1.0	0.3
P3 10% RF,30 Min	25	66	7.1	1.0	1.0	0.2
P4 14% RF,10 Min	27	68	4.4	0.4	0.7	0.3
P5 14% RF,20 Min	25	67	5.9	0.9	1.0	0.4
P6 14% RF,30 Min	27	68	3.5	0.5	0.8	0.3
Control	19	63	14	1.3	1.1	0.4

Note: ND indicates that the element was scanned but was not detectable.

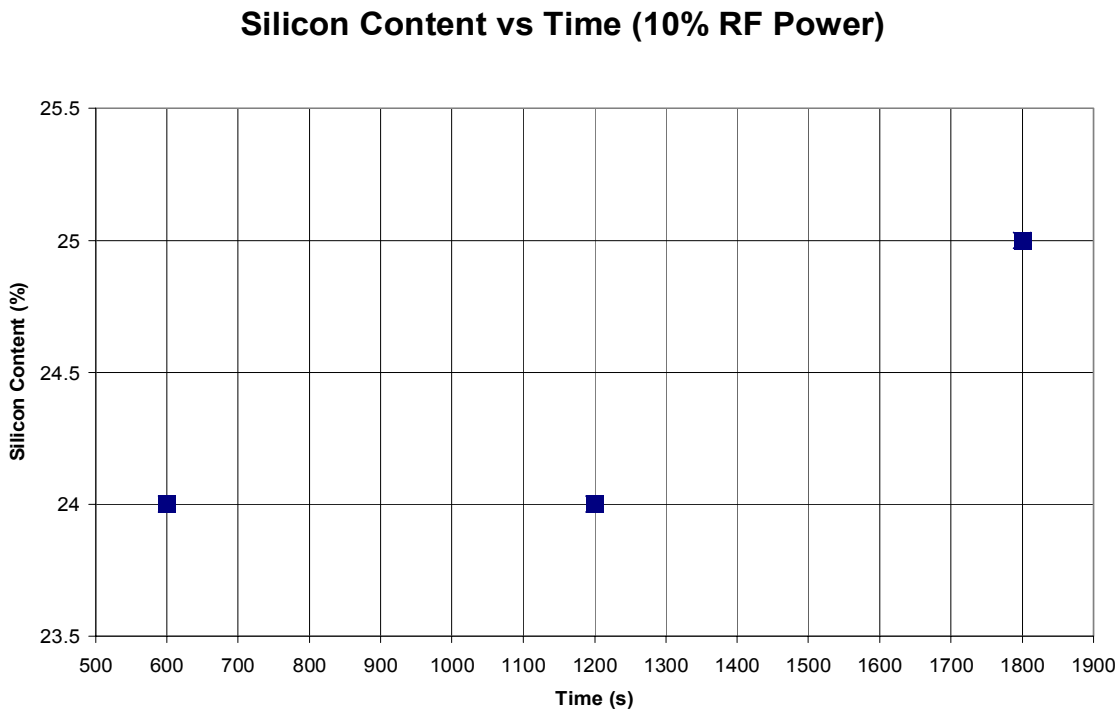

Figure V-30. Silicon Content vs Time (10% RF Power)

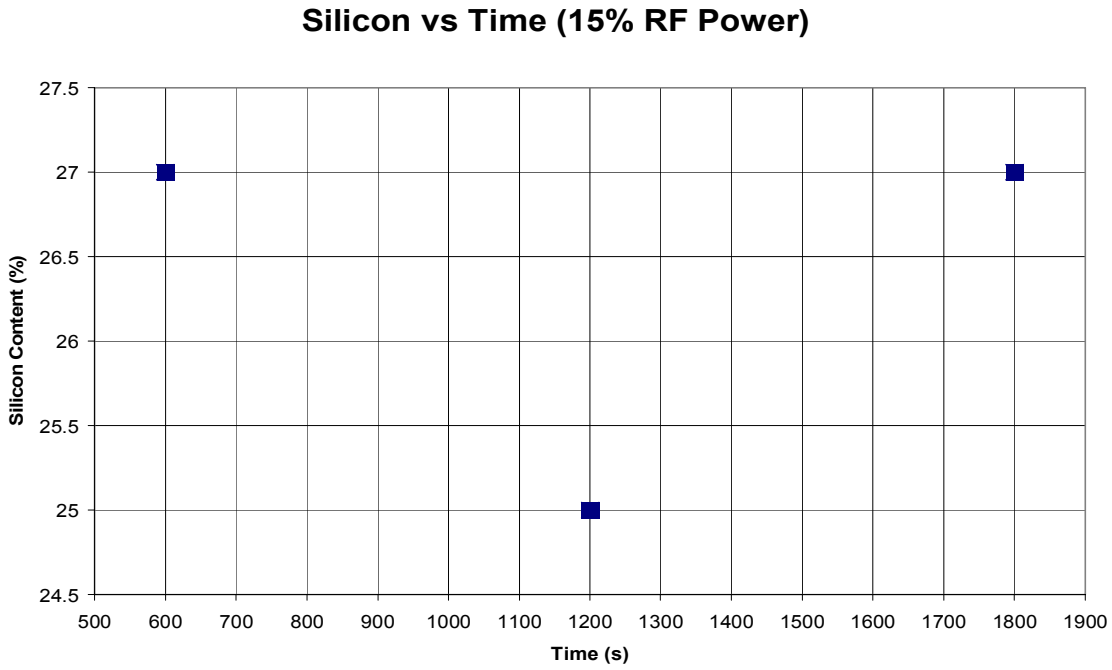

Figure V-31. Silicon Content vs Time (15% RF Power)

1. Weatherization of Glass Tubes

After a period of exposure to the atmosphere, the interior of the glass tubes appear to have a coating on them. This is due to weatherization of these tubes which involves the formation of water soluble sodium carbonate and sodium sulfate. This is powder which is formed by water vapor reacting with the glass surface. This reaction involves the exchange of H+ ions for Na+. This is followed by surface Na+ reacting with CO_2 and SO_2. This process takes several weeks to occur and the tubes shouldn't be used for experiments afterwards.

G. Process Control

Figure V-32 is a diagram of a section of the RF vacuum deposition system. Switch 1 is the electrical on/off switch for the nebulizer and Valve 1 is the mechanical valve for precursor flow control. Figure V-33 on the next page demonstrates the deposition procedure used in experiments Y20 through Y25. The tops of the curves represent the valve completely open or the switch on. The bottoms of the curves (horizontal axis) represent the valve completely closed or the switch off.

After starting the RF generator, Valve 1 was opened so as to allow Ar into the glass tube. Once a sufficient amount of Ar was present a glow discharge formed. This procedure is demonstrated in figure V-33 to the left of the vertical axis. Once a glow discharge was established the nebulizer power was set to one hundred percent and Switch 1 was turned on. This is shown in figure V-33 to the right of the vertical axis. With Valve 1 completely open and the nebulizer running the intensity of the plasma was greatly diminished. Valve 1 was then turned almost completely off and the intensity of the plasma increased. During the time the valve was almost closed the aerosol mist in the nebulizer chamber accumulated. After an amount of time passed, the coil region of the glass tube intensified to a bright white. At this time Valve 1 was opened completely and the contents of the nebulizer chamber was dumped into the plasma. This procedure was repeated numerous times during the deposition experiments.

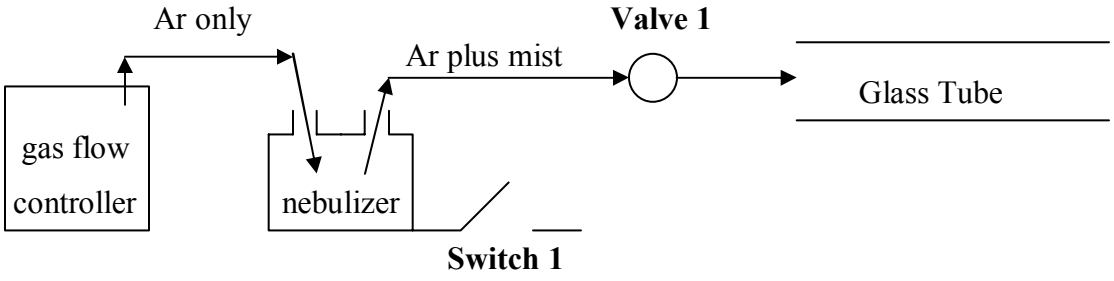

Figure V-32. Carrier Gas Control

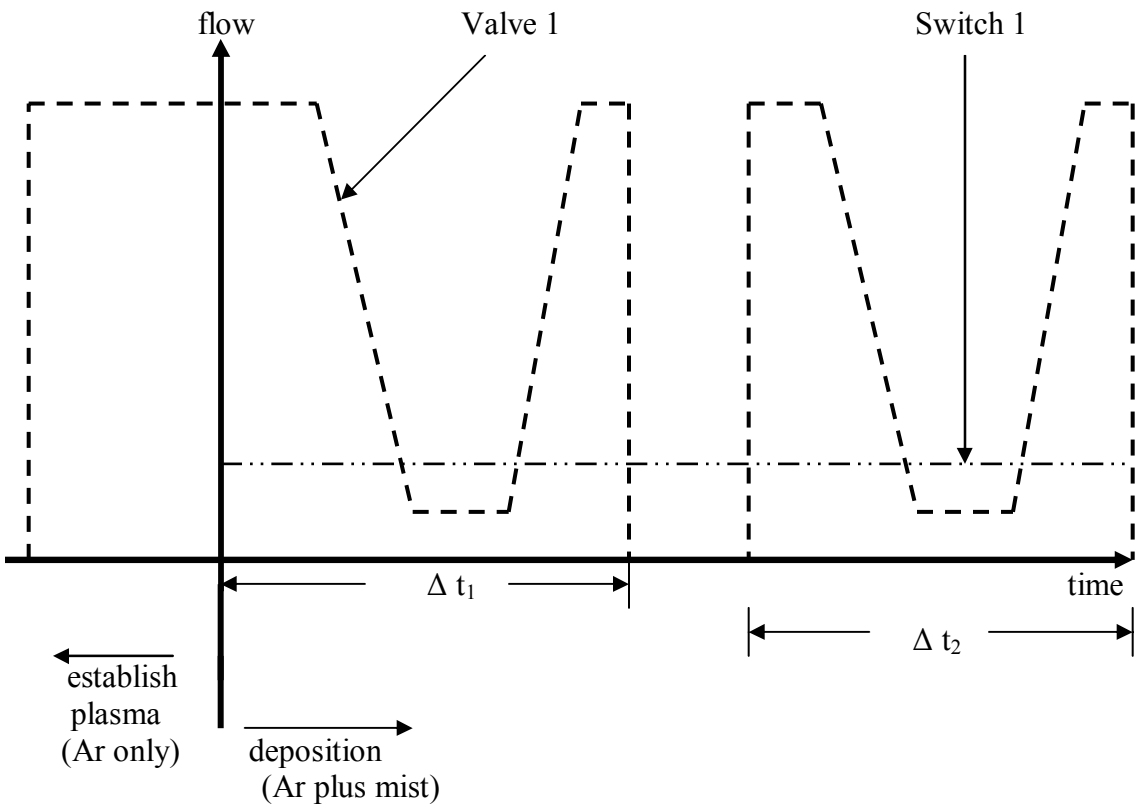

Figure V-33. Process Control

Results indicate that the morphology of the deposited films differed between experiments even though the deposition parameters were the same. The graph shown in Figure V-34 provides a possible explanation for the inconsistencies. The curves Y20, Y21, and Y22 represent the operation of the precursor flow valve for that particular experiment. The amount of time the precursor flow valve was opened and closed for each experiment was different. In addition, the degree to which the valve was open was probably different for each experiment.

Table XVIII shows the deposition conditions for each experiment.

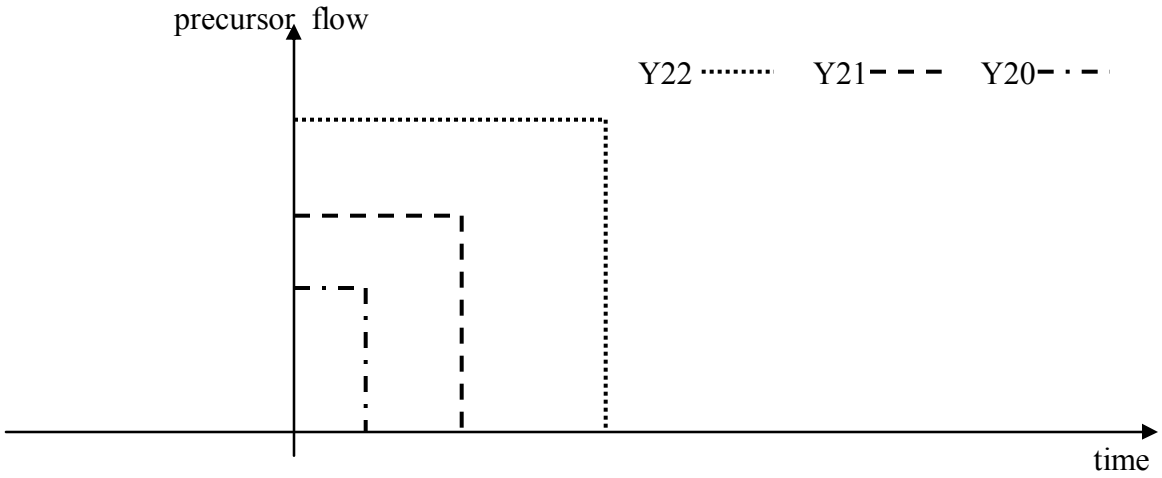

Figure V-34. Precursor Flow vs Time

Table XVII1. Process Conditions

Glass Tube #	Solution Concentration	Nebulizer Power (%)	RF Power (%)	Time (minutes)
Y1	25 g/l	60	30	10
Y2	25 g/l	60	14	30
Y3	25 g/l	100	20	30
Y4	25 g/l	100	25	30
Y5	25 g/l	100	25	30
Y6	25 g/l	100	20	30
Y7	25 g/l	100	30	30
Y8	50 g/l	100	20	30
Y9	50 g/l	100	25	30
Y10	50 g/l	100	15	30
Y11	100 g/l	100	20	7
Y12	100 g/l	100	25	7
Y13	100 g/l	100	30	7
Y14	100 g/l	100	15	7
Y15	100 g/l	100	20	12
Y16	100 g/l	100	35	12
Y17	100 g/l	100	35	14
Y18	100 g/l	100	30	4
Y19	100 g/l	100	30	6
Y20	25 g/l	100	25	5
Y21	25 g/l	100	25	5
Y22	25 g/l	100	25	5
Y23	25 g/l	100	25	8
Y24	25 g/l	100	25	8
Y25	25 g/l	100	20	8
Al 1	25 g/l	100	30	30
Al 2	25 g/l	100	25	30
Al 3	25 g/l	100	20	30
Al 4	50 g/l	100	15	15
Al 5	50 g/l	100	20	15
Al 6	50 g/l	100	25	15
Al 7	50 g/l	100	25	30
Al 8	50 g/l	100	20	30
Al 9	50 g/l	100	15	30
Al 10	100 g/l	100	15	7
Al 11	100 g/l	100	20	7
Al 12	100 g/l	100	25	7
Al 13	100 g/l	100	30	7
Al 14	500 g/l	100	25	15
Al 15	500 g/l	100	40	7

VI SUMMARY AND CONCLUSIONS

The atmospheric RF thin film deposition system was modified to work as a vacuum system. The current problems with the vacuum system are mostly related to the quality of the equipment and materials being used. These problems include a gas flow controller and a nebulizer not designed to operate in a vacuum. Another problem is the fittings and tubing that deform when exposed to the high temperatures required to deposit thin film.

The types of coatings deposited with the new system include silicon dioxide, yttrium containing, and possibly aluminum containing. Although the coatings deposited with this system were not continuous thin films, it is believed that the process can be refined to accomplish that.

Experiments involving tubes Y1 and Y20 through Y25 demonstrate that the objective of this study has been accomplished.

VII FUTURE WORK

Future work with this system should include the replacement of the existing vacuum pump with one capable of creating a better vacuum. The addition of a vacuum pressure gauge should also be included. A more complete temperature profile with an optical pyrometer is also needed.

The PVC inlet and outlet fittings and tubing should be replaced with high temperature resistant ceramic material. The PVC precursor delivery valve should be replaced with one capable of more refined control.

The gas flow controller should be replaced with one designed to work in a vacuum. A gas flow meter should also be added to the system so that flow rates can be more accurately measured.

Consideration should also be given to the idea of adding a second nebulizer in series with the existing one. This would allow more precursor to enter the plasma region.

A mechanical method of translating and rotating the glass tubes during deposition is needed. This will probably help in producing a continuous coating on the interior surface of the glass tubes.

REFERENCES

1. D. J. Hunt, "RF Plasma Deposition of Magnesium – Aluminum Oxide"; M.S. Thesis. Alfred University, Alfred, NY, 1998.

2. J. A. A. Williams, "RF Aerosol Mist Plasma Deposition of Tin Oxide Indium-Tin Oxide, and Silicon Oxide Thin Films on Float Glass"; M.S. Thesis. Alfred University, Alfred, NY, 1994.

3. B. G. Streetman, and B. SanJay, *Solid State Electronic Devices*; pp. 203-5. Prentice Hall, Upper Saddle River, NJ, 2000.

4. A. Schutze, J. Y. Jeong, S. E. Babayan, J. Park, G. S. Selwyn, and R. F. Hicks, "The Atmospheric-Pressure Plasma Jet: A Review and Comparison to Other Plasma Sources," *IEEE Trans. Plasma Sci.*, **26** [6] 1685-94 (1998).

5. J. McLaughlin, "Technological Plasmas" (2001) University of Ulster. Accessed on: May, 2003. Available at <http://www.engj.ulst.ac.uk/nibec/thinfilm/plasma.htm>

6. Lepel Technical Manual, Lepel High Frequency Induction Unit. Lepel Corporation, Edgewood, NY.

7. Devilbiss Instruction Manual, Ultra Neb 99 Ultrasonic Nebulizer, Devilbiss Health Care, Somerset, PA.

8. J. Klesel, "Using a Vacuum" (2003) Iowa State University. Accessed on: July, 2004. Available at <http://mse.iastate.edu/microscopy/vacuum.html>

9. J. Klesel, "Beam's Path through the Column" (2003) Iowa State University. Accessed on: July, 2004. Available at <http://mse.iastate.edu/microscopy/path.html>

10. "Energy Dispersive Spectroscopy" (2000) Bess TESTLAB. Accessed on: July, 2004. Available at <http://www.besstestlab.com/eds.html>

11. S. S. Zumdahl, and S. A. Zumdahl, *Chemistry*; pp. 471-8. Houghton Mifflin Company, New York, 2000.

12. Handbook of Chemistry and Physics, Vol. 57; pp. B86, B175. Edited by R. C. Weast. CRC Press, Cleveland, OH, 1976.

13. T. A. Barbari, "Physics and Astronomy: Atomic and Molecular Physics and Spectroscopy" (2000) John Hopkins University. Accessed on: July, 2004. Available at <http://www.stormingmedia.us/18/1874/A187483.html>

14. D. H. Lee, K. D. Vuong, R. A. Condrate Sr., and X. W. Wang, "FTIR Investigation of RF Plasma Deposited Indium-Tin Oxide Films on Glasses," *J. Mater. Res*., **11** [4] 901 (1996).

APPENDIX

Physical Properties and Chemistry of SG80 Lime Glass:

Composition (wt%)	SG80
SiO2	74.0
Na2O	16.4
K2O	0.3
CaO	4.6
MgO	3.3
Al2O3	1.4

Physical Properties	
Thermal Expansion	92.4
23-300°C (x 10-7/°C)	
Working Point (°C)	1018
Softening Point (°C)	700
Annealing Point (°C)	514
Strain Point (°C)	473
Electrical Resistivity (log ohm-cm)	
@ 250°C	6.4
@ 350°C	5.1
Density (g/cc)	2.47

Temperature Profile

time (s)	temp degrees C
20	119.7
40	130.8
60	135
120	142.3
180	144.8
240	149.1
300	152.2
360	153.2
420	154.8
480	156.5
540	158
600	157.8
660	159

Table XIX. Temperature Profile of First System

Plasma Treated Tubes

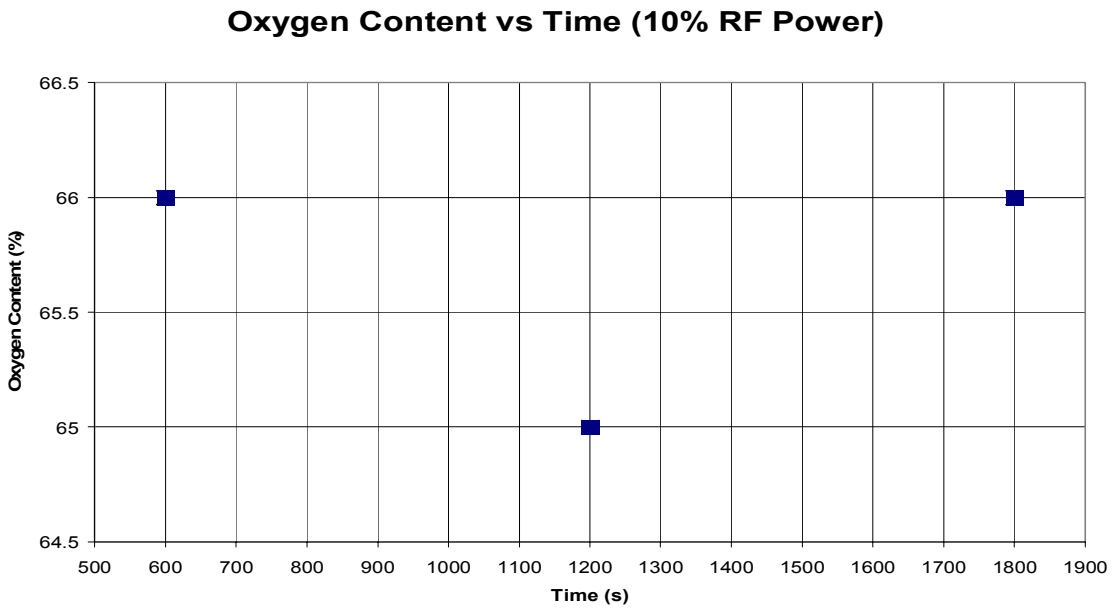

Figure A-1. Oxygen Content vs Time (10% RF Power)

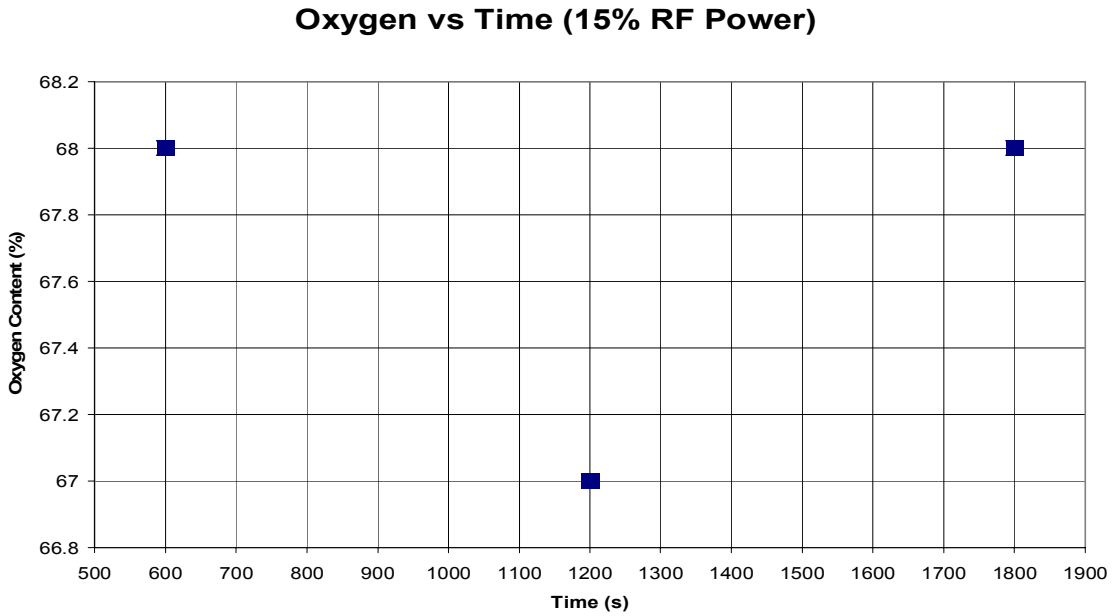

Figure A-2. Oxygen Content vs Time (15% RF Power)

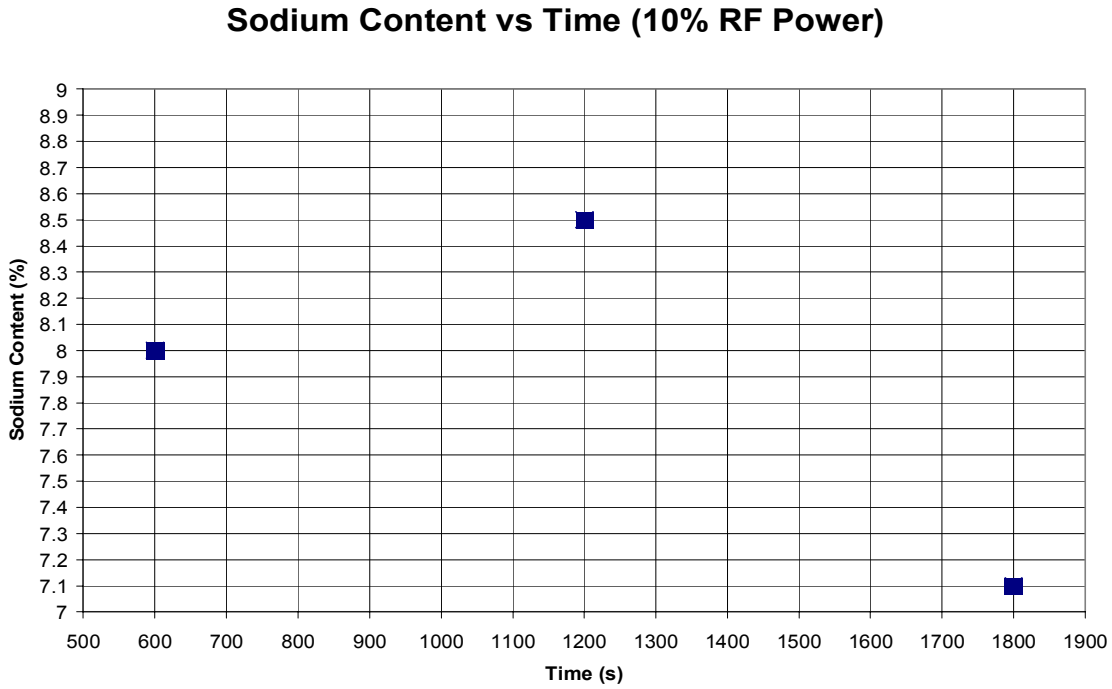

Figure A-3. Sodium Content vs Time (10% RF Power)

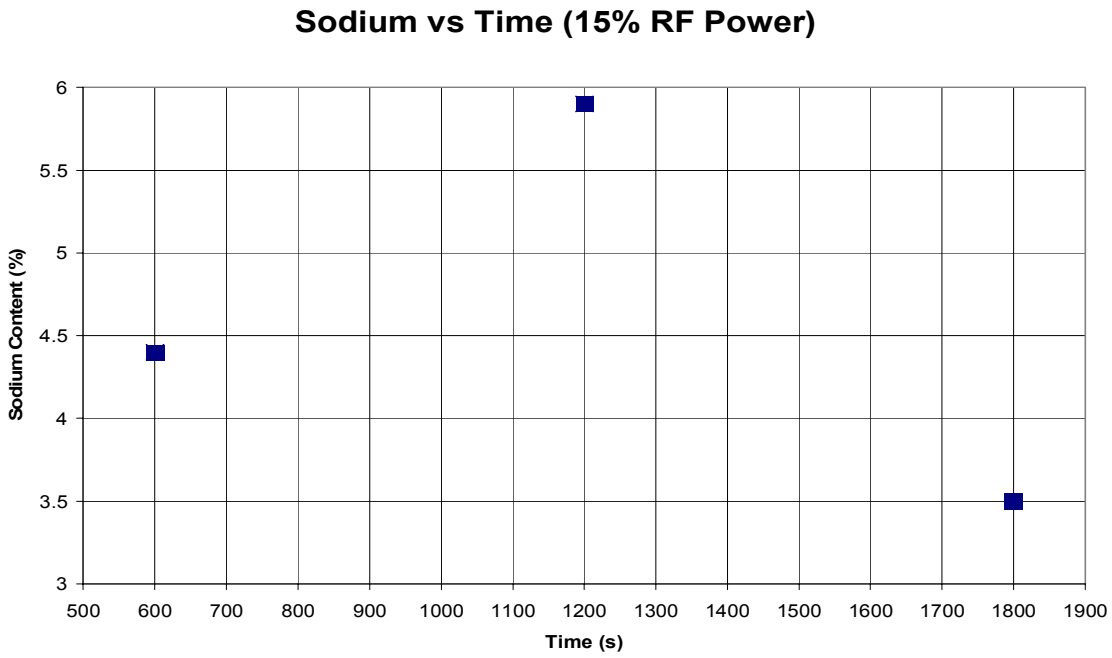

Figure A-4. Sodium Content vs Time (15% RF Power)

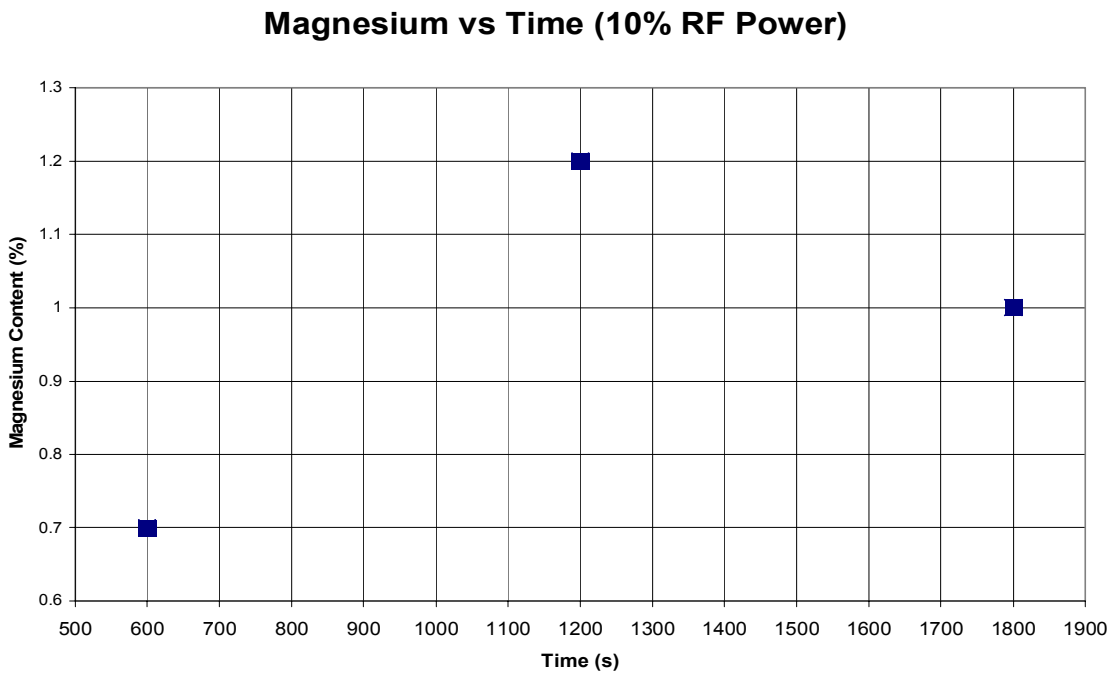

Figure A-5. Magnesium Content vs Time (10% RF Power)

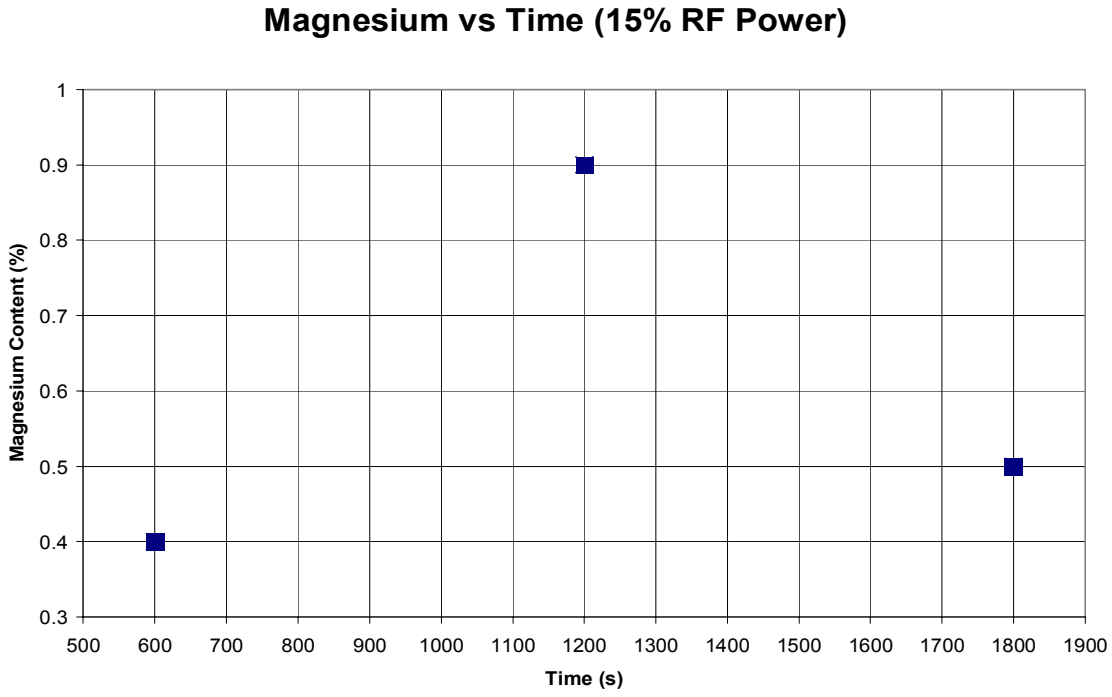

Figure A-6. Magnesium Content vs Time (15% RF Power)

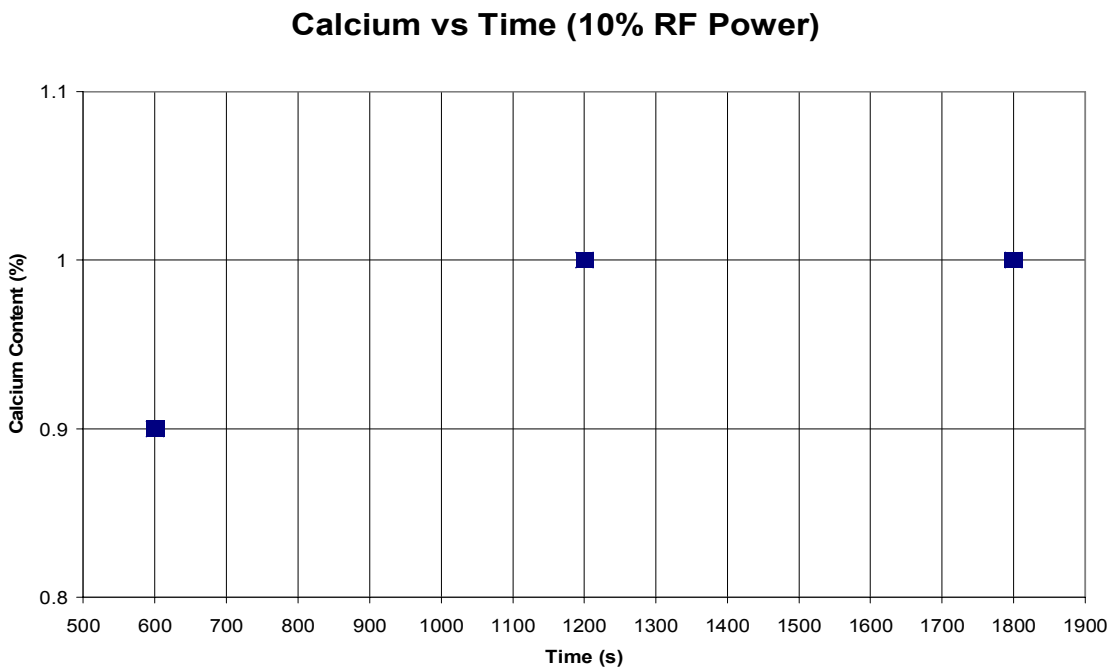

Figure A-7. Calcium Content vs Time (10% RF Power)

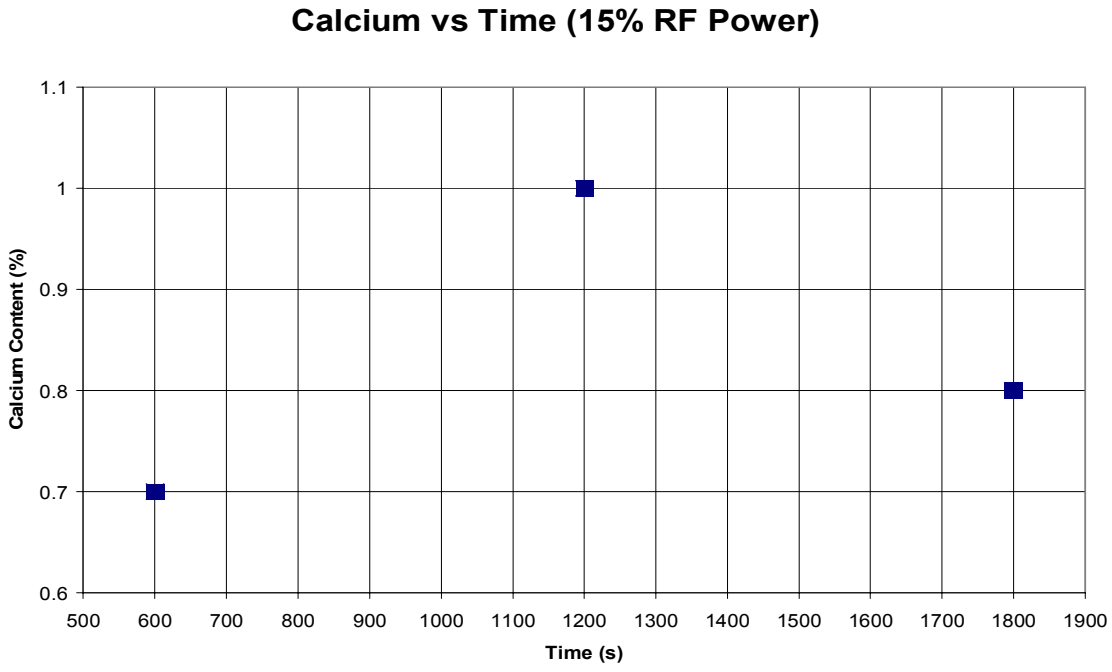

Figure A-8. Calcium Content vs Time (15% RF Power)

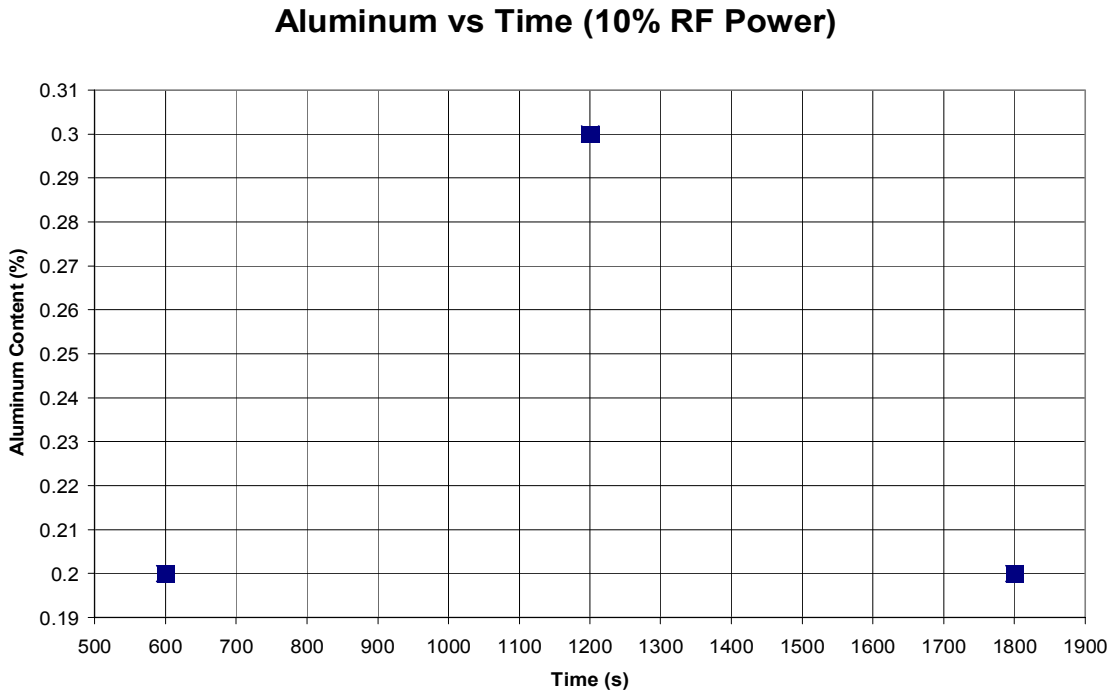

Figure A-9. Aluminum Content vs Time (10% RF Power)

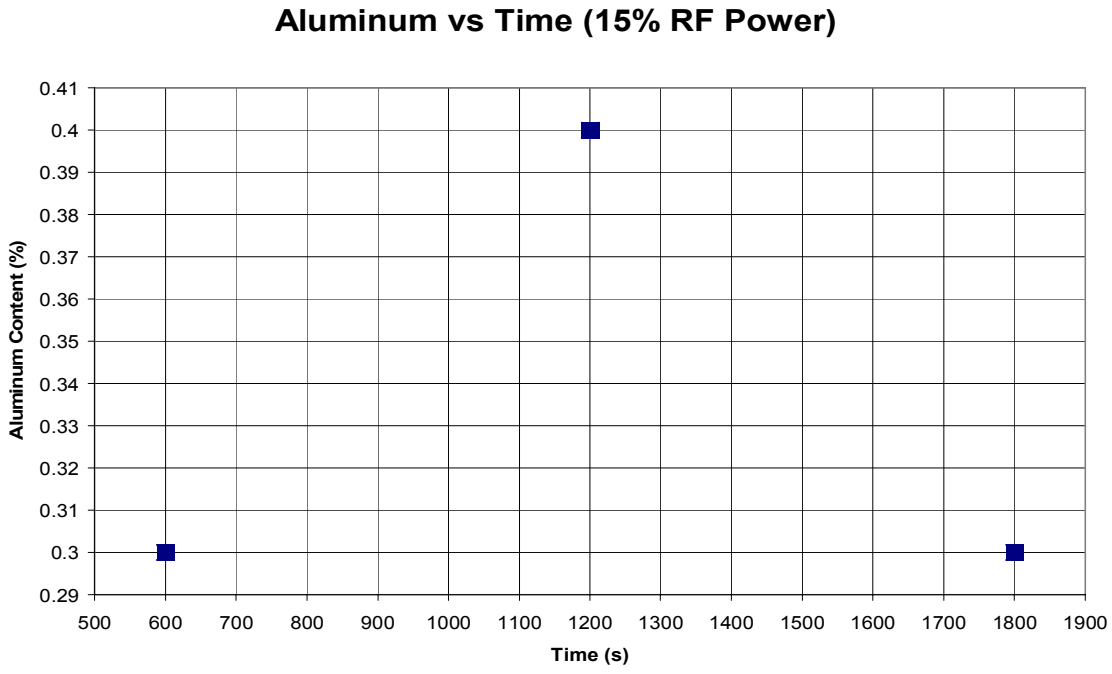

Figure A-10. Aluminum Content vs Time (15% RF Power)

To: Chris Norton

From: Erik Pavlina

Date: 22 January 2004

RE: SEM/EDS Analysis of Y15 Glass Tube

The inside surface of the Y15 glass tube was analyzed at two locations by SEM/EDS analysis. First, the inside surface of the middle section of the tube was analyzed. Visually, no surface layer or particles were observed. Due to the smoothness of the surface it was not possible to obtain a photomicrograph of this surface. EDS analysis also indicates that no yttrium-rich surface layer or particles are present (Figure 1).

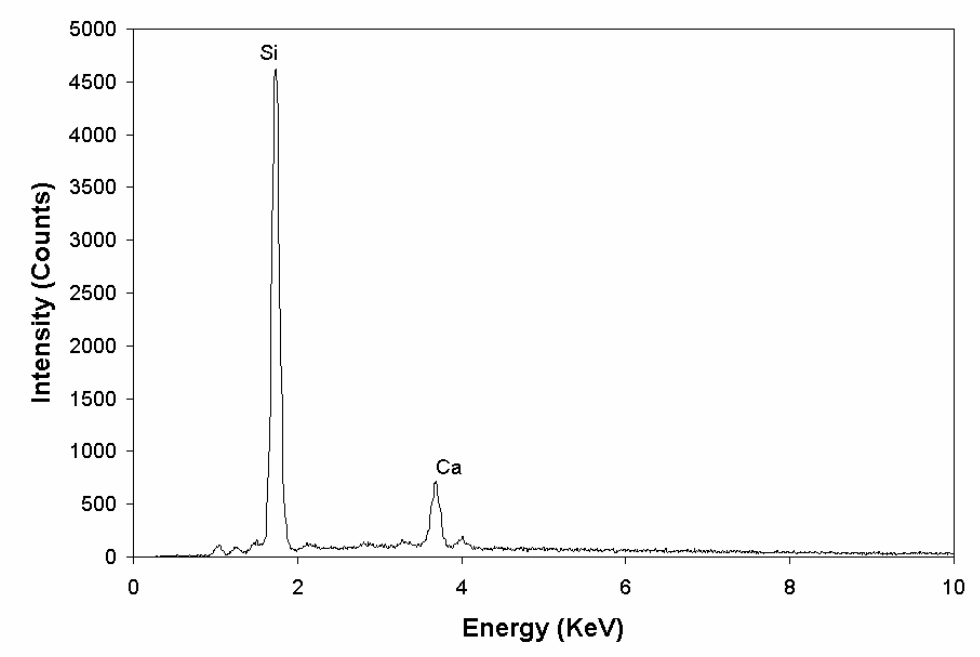

Figure 1 EDS spectra of the inside surface of middle of the Y15 glass tube.

The inlet end of the tube was also examined. Again, no surface layer or particles were detected. Yttrium was not detected by EDS analysis (Figure 2). The surface at this end

of the tube was rougher than in the middle of the tube and some surface topography was observed (Figure 3).

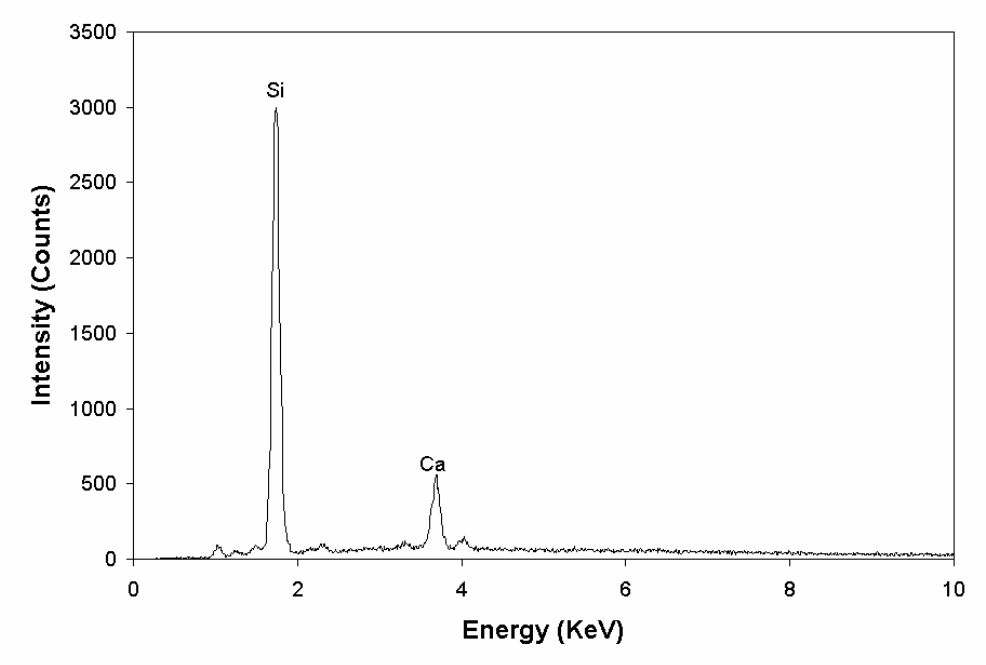

Figure 1 EDS spectra of the inside surface of the inlet of the Y15 glass tube.

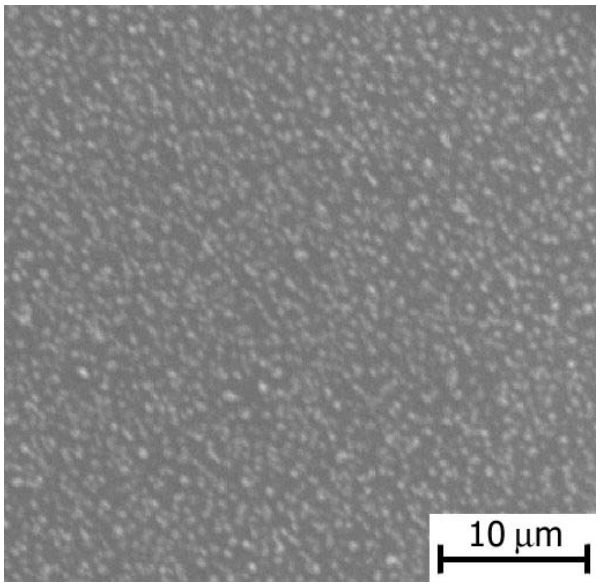

Figure 3 SEM photomicrograph of the inside surface of the inlet on the Y15 glass tube. Taken at 2000x.

To: Chris Norton

From: Erik Pavlina

Date: 21 January 2004

RE: SEM/EDS Analysis of Y1 Glass Tube

The inside surface of the sample Y1 was examined by SEM/EDS analysis. Spherical particles were present on the inside surface a foggy section of the glass tube (Figures 1-2). Incomplete coverage of the glass surface was observed. The spherical particles were yttrium rich (Figure 3). The silcon, aluminum, and calcium peaks are observed due to the interaction volume of the electron beam with the glass tube.

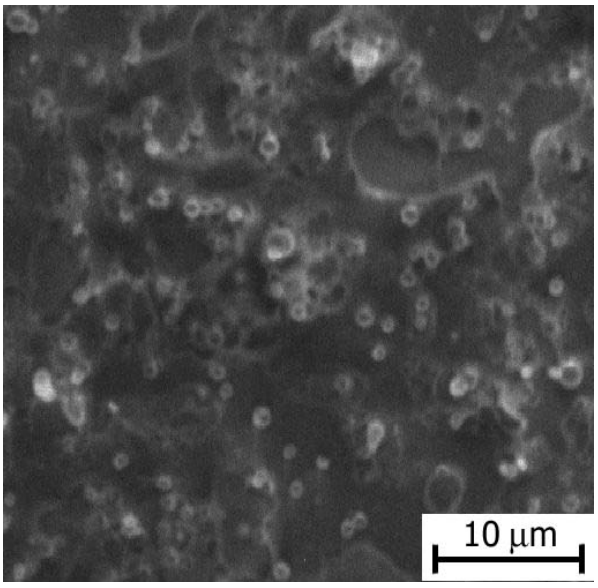

Figure 1 SEM photomicrograph of the inside surface of Y1 glass tube. Taken at 2000x.

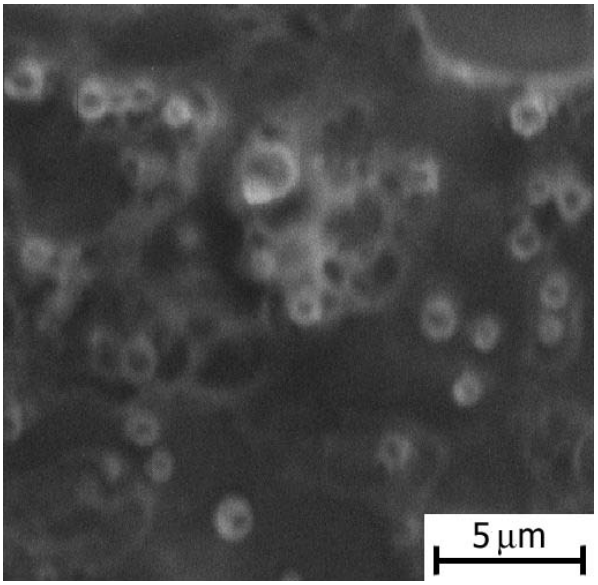

Figure 2 SEM photomicrograph of the inside surface of Y1 glass tube. Taken at 4000x.

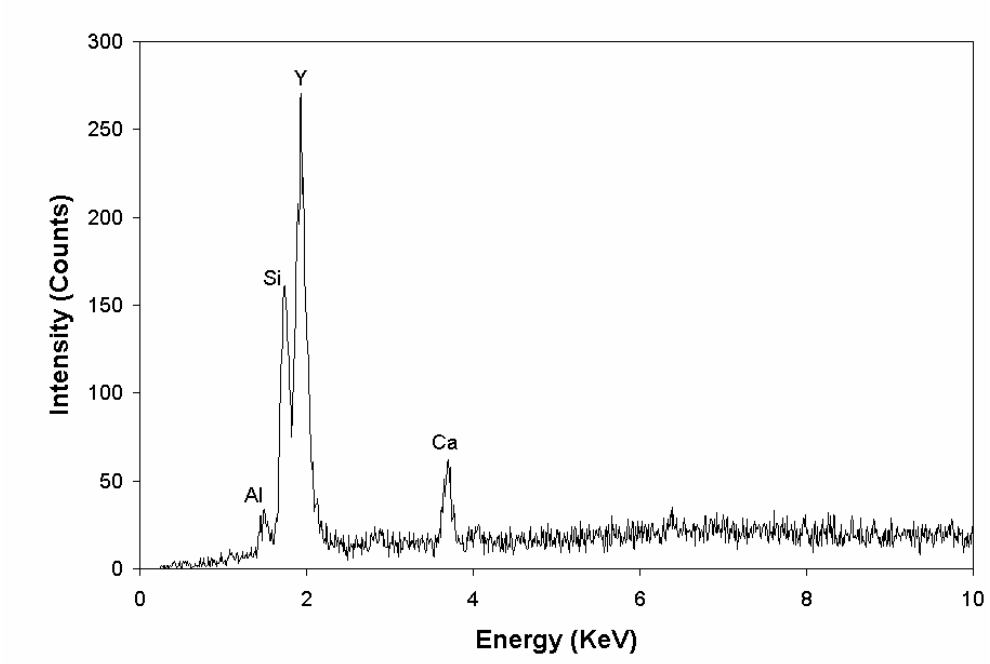

Figure 3 EDS spectra of spherical particles on the inside surface of Y1 glass tube.

To: Chris Norton

From: Erik Pavlina

Date: 29 January 2004

RE: SEM/EDS Analysis of Y16 Glass Tube

Sections of the Y16 glass tube were analyzed via SEM/EDS in order to determine if a yttrium coating is present on the inside surface of the tube. There was no yttrium detected at both the inlet of the precursor and in the middle of the tube length. Bright spots were observed at on the surface at the middle of the tube (Figure 1). EDS analysis indicates that these spots contain no yttrium (Figure 2). This surface contrasts with that of sample Y15 and an uncoated tube, both of which had a smooth surface at this location.

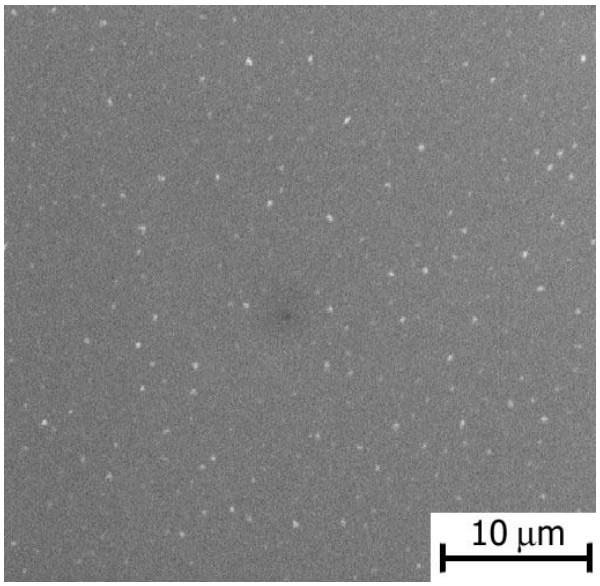

Figure 1 SEM photomicrograph of the inside surface at the middle of the Y16 glass tube. Taken at 2000x.

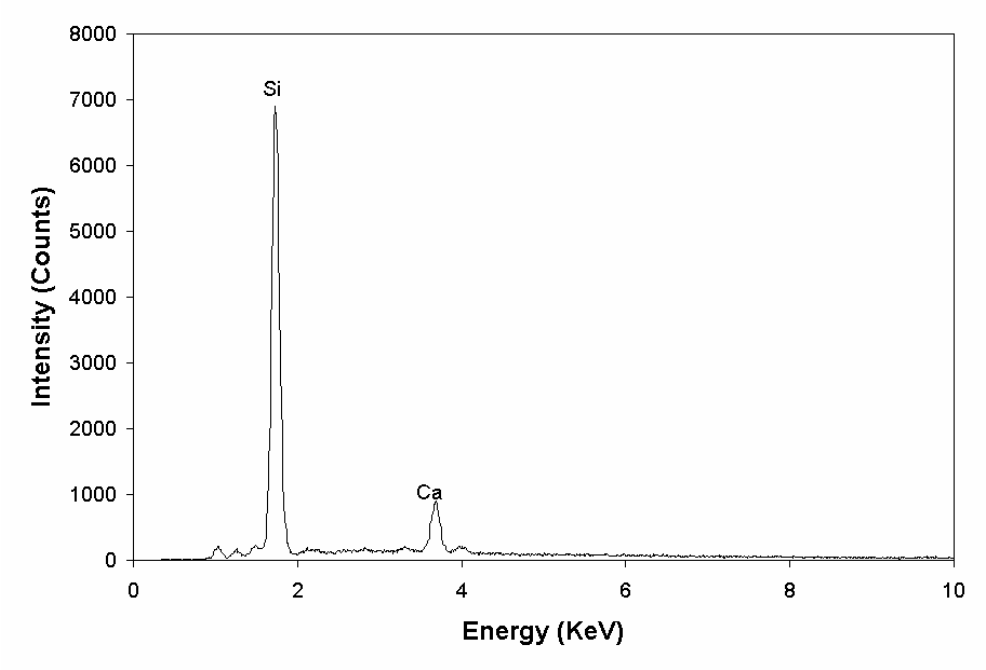

Figure 2 EDS spectra of a bright spot seen on the inside surface of the middle of the Y16 glass tube. Refer to the photomicrograph in Figure 1.

The inlet end of the tube was also examined. The surface at this end of the tube was rougher than in the middle of the tube and some surface topography was observed (Figure 3). Again, no surface layer or particles were detected. Yttrium was not detected by EDS analysis (Figure 4). The surface topography and features at this location of the tube are different than those observed on an uncoated tube (Figure 5).

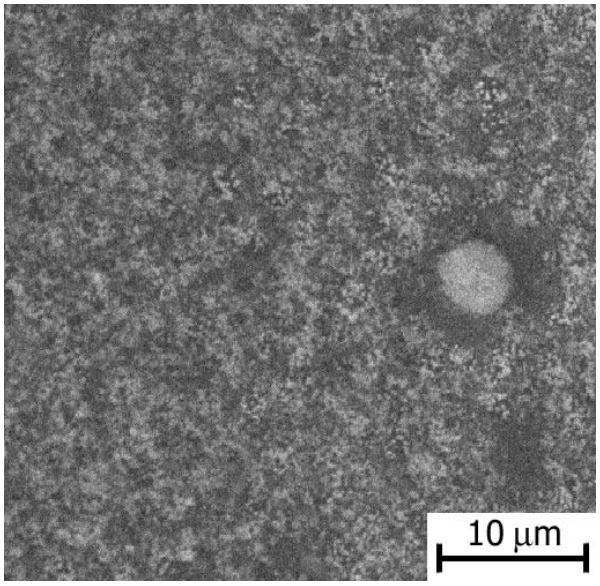

Figure 3 SEM photomicrograph of the inside surface of the inlet on the Y15 glass tube. Taken at 2000x.

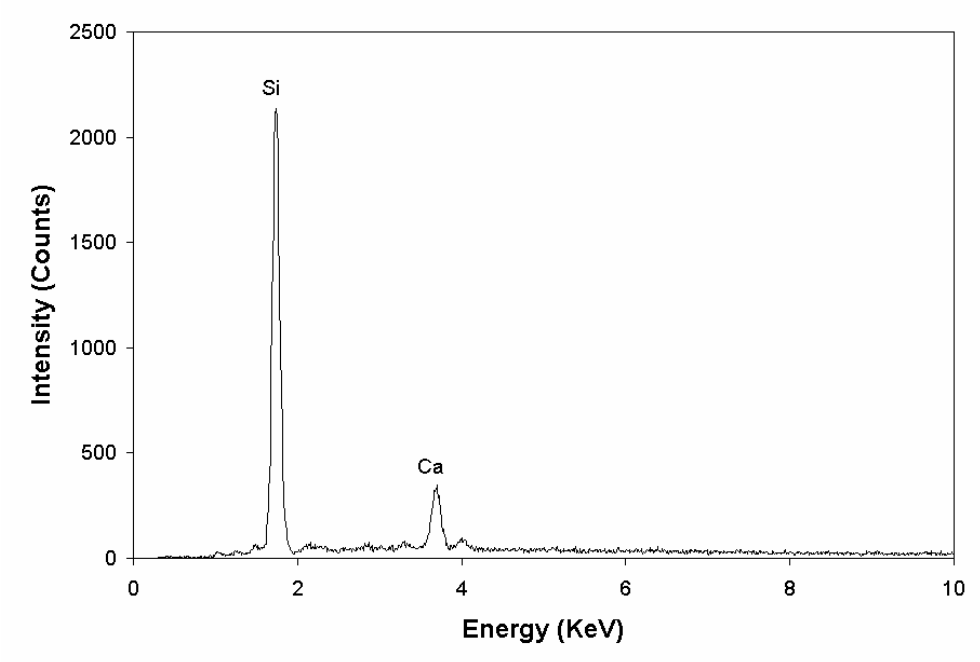

Figure 3 EDS spectra of the inside surface of the inlet of the Y16 glass tube.

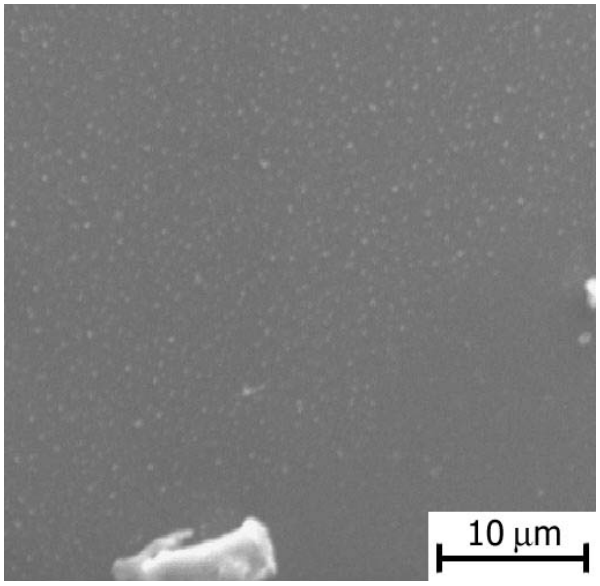

Figure 5 SEM photomicrograph of the inside surface of the inlet on an uncoated glass tube. Taken at 2000x.

To: Chris Norton
From: Erik Pavlina
Date: 12 February 2004
RE: SEM/EDS Analysis of Al14 and Al15 Samples

Analysis was conducted on coated glass tubes via SEM/EDS. The samples analyzed were Al14 and Al15. A non-continuous, spherical deposit was observed on both samples. The composition of the deposition could not be verified using EDS techniques. Since alumina is a component of the glass tube composition, aluminum peaks are observed due to the electron beam interaction with the deposition particles and with the glass itself.

IV AL14

A regular deposition was observed at the mid-point and inlet of the glass tube (Figures 1 and 2). The deposition had a spherical morphology. As stated earlier, the interaction of the electron beam with the glass essentially masks any aluminum peaks that would be

observed for the deposition particles since alumina is a part of the glass composition (Figure 3).

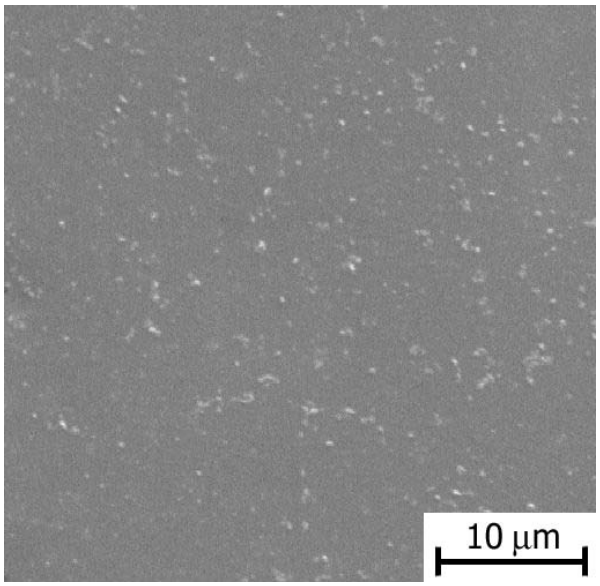

Figure 1 SEM photomicrograph of the deposition particles at the mid-point of sample Al14. Taken at 2000x.

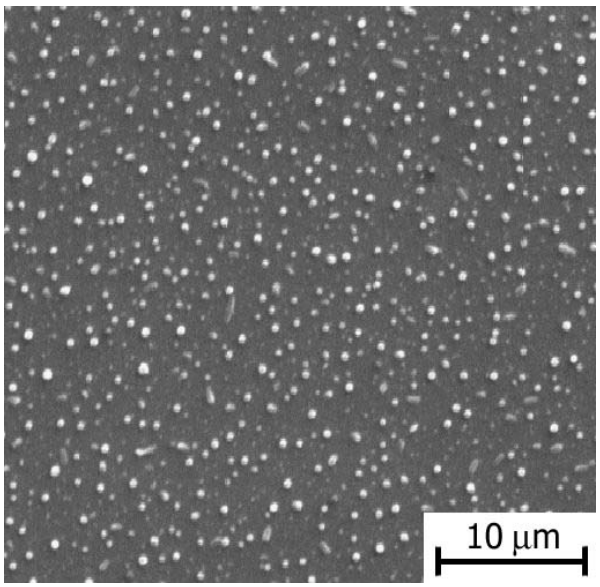

Figure 2 SEM photomicrograph of the deposition particles at the inlet of sample Al14. Taken at 2000x.

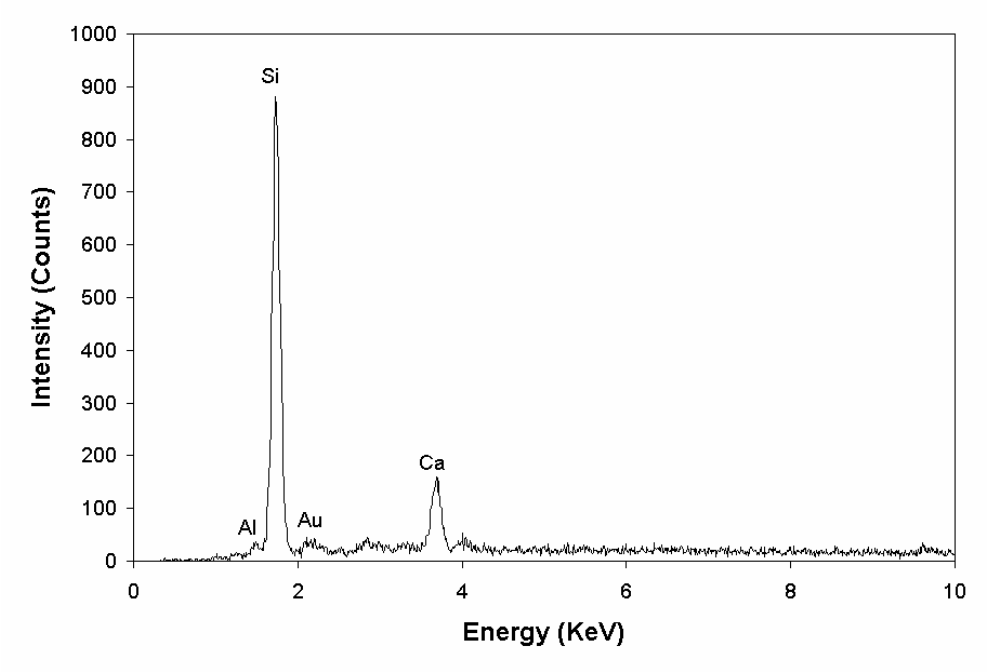

Figure 3 EDS spectra of surface particles on sample Al14.

V AL15

The deposition particles on the Al15 sample also had a spherical morphology (Figures 4 and 5). Also, larger particles were also observed on the surface, especially around the mid-point of the glass tube (Figure 6). Elemental analysis of the larger particles indicated the presence of sodium and chlorine (Figure 7). Chlorine peaks were observed on all EDS spectra obtained from the smaller spherical deposition particles as well (Figure 8).

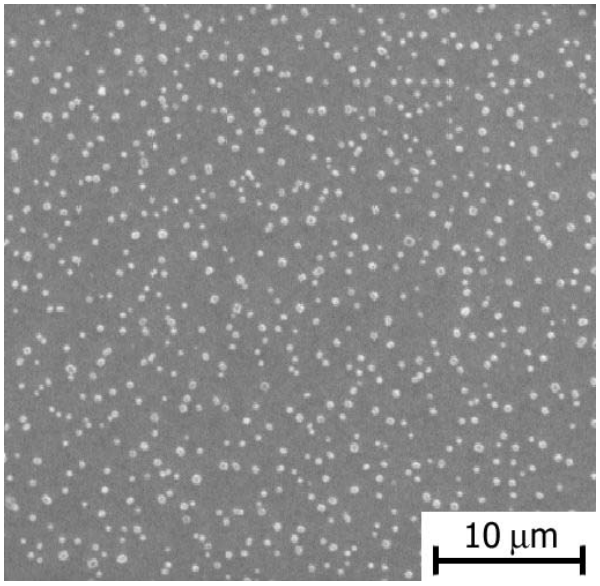

Figure 4 SEM photomicrograph of the deposition particles at the mid-point of sample Al15. Taken at 2000x.

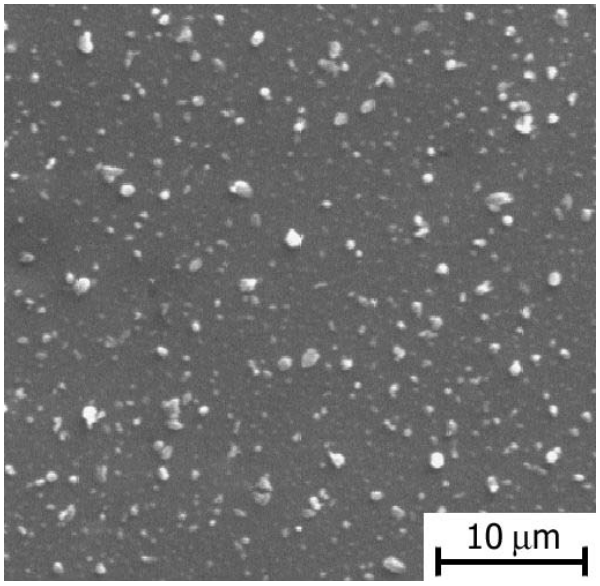

Figure 5 SEM photomicrograph of the deposition particles at the inlet of sample Al14. Taken at 2000x.

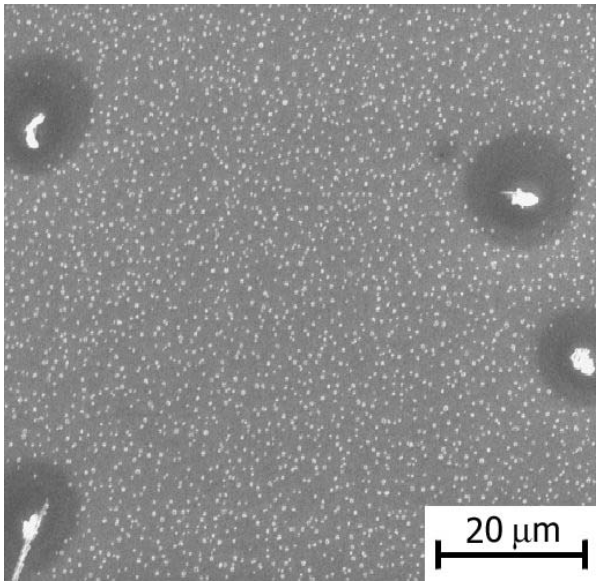

Figure 6 SEM photomicrograph of the large particles at the mid-point of sample Al15. Taken at 1000x.

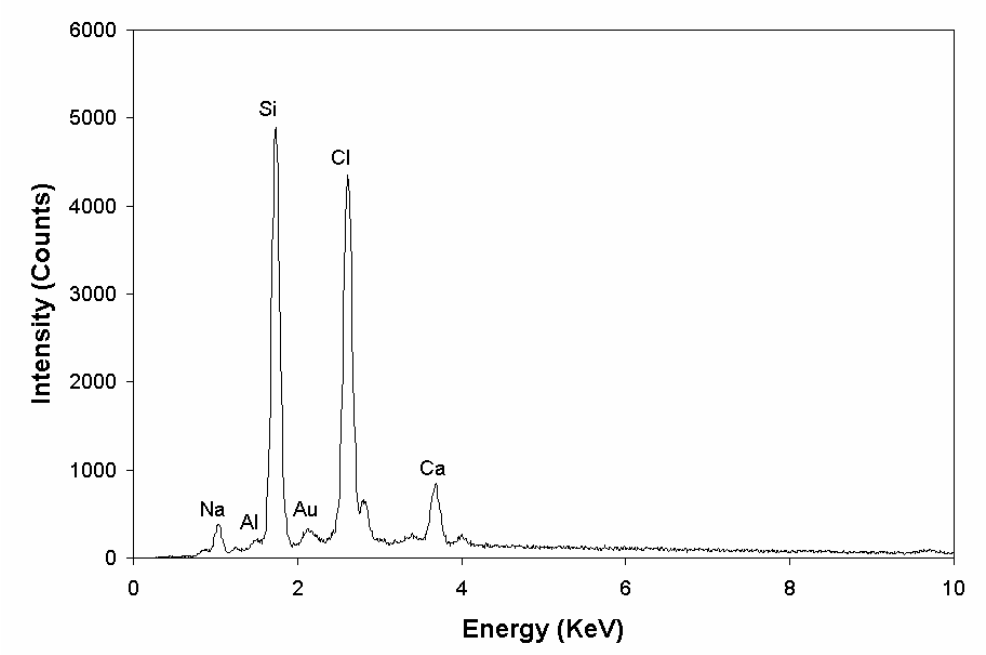

Figure 7 EDS spectra of the large surface particles at the mid-point of sample Al15.

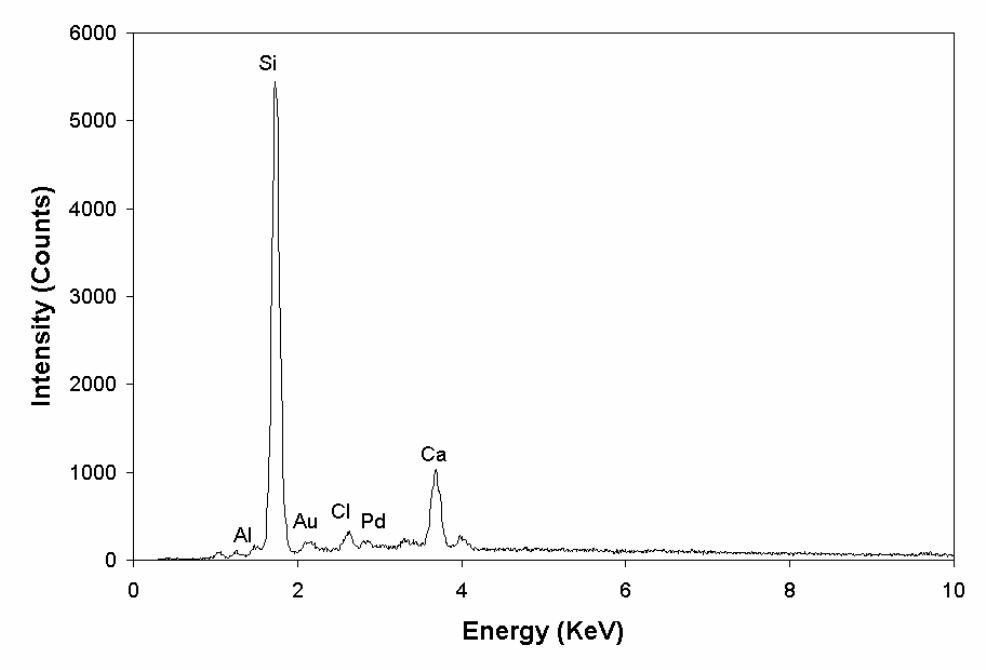

Figure 8 EDS spectra of the deposited surface particles on sample Al15.

Attached are SEM photomicrographs and EDS spectra for the Y17 sample. It does not appear to a yttrium coating.

Erik

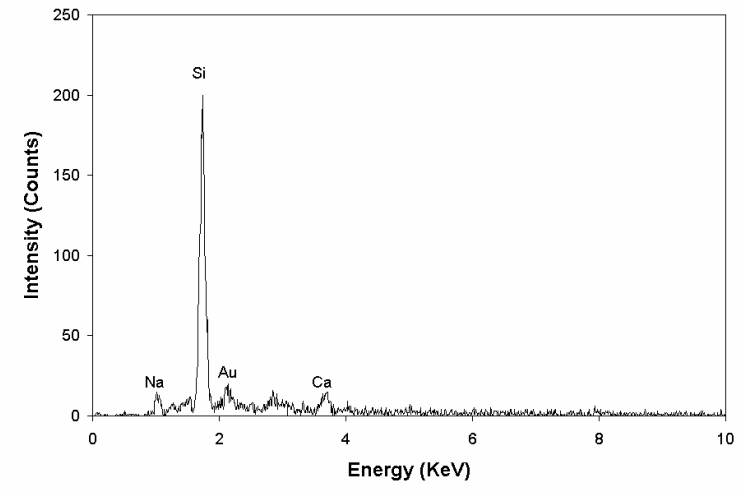

To: Chris Norton, Xingwu Wang, Richard Marlor, and Tuan Dang

From: Erik Pavlina

Date: 8 March 2004

RE: SEM/EDS Analysis of Filter Paper

Filter paper containing an yttrium salt precursor was compared with an as-received filter paper via SEM/EDS analysis. The filter paper is composed of soda-lime-silicate glass fibers that also contain some magnesia, potash, and alumina (Figure 1). Yttrium was detected in the paper containing the precursor (Figure 2). When compared visually, there are no prominent differences observed between the as-received filter paper and the precursor-containing filter paper (Figures 3-5).

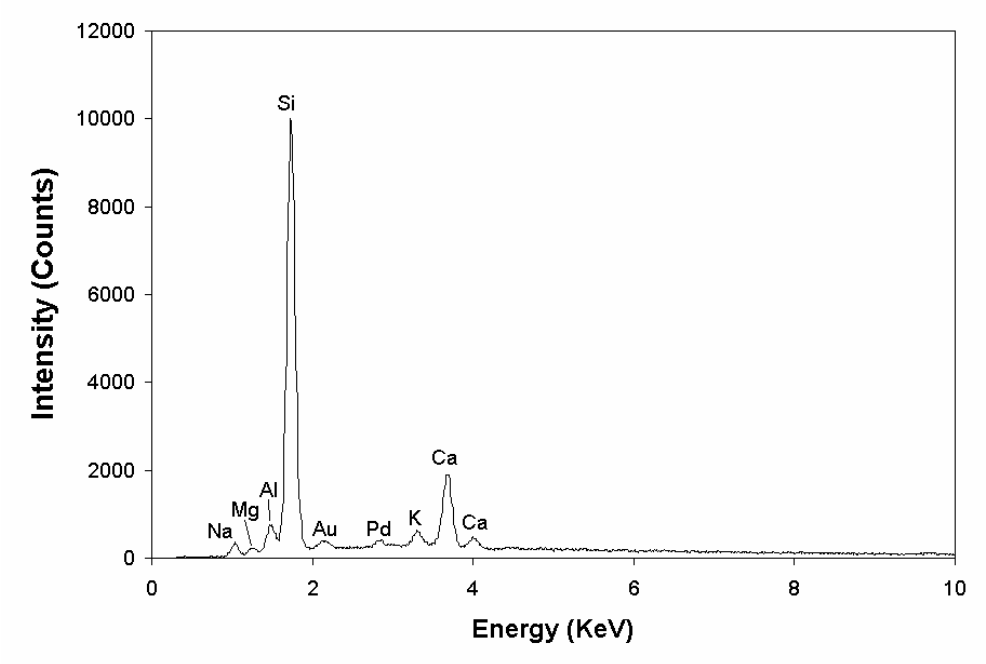

Figure 1 EDS spectra of the as-received filter paper.

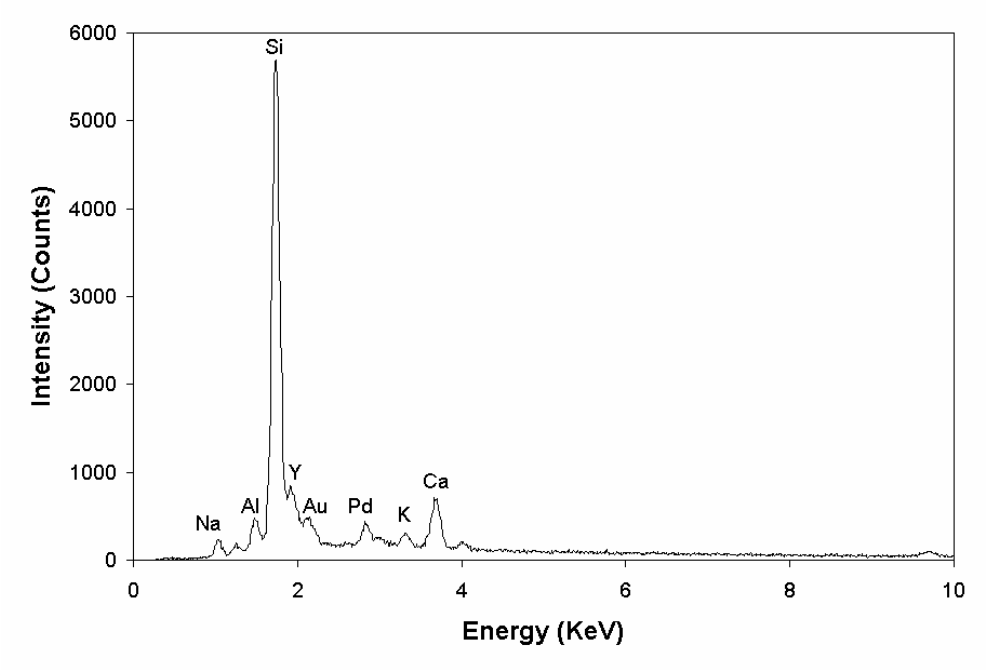

Figure 2 EDS spectra of filter paper containing the yttrium salt precursor.

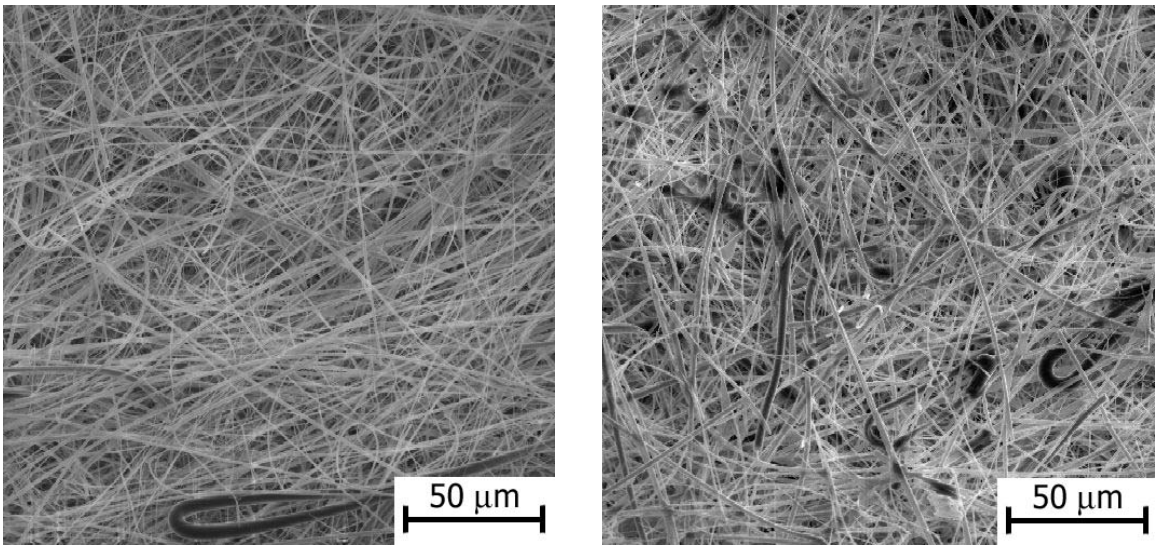

(a) (b)

Figure 3 SEM Photomicrographs of (a) as-received filter paper and (b) precursor-containing filter paper. Taken at 400x.

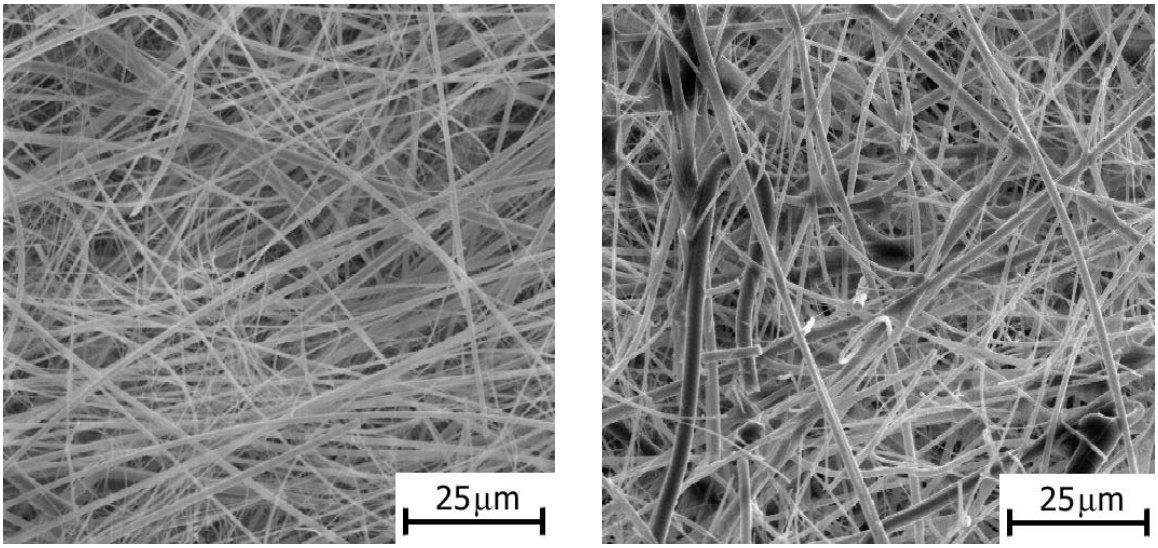

(a) (b)

Figure 4 SEM Photomicrographs of (a) as-received filter paper and (b) precursor-containing filter paper. Taken at 800x.

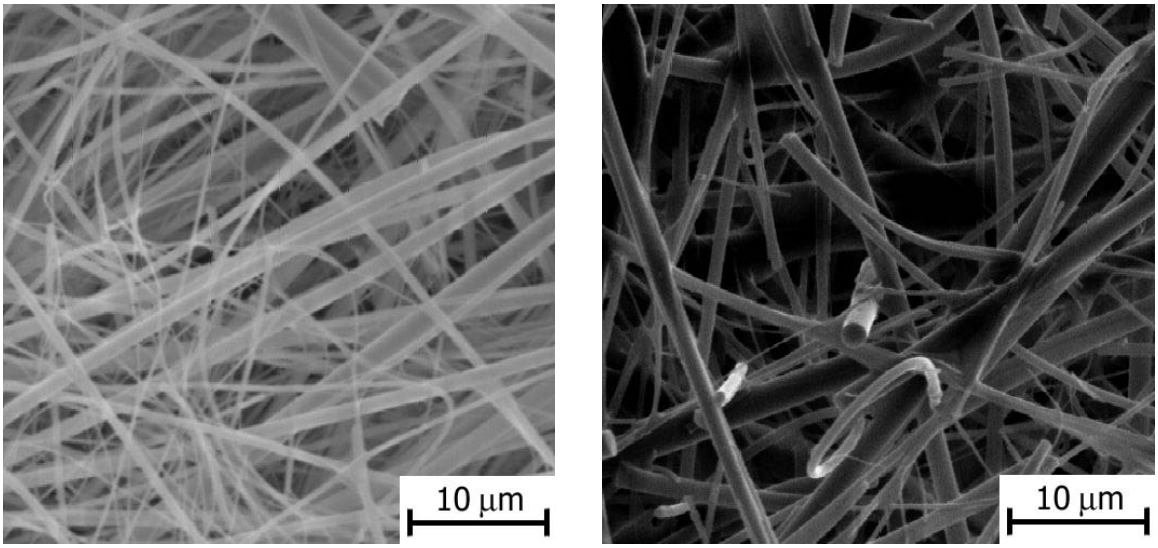

(a) (b)

Figure 5 SEM Photomicrographs of (a) as-received filter paper and (b) precursor-containing filter paper. Taken at 2000x.

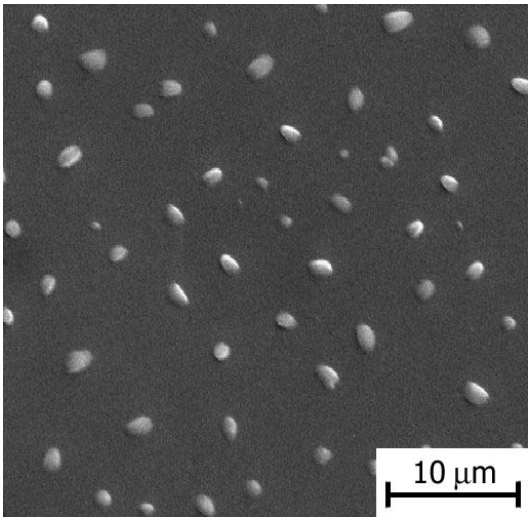
10 µm

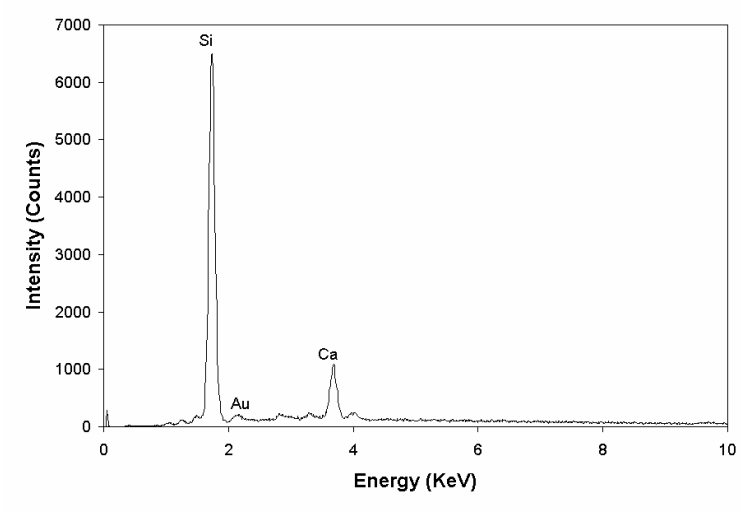
Intensity (Counts)
Energy (KeV)
Si
Au
Ca
0
1000
2000
3000
4000
5000
6000
7000
0
2
4
6
8
10

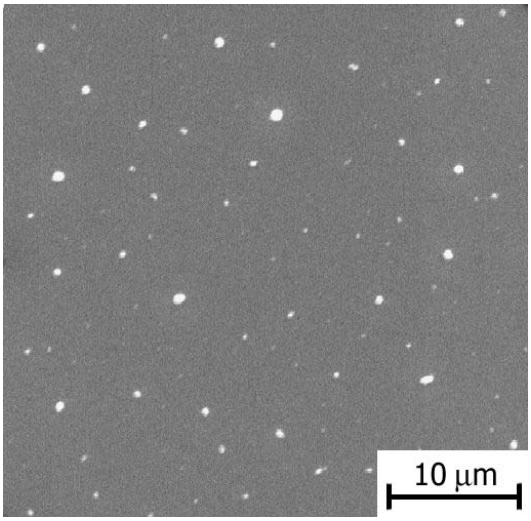
10 µm